NLRP3 INFLAMMASOME ACTIVITY IN RPE: ROLE IN AMD PATHOGENESIS

by

Jiangyuan Gao

B.Sc., Fudan University, 2010

A THESIS SUBMITTED IN PARTIAL FULFILLMENT OF

THE REQUIREMENTS FOR THE DEGREE OF

DOCTOR OF PHILOSOPHY

in

THE FACULTY OF GRADUATE AND POSTDOCTORAL STUDIES

(Cell and Developmental Biology)

THE UNIVERSITY OF BRITISH COLUMBIA

(Vancouver)

August 2017

Abstract

Purpose:

Age-related macular degeneration (AMD) is a devastating eye disease causing irreversible vision loss in the elderly. Retinal pigment epithelium (RPE), an important cell type afflicted in AMD, undergoes cell death in the late stages of the disease. Salient factors underlying AMD pathogenesis are aging, drusen components and NLRP3 inflammasome activity. The purpose of this dissertation is to elucidate the molecular interactions among these factors and how they contribute to RPE damage.

Methods:

The effects of aging on drusen components, in particular the membrane attack complex (MAC) and amyloid beta (Aβ) were examined in rats at different age. To determine the role of MAC in inflammasome activation in RPE, aurin tricarboxylic acid complex (ATAC), was administrated to naïve rats. To understand Aβ's role in inflammasome activation, Aβ intravitreal injections were made into rat eyes *in vivo* and Vinpocetine was used to ameliorate the inflammatory responses. An *in vitro* RPE cell culture model was established to further investigate the relationship between inflammasome and X-chromosome linked inhibitor of apoptosis (XIAP). Statistical significance was set at $p \leq 0.05$.

Results:

An age-dependent increase in MAC, Aβ, and NF-κB activation was observed in the RPE-choroid *in vivo*. Blocking MAC formation with ATAC led to a prominent reduction in inflammasome

activity (caspase-1 cleavage and cytokine secretion), but not in NF-κB activity. Aβ intravitreal injections triggered inflammasome activation evidenced by enhanced caspase-1 cleavage and IL-1β/IL-18 release, which was suppressed by Vinpocetine mediated NF-κB inhibition. The robust inflammasome activity further led to gasdermin D-mediated activation of the pyroptotic pathway and a significant reduction in XIAP, which in turn enhanced IL-18 secretion.

Conclusion:

Aging is a strong risk factor for AMD, which increases the deposition of MAC and Aβ in the outer retina. The elevated levels of MAC and Aβ are triggers for inflammasome activation. By demonstrating a causal relationship between inflammasome activation and XIAP reduction, this dissertation suggests the precise regulation of XIAP, together with the suppression of MAC and NF-κB, may be crucial for controlling inflammasome activity and hence provides new avenues to prevent AMD.

Lay Summary

Age-related macular degeneration (AMD) is a common eye condition that occurs to the central part of retina, the macula. In one of the late stages of AMD, retinal pigment epithelium (RPE) cell death is the major cause of irreversible vision loss that we do not have a cure for. It is therefore paramount to understand how normal aging transitions into such a state of RPE cell loss and what are the key forces behind it. This dissertation focuses on the age-related accumulation of pro-inflammatory molecules and the pathological pathways that potentially lead to RPE cell damage. My study revealed a crucial role of inflammasome, an immune protein complex, in connecting the elevated pro-inflammatory molecules with declined RPE homeostasis. These novel findings will advance the goal of developing new treatment strategies to preserve vision in AMD patients.

Preface

A version of *chapter 1* has been published. [Gao, J.], Liu, R.T., Cao, S., Cui, J.Z., Wang, A., To, E., Matsubara, J.A. NLRP3 inflammasome: activation and regulation in age-related macular degeneration. Mediators of Inflammation. Vol. 2015, Article ID 690243, 11 pages, 2015. I prepared the first draft and revised the manuscript until its acceptance for publication. Under the Creative Commons Attribution License, as the author and copyright holder of the published article (http://dx.doi.org/10.1155/2015/690243), I am permitted to reuse the contents of the article in this dissertation.

A version of *chapter 2* has been published. Zhao, T., [Gao, J.], Van, J., To, E., Wang, A., Cao, S., Cui, J.Z., Guo, J.P., Lee, M., McGeer, P.L., Matsubara, J.A. Age-related increases in amyloid beta and membrane attack complex: evidence of inflammasome activation in the rodent eye. Journal of Neuroinflammation. Jun 2015;12:121. I participated in the study design, performed 40% of the experiments, analyzed and interpreted data, prepared the first draft and revised the manuscript until its acceptance for publication. The study was approved by the Animal Care Committee of the University of British Columbia (Certificate number: A16-0168). Under the Creative Commons Attribution License, as the author and copyright holder of the published article (http://dx.doi.org/10.1186/s12974-015-0337-1), I am permitted to reuse the contents of the article in this dissertation.

A version of *chapter 3* has been published. Liu, R.T., [Gao, J.], Cao, S., Sandhu, N., Cui, J.Z., Chou, C.L., Fang, E., Matsubara, J.A. Inflammatory mediators induced by amyloid-beta in the

retina and RPE *in vivo*: implications for inflammasome activation in age-related macular degeneration. Investigative Ophthalmology and Visual Sciences. Mar 2013;54(3):2225-2237. I participated in the study design, performed 40% of the experiments in the manuscript, analyzed and interpreted data, and revised the manuscript until its acceptance for publication. The study was approved by the Animal Care Committee (Certificate number: A16-0168) and the Clinical Research Ethics Board (Certificate number: H11-02772, H00-70411) of the University of British Columbia. The Association for Research in Vision and Ophthalmology, as the copyright holder, has generously permitted the reuse of the article (doi:10.1167/iovs.12-10849) in this dissertation.

A version of *chapter 4* has been published. Liu, R.T., Wang, A., To, E., [Gao, J.], Cao, S., Cui, J.Z., Matsubara, J.A. Vinpocetine inhibits amyloid-beta induced activation of NF-κB, NLRP3 inflammasome and cytokine production in retinal pigment epithelial cells. Experimental Eye Research. Oct 2014;127:49-58. I participated in the study design, performed 25% of experiments in the manuscript, analyzed and interpreted data, and revised the manuscript until its acceptance for publication. The study was approved by the Animal Care Committee of the University of British Columbia (Certificate number: A16-0168). As the copyright holder, Elsevier has generously permitted the reuse of the article (http://dx.doi.org/10.1016/j.exer.2014.07.003) in this dissertation.

A version of *chapter 5* has been submitted for publication. [Gao, J.], Cui, J.Z., Cao, S., Matsubara, J.A. Evidence for the activation of pyroptotic and apoptotic pathways in RPE cells associated with NLRP3 inflammasome in the rodent eye. Journal of Neuroinflammation, 2017. I participated in the study design, performed 80% of the experiments, analyzed and interpreted

data, prepared and revised the manuscript for publication. The study was approved by the Animal Care Committee of the University of British Columbia (Certificate number: A16-0168).

Chapter 6 is based on the work conducted in the Department of Ophthalmology and Visual Sciences by [Gao, J.], Cui, J.Z., Wang, A., Matsubara, J.A. I designed the study, performed all the experiments, analyzed and interpreted data. The results are being prepared for submission to a scientific journal. This study was approved by the Animal Care Committee of the University of British Columbia (Certificate number: A16-0168).

Table of Contents

List of Tables

List of Figures

List of Abbreviations

Aβ	amyloid beta
AD	Alzheimer's disease
AEC	3-amino-9-ethylcarbazole
AMD	age-related macular degeneration
ANOVA	analysis of variance
APP/PS1	amyloid precursor protein/presenilin
ASC	apoptosis-associated speck-like protein containing a carboxy-terminal CARD
ATAC	aurin tricarboxylic acid complex
BM	Bruch's membrane
CFH	complement factor H
CMV	cytomegalovirus
CNS	central nervous system
CNV	choroidal neovascularization
CRALBP	cellular retinaldehyde-binding protein
DAMPs	danger-associated molecular patterns
DMEM	Dulbecco's modified essential medium
DMSO	dimethyl sulfoxide
DPBS	Dulbecco's phosphate-buffered saline
DUBs	deubiquitinating enzymes
ECL	enhanced chemiluminescence
ELISA	enzyme-linked immunosorbent assay

FBS	fetal bovine serum
GA	geographic atrophy
GAPDH	glyceraldehyde 3-phosphate dehydrogenase
GCL	ganglion cell layer
GRO/KC	chemokine (C-X-C motif) ligand 1
GSDMD	gasdermin D
HA	hemagglutinin
HFIP	1,1,1,3,3,3-hexafluoro-2-propanol
IC_{50}	half maximal inhibitory concentration
IL-1α	interleukin-1alpha
IL-1β	interleukin-1beta
IL-6	interleukin-6
IL-18	interleukin-18
INL	inner nuclear layer
IPL	inner plexiform layer
IS	inner segment
LLOM	Leu-Leu-OMe (L-leucyl-L-leucine methyl ester)
MAC	membrane attack complex
MCP-1	monocytes chemoattractant protein 1
MES	2-(N-morpholino)ethanesulfonic acid
MFI	median fluorescent intensity
MIP-3α	macrophage inflammatory protein 3 alpha
MW	molecular weight

NF-κB	nuclear factor kappa B
N-GSDMD	N-terminal fragment GSDMD
NLRP3	nod-like receptor family pyrin domain containing 3
NSAIDs	non-steroidal anti-inflammatory drugs
ONL	outer nuclear layer
OPL	outer plexiform layer
OS	outer segment
PAMPs	pathogen-associated molecular patterns
PBS	phosphate buffered saline
PVDF	polyvinylidene fluoride
RAGE	receptor for advanced glycation end product
RIPA	radio immunoprecipitation assay
ROS	reactive oxygen species
RPE	retinal pigment epithelium
RPE65	retinoid isomerohydrolase
RT-PCR	reverse transcription polymerase chain reaction
SAPE	streptavidin-phycoerythrin
SD	standard deviation
SDS-PAGE	sodium dodecyl sulfate polyacrylamide gel electrophoresis
siRNA	small interfering RNA
SNP	single nucleotide polymorphism
TLR	toll-like receptor
TNF-α	tumor necrosis factor-alpha

TUNEL	terminal deoxynucleotidyl transferase dUTP nick-end labeling
VEGF	vascular endothelial growth factor
WB	western blot
XAF1	XIAP-associated factor 1
XIAP	X-chromosome linked inhibitor of apoptosis protein
XLP2	X-linked lymphoproliferative syndrome 2

Glossary

ARPE-19 A spontaneously immortalized cell line of human retinal pigment epithelium, which is widely used to study RPE cellular responses in various physiological and pharmaceutical conditions.

Pyroptosis A specialized form of inflammatory programmed cell death that requires Caspases 1 or 11 in mice and Caspases 1, 4 or 5 in humans.

Nod-like Receptor Family, Pyrin Domain Containing 3 (NLRP3) Inflammasome A well-studied intracellular innate immune multi-protein machinery capable of sensing a diversity of pathogen-/danger-associated molecular patterns, which leads to elevated cytokine secretion and ultimately pyroptosis.

Gasdermin D A member of the evolutionarily conserved gasdermin family, functions as an executioner of pyroptosis when cleaved by inflammatory Caspases.

Geographic Atrophy (GA) A non-exudative type of late stage AMD, clinically defined as any sharply delineated round or oval area of hypopigmentation (due to RPE and photoreceptor cell death) that must be ≥ 175 μm in diameter.

Membrane Attack Complex (MAC) The terminal product of complement activation that forms hydrophilic pores to disrupt lipid bilayers and lyse the cell.

Small Interfering RNA (siRNA) A class of single-stranded RNA molecules (often 21-25 nucleotides in length) that bind to complementary sequences in mRNA and brings about the cleavage and degradation of the mRNA.

Intravitreal Injection A surgical procedure to deliver substances (e.g. treatment drugs, Aβ) into the eye. The injected substances then reach the retina mostly by passive diffusion.

Interleukin-18 (IL-18) A member of the IL-1 family of cytokines, synthesized as an inactive precursor that requires caspase-1 mediated processing into an active cytokine.

Interleukin-1β (IL-1β) A member of the IL-1 family of cytokines, synthesized as an inactive precursor that requires caspase-1 mediated processing into an active cytokine.

Vitreous A gel-like filling substance that helps the eye maintain a round shape. It contains millions of fine intertwining fibers that are attached to the surface of the retina.

RPE-Choroid Complex A sample type of *in vivo* eye tissues, composed of both RPE and choroid that are surgically difficult to separate. It is commonly used as a substitute for the theoretically hard-to-obtain homogeneous RPE tissue in AMD research.

CH50 Hemolysis Assay A type of experimental assay measures the degree of hemolysis in blood samples due to complement activation.

Complement Activation An innate immune response triggered by antigen-antibody complexes, pathogens or mannan-binding lectin, generating effector complement molecules, and leading to the opsonization of pathogens, the recruitment of inflammatory cells, and the formation of membrane attack complex to directly kill the affected cells.

Nuclear Factor Kappa B (NF-κB) A eukaryotic transcription factor that is involved in the control of key cellular processes, such as inflammatory responses and cell death.

Acknowledgements

I offer my enduring gratitude to Dr. Joanne A. Matsubara for accepting me into the research group, generously offering her supervision and guidance through the course of my PhD study.

I would like to thank my supervisory committee members, Dr. Calvin D. Roskelley, Dr. Matthew C. Lorincz and Dr. Orson L. Moritz for enlarging my vision of science and providing coherent, inspiring answers to my questions during annual committee meetings. I thank them for their expertise, time and efforts to help me complete my study.

I owe particular thanks to Dr. Jing Z. Cui for her help with my study design, lab work as well as my personal life, especially during the transition times at the beginning of my Canadian graduate studies.

I would also like to thank Dr. Aikun Wang for his technical assistance in molecular biology and animal studies; Eleanor To for her help with immunohistochemical experiments, analyses and administrative work; Sijia Cao, Tom Ruozhou Liu, Tom Zhao, Matthew Wong and Alison Fong for their kind support and constructive discussions in various research projects presented in this dissertation.

I would also like to express my gratitude to the faculty members in the Department of Ophthalmology and Visual Sciences, especially Dr. Paul Mackenzie, Dr. Simon J. Warner, Dr.

David Maberley, and Dr. Valerie A. White, who have inspired me with their in-depth knowledge and clinical insights.

Special thanks are owed to my parents and my wife, who have supported me throughout my years of education, both morally and financially.

This work was jointly supported by Canadian Institutes of Health Research (CIHR) grants MOP-97806 and MOP-126195 to Dr. Joanne A. Matsubara and by the Vancouver Hospital + UBC Foundation.

Dedication

This dissertation is dedicated to my loving parents, Mr. Feng Gao and Mrs. Meilan Jiang, my in-laws, Mr. Yongqi Luo and Mrs. Lijuan Yan, my beloved wife, Mrs. Wei Luo, my son, Mason Luoxuan Gao, and my friends, especially Yichun Qiu, Wu Yang Jin, Leon Lin Li, Zhechen Wang and Junchao Yu.

The path to the completion of this PhD program was challenging, stressful and full of obstacles. If it were not for the love, support and patience of my family and friends, I can honestly say that I would not have been able to accomplish it. Thank you all for everything.

Chapter 1: Introduction

1.1 Background

1.1.1 Anatomy of the human eye

The eye is a marvelous sensory organ that allows us to see the beautiful world we live in and to communicate with others. Coined as the "windows to the soul", our eyes are physically connected to the brain, serving as an outpost of the central nervous system (CNS). For the eye to sense light and information from the outside world, it needs a system that is optically and neurologically sophisticated to efficiently compartmentalize the input. Such an optical system consists of cornea, aqueous humor, lens, vitreous humor and the multi-layered retina (Figure 1-1). Light rays are focused through the transparent cornea and lens upon the retina, where visual signals are converted into electrical neural signals by the photoreceptors and then relayed into the visual cortex through the visual pathway, photoreceptors—retinal interneurons—ganglion cells—optic nerve/tract—lateral geniculate nucleus—primary visual cortex. In the center of retina, there is macula, a specialized region responsible for fine visual acuity that is required for tasks such as reading, facial recognition, and driving.[1] In the center of macula lies the fovea, an area containing the highest density of cone photoreceptors, which allows us to see fine details. Although the macula only covers 4% of retinal area, it almost accounts for 10% of our visual field.[2] Hence, losing functional cells in the macular region can lead to vision impairment.

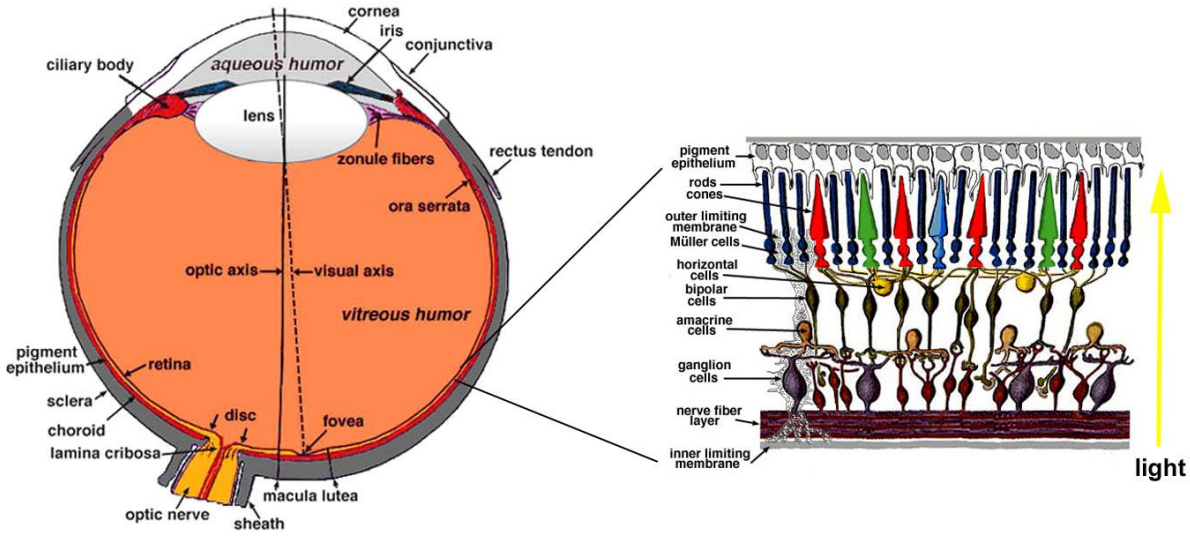

Figure 1-1 A schematic diagram of an adult human eye and the sagittal view of retina.

(Left) Light comes into the eye through the anterior (cornea and lens) and focuses on the retina, the centre of which is macula. (Right) Human retina is a well-organized multi-layered structure that efficiently utilizes the light signals and converts them into neurological signals. Note that the retina is aligned by placing the inner limiting membrane at the bottom of this panel for illustration purpose only, which should be interior facing towards the vitreous humor in its native anatomical position. (©Webvision, http://webvision.med.utah.edu, reproduced with permission)

1.1.2 The development of retina

The development of the human eye is an intricate process, each stage of which requires exquisite coordination of time and space. During gastrulation, the process known as neural induction transforms a region of ectoderm into the precursors of the CNS, called the neural plate. Like the rest of the CNS, the retina is embryonically derived from the neural plate. Both the neural retina and the retinal pigment epithelium (RPE) arise from the optic vesicle region of the neural tube. The mitotic retinal progenitors undergo repeated mitotic cell divisions to produce the different types of human retinal cells in a sequence that is conserved in all vertebrates.[3]

1.1.3 Histology and function of RPE

The RPE is a terminally differentiated monolayer of highly specialized neuroectoderm-derived pigmented cells formed embryonically by cells of the developing outer layer of the optic cup.[4] There are approximately 3.5 x 10^6 RPE cells lining the back of the eye, between the neural retina and the choroid, in the adult human eye, with the highest cell density at the foveal area.[5] RPE cells are cobblestone-like, highly polarized cells. Their apical microvilli interdigitate with the outer segments of the photoreceptors, and their basal surface is firmly attached to the underlying Bruch's membrane (BM). Given their unique position in the eye, RPE cells mediate functions essential for outer retinal physiology that include recycling components of the visual cycle, phagocytosis of shed photoreceptor outer segments, maintenance of the outer blood-retinal barrier, secretion of trophic and inflammatory factors, and regulation of ion/metabolic transport between retina and choroid.[6, 7] Therefore, the loss of RPE cells due to disease often results in devastating outcomes such as vision impairment in the age-related macular degeneration (AMD) and other retinal dystrophies.

1.1.4 AMD: a multi-factorial disease

Age-related macular degeneration (AMD) is a neurodegenerative disease characterized by the deterioration of photoreceptors in the macula. According to the World Health Organization, AMD currently ranks as the third global leading cause of blindness, second only to cataract and glaucoma.[8] However, among the elderly, AMD is the most common cause of irreversible vision loss in developed countries. Approximately 30-50 million individuals worldwide are afflicted with AMD. The economic costs for treatment and care of individuals who suffer vision loss from

AMD are projected to be more than US$ 300 billion annually, a heavy toll that will significantly impact global social and public health systems and one that prompts an urgent need to decipher its underlying mechanisms.[9]

The pathogenesis and progression of AMD are influenced by a variety of risk factors. Among them, advanced chronologic aging is the strongest.[10-12] The prevalence of AMD steadily increases with age, affecting 2% of the population at age 40 and 25% by age 80.[13] Besides aging, other risk factors such as cigarette smoking and diet also contribute to the development of the disease.[14-17] Clinically, early stages of AMD are defined by the presence of drusen, the extracellular yellowish proteinaceous deposits located between the RPE and BM (Figure 1-2).[18] Despite the fact that early AMD is usually not associated with appreciable vision loss, the number and the size of drusen deposits serve as indicators of disease progression.[19] When the disease progresses into the late stage, it takes one of two forms: geographic atrophy (GA), featured by confluent regions of RPE and photoreceptor degeneration, or choroidal neovascularization (CNV), characterized by the abnormal growth of leaky choroidal vessels invading retina. Central to AMD pathogenesis, the RPE undergoes significant changes in structure and function that predispose individuals to disease processes associated with AMD. Suggestive of an associated, and perhaps causal, role in RPE dysfunction is the finding that RPE cells overlying drusen appear swollen and vacuolated.[20] It is further proposed that the spontaneous release of drusen components during drusen regression in AMD development may result in RPE loss in GA.[21]

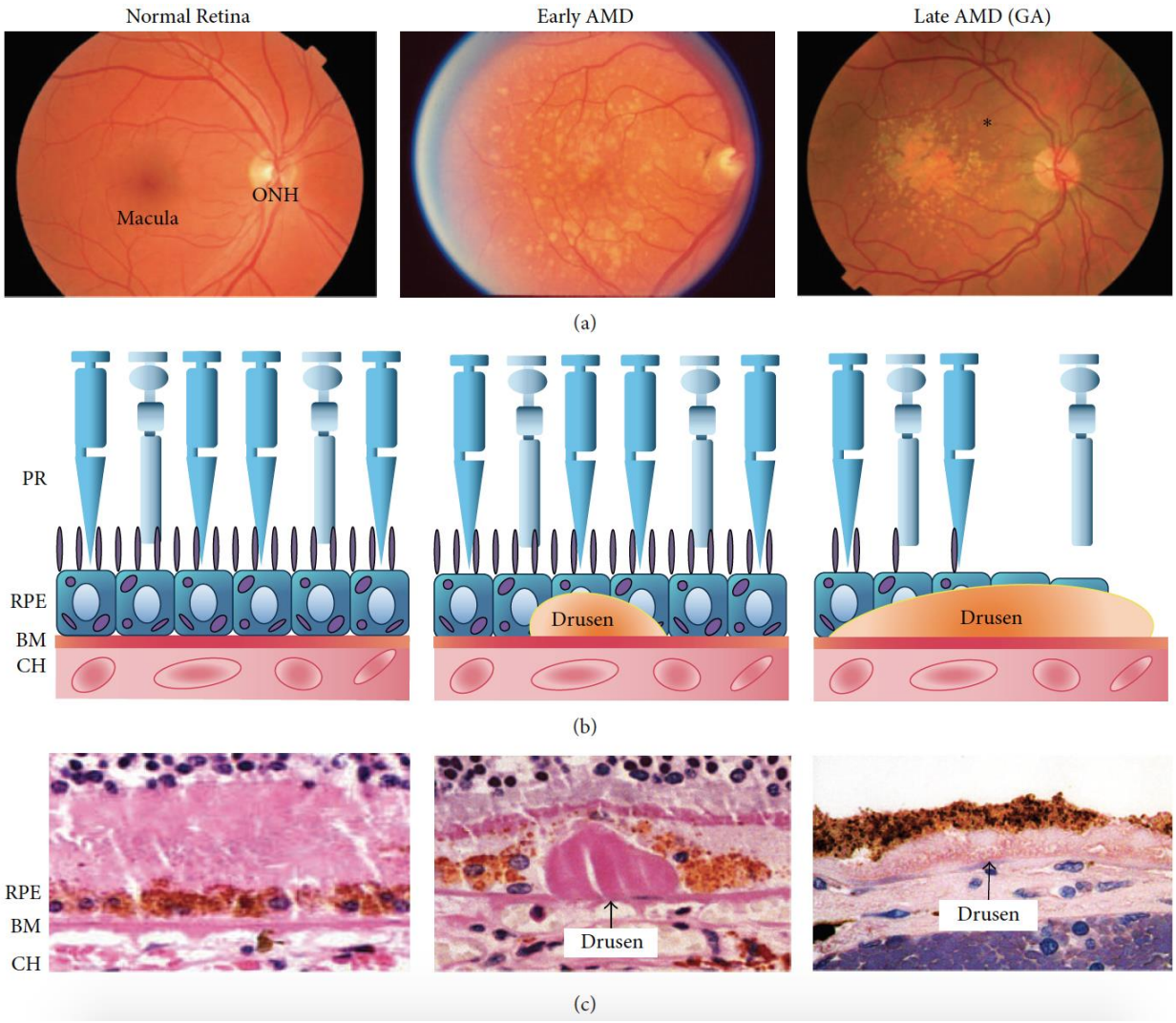

Figure 1-2 Clinical stages and signs of age-related macular degeneration.

(a) Fundus photos demonstrate clinical features of AMD at different stages. Early AMD shows yellow extracellular drusen deposits surrounding macular area. Late AMD (GA) shows hypopigmentation or background darkening (*) around drusen. A large number of drusen deposits are observed accumulated in the macular area. (b) Schematic diagram of drusen accumulation and RPE/photoreceptor degeneration from early to late stage AMD (GA). (c) Staining of human postmortem donor eye tissues depicting normal, early AMD, and late AMD. Arrows point to different forms of drusen: a large hard drusen in an early AMD eye and a diffuse, soft drusen in a late AMD (GA) eye. GA, geographic atrophy; ONH, optic nerve head; PR, photoreceptors; RPE, retinal pigment epithelium; BM, Bruch's membrane; CH, choroidal capillaries.

1.1.5 NLRP3 inflammasome

Recent advances have highlighted the essential role of immune processes in the development, progression, and treatment of AMD.[1] Both the innate and adaptive immune systems have been shown to contribute to AMD pathogenesis.[22, 23] The innate immune system is an evolutionarily conserved system that constitutes the first line of defense against pathogens. Inflammasome activation is a key component of innate immunity, which when overactive has been linked with many human immune diseases.[24-27] The inflammasome is an intracellular, multi-protein complex whose molecular composition is stimulus dependent. The canonical inflammasome complexes are assembled around protein members of the nod-like receptor (NLRs) or HIN-200 protein families, converting the pro-caspase-1 zymogen into a catalytically active enzyme. The canonical inflammasome family is further categorized based on the presence of an apoptosis-associated speck-like protein containing a caspase recruitment domain (ASC) into ASC-dependent (NLRP3 and AIM2) and ASC-independent (NLRP1 and NLRC4) subtypes.[28] The non-canonical inflammasome complex with an, as yet, unknown structural composition is proposed to promote the activation of caspase-11.[29] Despite the gap in knowledge of the structure of the non-canonical inflammasome, there is a wealth of evidence to firmly establish the mode of action for several canonical inflammasomes in the immune signaling pathway, especially the most widely studied NLRP3 inflammasome.[30] The NLRP3 inflammasome senses and responds to a diversity of pathogen- or danger-associated molecular patterns (PAMPs or DAMPs), including bacterial/viral/fungal pathogens, pore-forming toxins, uric acid crystals, particulate aggregates, and adenosine triphosphate (ATP). To be activated, the NLRP3 inflammasome requires the presence of two signals, a “priming signal” and an “activation signal,” both of which are vital to

control the degree of immune response driven by the products of inflammasome activation. In most cases, the "priming signal" channels through the nuclear factor kappa B (NF-κB) pathway, upregulating the transcription of NLRP3 and pro-interleukin-1β (pro-IL-1β).[31] In both immune and RPE cells, pro-IL-1β is not constitutively expressed and the endogenous level of NLRP3 appears to be inadequate for inflammasome activation, thus making the priming process critical.[32, 33] In contrast, other inflammasome-related proteins, ASC, pro-caspase-1, and pro-IL-18, are constitutively expressed in RPE cells and therefore priming may, or may not, further increase their protein levels.[32, 34-36] In addition to the classic, transcription-dependent priming, it is now known that the NLRP3 inflammasome can be "primed" post-translationally, adding another layer of regulation.[37] Common priming signals for immune cells of the body and human RPE cells are lipopolysaccharide (LPS), tumor necrosis factor-α (TNF-α), nitric oxide, and IL-1α.[32, 38] In the presence of foreign or endogenous "activation signals," NLRP3 senses one or more of the following intracellular changes: K^+ efflux,[39] release of lysosomal resident cathepsin B,[40] overproduction of reactive oxygen species (ROS),[41] NLRP3 translocation to mitochondria,[42] cell volume change, and Ca^{2+} disequilibrium.[38] Once the NLRP3 is activated, it recruits ASC and mediates the proximity-induced pro-caspase-1 auto-activation. The assembled NLRP3 inflammasome then turns itself into a cytokine processing platform, cleaving pro-IL-1β/pro-IL-18 into mature peptides and releasing them into extracellular space for downstream effects (Figure 1-3). Despite the rapid development of inflammasome research towards chronic inflammatory diseases such as AMD, the biological significance of inflammasome activation in the outer retina remains controversial. One of the inflammasome activation mature products, IL-18, is hypothesized to carry out dual functions in different target cell types: as a destructive factor in GA[36] and as a protective, antiangiogenic factor in CNV.[43] Of note, the generalized

NLRP3 inflammasome activation process summarized above is clearly an oversimplification of the intricate process that occurs *in vivo*, but nevertheless provides the foundation for studies of the role of the inflammasome in disease processes.

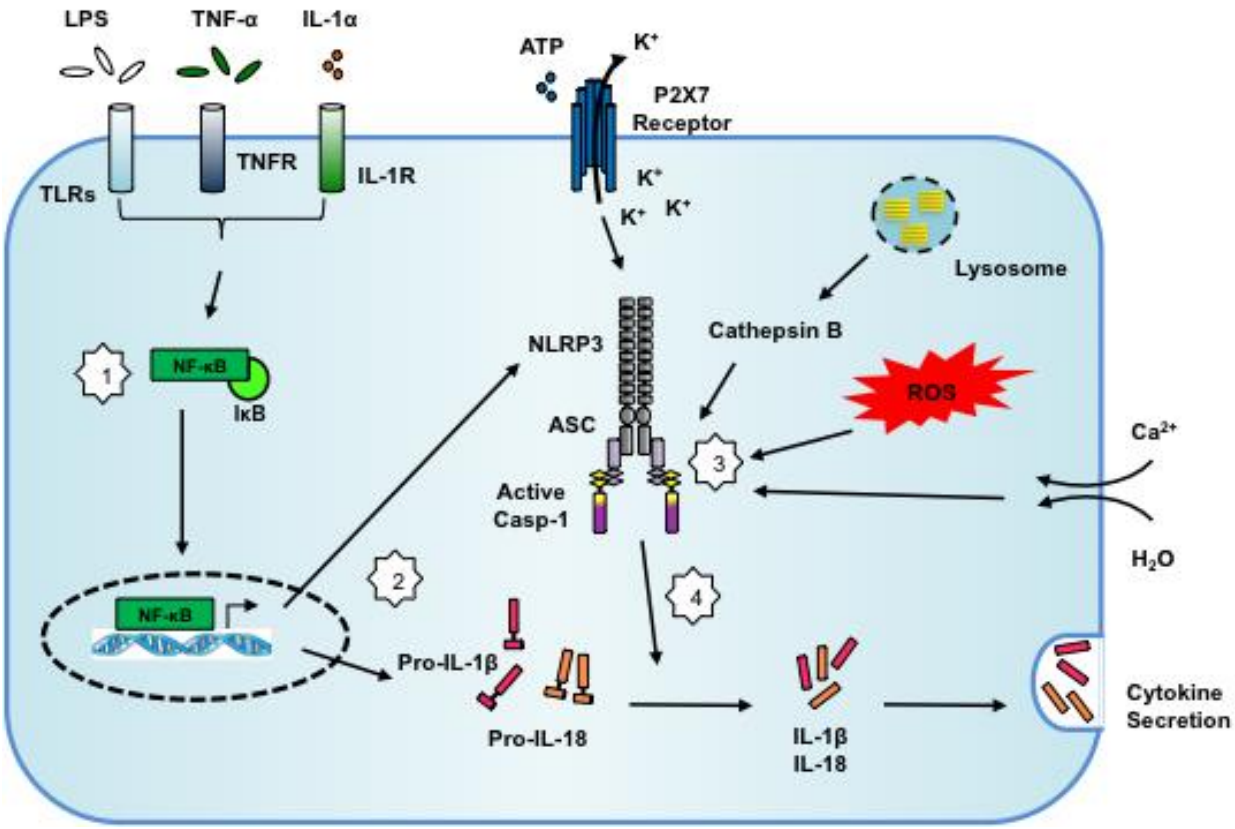

Figure 1-3 Generalized model of NLRP3 inflammasome activation.

(1) Priming of the cells by LPS, TNF-α, or IL-1α is required for activation of the NF-κB pathway. (2) Once the NF-κB pathway is active, it promotes the transcription of NLRP3 and pro-IL-1β. (3) Separate inflammasome components are assembled as a multi-protein complex triggered by one of the following mechanisms: K^+ efflux via P2X7 receptor activation in response to extracellular ATP accumulation; cytoplasmic cathepsin B released from the destabilized lysosomes; reactive oxygen species (ROS) overproduction; cell swollen and Ca^{2+} disequilibrium. (4) Successful assembly of NLRP3 inflammasome triggers autoproteolysis of pro-caspase-1 into active caspase-1, which further oligomerizes to convert pro-IL-1β and pro-IL-18 into bioactive peptides for secretion.

1.1.6 Complement factors and their associations with NLRP3 inflammasome

As part of the innate immunity, the complement system is one of the first defenders that responds to tissue damage during aging and is activated by cell death.[44] In this regard, stressed, damaged, or dying RPE could trigger local complement activation, which is supported by the fact that activated complement components as well as complement regulators are present in drusen.[45] The degree of complement activation is precisely regulated in healthy retina and is thus beneficial for tissue homeostasis and longevity. However, when the complement system is overactive due to either genetic polymorphism[45] or chronic, sustained pathological stimulation, it generates elevated levels of activated complement factors, facilitating the formation of terminal membrane attack complex (MAC), and thus advances AMD pathology[46]. Consistent with this model, Doyle and colleagues have shown that drusen extracts isolated from AMD donor eye tissues are able to activate the NLRP3 inflammasome in LPS-primed macrophages.[43] They further revealed the role of complement factor 1q (C1q) as an NLRP3 inflammasome "activation signal" by showing caspase-1 cleavage and elevated IL-1β secretion after C1q stimulation on LPS-primed mouse bone marrow derived macrophages and THP1 human monocytic cells. Moreover, in addition to C1q stimulation, other studies have suggested complement factor 3a (C3a) and MAC may also mediate the activation of the inflammasome, further linking many components of the complement pathway with IL-1β and IL-18 production[47-49] by unique underlying mechanisms. For instance, sublytic MAC is known to activate NLRP3 inflammasome through Ca^{2+} influx and/or K^{+} efflux, whereas C3a activation of the NLRP3 inflammasome is initiated by the release of ATP into the extracellular space. These studies were primarily conducted on monocytes, dendritic cells, or lung epithelial cells. Although the aforementioned mechanisms are yet to be

confirmed in AMD models, they do lend to the biological plausibility that similar processes can happen in ocular tissue.

1.1.7 Amyloid beta

Amyloid-beta (Aβ) is a drusen component found in AMD eyes;[50-52] more recently, there is growing interest in Aβ for its capacity to stimulate inflammasome activation and potentially contribute to AMD pathogenesis. As a pathological peptide best known for its neurotoxicity in Alzheimer's disease (AD), Aβ is generated through the amyloidogenic pathway by cleaving the amyloid precursor protein (APP) into the intramembrane Aβ domain of 36-43 amino acids in length.[53] The accumulation of Aβ in tissue results from its disturbed balance between production and clearance, the latter of which is largely controlled by the membrane-bound degradation enzyme, neprilysin.[54, 55] Aβ's intrinsic cytotoxicity lies in its aggregated forms as soluble oligomers or insoluble fibrils. Originally considered a primary toxic structure, Aβ fibrillar plaques are now believed to be less harmful to brain neurons than the small spherical oligomers that damage cell membranes and cause cell death.[53, 56-60] Aβ's ocular presence has been reported in studies of postmortem human donor eyes[52, 61] showing specific deposition within drusen from AMD eyes.[62] The age-dependent deposition of Aβ in the outer retina[51, 63] can be, at least partially, attributed to local RPE synthesis[50]. In this regard, transgenic animals lacking neprilysin exhibited Aβ accumulation in both RPE and sub-RPE deposits, concomitant with significant RPE atrophy.[64] When incubated with Aβ oligomers, human primary RPE cells demonstrated a prominent decrease in cell viability.[65] These findings point towards Aβ's potential role in promoting RPE atrophy. Nevertheless, the exact mechanism by which Aβ contributes to RPE atrophy is still poorly understood but may involve inflammasome-related caspase-1 dependent

cell death. In addition to its cytotoxicity, Aβ is also a major pro-inflammatory factor that has been extensively studied in the context of AMD. The presence of Aβ in drusen is found to overlap with complement activation sites.[50, 66] In an RPE cell culture model, Kurji et al. discovered that inflammation associated genes and immune response pathways were the predominant responses of RPE to oligomeric Aβ stimulation.[65]

1.1.8 Cell death pathways involved in AMD

A salient factor in the development and homeostasis of all organs and tissues is the balance between cell death and cell survival. The maintenance of tissues throughout an organism's lifetime necessitates the recognition and removal of unwanted danger signals (e.g. DAMPs) and clearance of dying cells. An important example is seen in the retina, specifically the RPE, which is very susceptible to molecular and cellular dysregulation during the aging process, just like other long-lived post-mitotic cells.[67, 68] There are three distinct cell death pathways currently proposed to contribute to AMD pathology, necrosis, apoptosis, and pyroptosis.[36, 69, 70] It is well accepted that as AMD progresses, RPE cells follow a common fate: (1) accumulation of lipofuscin; (2) enlarged cell body; (3) decrease in phagocytosis capacity; (4) formation of drusen; (5) morphological rounding; (6) hyperpigmentation; (7) hypopigmentation; (8) RPE loss.[71] In sections of human postmortem donor eyes diagnosed with GA, Sarks et al. identified double-layered hyperpigmented RPE in the GA lesion, characteristic of necrosis,[69] which was further supported by the discovery that RPE cells adjacent to excessive drusen accumulation die of necrosis.[72] Consistent with this description is the finding that necrosis, particularly the released ATP, is a trigger for NLRP3 inflammasome activation.[73] The potential involvement of an apoptotic mechanism is also supported by several studies[36, 74] discussed earlier in this chapter

and by a recent transcriptome analysis on AMD eyes.[75] However, insufficient knowledge of definitive pyroptosis markers makes it even more challenging to determine the exact role that pyroptosis may play in RPE atrophy in the late stage of dry AMD, including GA. Further studies are needed to understand, more fully, the combination of cell death mechanisms in RPE associated with dry AMD and GA.

1.1.9 X-chromosome linked inhibitor of apoptosis (XIAP)

XIAP is a well-studied neuroprotective protein in many retinal degeneration models [76-79]. Its anti-apoptotic potency lies in its abilities to directly inhibit caspase (-3, -7, -9), degrade pro-apoptotic factors and activate pro-survival signals. Recently, it has been shown that XIAP suppresses apoptosis in the immortalized RPE cell line, ARPE-19, which undergoes oxidative stress by hydrogen peroxide.[80] More intriguing is the idea that XIAP may be involved in the inflammasome activation, a model bolstered by several recent studies using non-ocular cell types. Macrophages from XIAP knockout mice exhibit enhanced caspase-1 cleavage and IL-1β secretion when compared to wild type cells under inflammasome activation. Pharmaceutical suppression of XIAP by Smac-mimetic compounds leads to an increased secretion of IL-1β.[81] Knocking out NLRP3 in dendritic cells promotes XIAP expression, suggesting a potential negative regulation.[82] And, most interestingly, in rat spinal cord neurons, there is evidence that XIAP constitutively binds to the inactive inflammasome complex, while in response to spinal cord injury, the inflammasome becomes activated and XIAP is degraded.[83]

1.2 Objectives and hypotheses

The overarching goal of this dissertation is to elucidate the molecular and cellular mechanisms underlying RPE atrophy in GA. Literature suggests the inflammasome cascade is involved in the RPE cell death, but the exact triggers remain unidentified. Given that aging and drusen components are both strong risk factors for AMD, my aim was to focus on the interactions among aging, drusen components and inflammasome activity, and the factor(s) associated with their regulation. ***We hypothesize that age-dependent accumulation of drusen components, in particular MAC and Aβ, leads to inflammasome hyperactivity, XIAP downregulation and subsequent RPE cell death.*** This hypothesis was addressed in the following four Aims.

1.2.1 Aim 1: evaluate the role of aging on the accumulation of MAC, Aβ, and inflammasome activity

This *in vivo* study provided insights on MAC's role in the inflammasome pathway and assessed the merit of using anti-MAC inhibitor as a treatment strategy to regulate inflammasome activity (see Chapter 2).

1.2.2 Aim 2: investigate the role of Aβ in the induction of inflammasome activation

This *in vivo* study presented the first experimental evidence to demonstrate Aβ's capacity to trigger inflammasome activation in RPE tissues and the associated signaling pathways (see Chapters 3 and 4).

1.2.3 Aim 3: delineate the cell death pathway(s) triggered by Aβ in RPE

Knowledge from this *in vivo* study sheds light on the complex regulatory networks involved in RPE cell death in response to chronic Aβ exposure (see Chapter 5).

1.2.4 Aim 4: understand the role of XIAP in inflammasome activation

This *in vitro* study unveiled the novel regulatory role of XIAP in RPE inflammation and in potential therapies for AMD (see Chapter 6).

Chapter 2: Age-related increases in amyloid beta and membrane attack complex: evidence of inflammasome activation in the rodent eye

2.1 Introduction

Advanced chronological age is an important risk factor for AMD. Key to understanding the effects of aging on the pathogenesis of retinal degenerative diseases are the cellular pathways that become dysregulated with age.[84-86] For example, aging is associated with the dysregulation in the complement cascade, part of the innate immune response. The complement cascade causes opsonization and agglutination, as well as cell lysis by the MAC formation.[87] Genetic studies showed that certain variants of the complement factor H (CFH) gene, an inhibitor of the alternative pathway, can increase the risk of AMD by up to six-fold in patients with the at-risk variant.[45] Postmortem eyes genotyped for CFH Y402H (T->C conversion resulting in a tyrosine->histidine switch, rs1061170) at-risk variants have increased MAC levels in the RPE-choroid.[88, 89] Moreover, in dry AMD patients, those with a CFH Y402H at-risk variant have elevated systemic levels of IL-6, TNF-α, and IL-18.[90] In addition to genetic influences, aging also contributes to the dysregulation of the complement system, as evidenced by the association of activated complement products and increased MAC deposition in the RPE-choroid with advanced age.[91-94]

While MAC deposition may cause cell lysis, it may also occur at sublytic levels that promote chronic, low-grade pro-inflammation.[95, 96] This type of chronic, local inflammation in the outer retina has been hypothesized to lead to degenerative changes in RPE function.[97] Recent studies

have suggested that MAC may mediate activation of the NLRP3 inflammasome.[48, 49] Whether MAC promotes inflammasome activation in the RPE-choroid is not known and is the premise of this chapter. We postulate that sublytic MAC increases with age, promotes activation of the inflammasome, and thereby, dysregulates RPE function. To ameliorate MAC-induced inflammasome activation on RPE, we also explore the effects of an agent, aurin tricarboxylic acid complex (ATAC), which has been shown to inhibit MAC formation in mice and humans. Specifically, ATAC acts both to inhibit the formation of the C3 convertase and to block the addition of C9 to the C5b-8 complex and thereby inhibits MAC.[98, 99] Here, we examine the age-related increase in MAC, the efficacy of ATAC in lowering levels of sublytic MAC, and a subsequent, corresponding reduction in inflammasome activation in the rat RPE-choroid.

2.2 Methods

2.2.1 *In vivo* studies

The animal procedures were approved by the Animal Care Committee of the University of British Columbia, conformed to the guidelines of the Canadian Council on Animal Care and were in accordance with the Resolution on the Use of Animals in Research of the Association of Research in Vision and Ophthalmology. Adult Long-Evans rats (Charles River, Wilmington MA) were divided into four groups. Group 1 (N = 6) comprised 6-month-old rats treated with oral administration of ATAC for 40 days and sacrificed at the age of 7.5 months. A dosage of 60 mg / 100 mL (in drinking-water) was chosen based on efficacy observed in an earlier study.[98] Group 2 (N = 6) comprised untreated 6-month-old rats (controls) sacrificed at the age of 7.5 months. Group 3 (N = 6) comprised 10-month-old rats treated with ATAC in drinking water (60

mg / 100 mL) for 40 days and sacrificed at the age of 11.5 months. Group 4 (N = 6) comprised untreated 10-month-old rats (controls) sacrificed at 11.5 months. Additional untreated naive animals were sacrificed at 2.5, 6, 7.5, or 11.5 months, and retinal tissues were used to demonstrate age-related changes in MAC, Aβ, and NF-κB activation. At the study endpoints, animals were anesthetized, whole blood drawn for serum analysis, and then euthanized. Eyes were immediately enucleated and frozen (western blot and enzyme-linked immunosorbent assay, i.e. ELISA) or fixed in 4 % paraformaldehyde in Dulbecco's phosphate-buffered saline (DPBS, Invitrogen, Carlsbad CA) for 48-72 h prior to embedding in paraffin.

2.2.2 Quantification of ATAC and CH50 assay

ATAC synthesis and its serum concentration analysis followed published methods.[98, 99] The final ATAC concentration was expressed in μg per 500 μL of blood (N = 6). A CH50 hemolysis assay was used to assess complement activation in rat serum before and after ATAC administration, following published procedures.[98]

2.2.3 Immunohistochemistry (MAC, IL-18, Aβ, and NF-κB)

Paraffin-embedded eye tissues were prepared and sectioned following established protocols.[100] Sections from the paired groups (7.5 m ATAC and No ATAC; 11.5 m ATAC and No ATAC) and the three age groups (2.5, 7.5, and 11.5 m) were processed simultaneously in order to make intensity comparisons. Primary antibodies targeting MAC, IL-18, and Aβ are described in Table 2-1. For the negative control sections, the primary antibody was replaced with a matched non-specific isotype IgG (Sigma Aldrich). For visualization, the slides were developed using either

the Vector® VIP peroxidase substrate kit or Vector® AEC peroxidase substrate kit (Vector Laboratories, Burlingame CA).

Two independent scorers graded MAC, Aβ, and IL-18 immunoreactivity semi-quantitatively in a masked fashion based on a 0-3 point scale. A score of 0 indicates no detectable immunoreactivity above background as compared to the negative controls. The slides with the strongest immunoreactivity were given a score of 3 and samples with the weakest or intermediate levels of immunoreactivity were given a score of 1 or 2, respectively.[101] Analysis and micrographs were taken using a ×60 objective lens and ×10 eyepieces (N = 3). The immunoreactivity scores of MAC, Aβ, and IL-18 were averaged and normalized to the 7.5-month-old group or the untreated control group (No ATAC).

To detect the active NF-κB, an antibody against the NF-κB p65 subunit was used (Table 2-1). Immunoreactivity was scored quantitatively, in a masked fashion, using a ×60 objective lens and ×10 eyepieces (N = 3). Positive RPE nuclei were identified as containing both the red (AEC) chromogen and blue hematoxylin counterstain, thus resulting in a purple appearance distinct from the unlabeled RPE nuclei that were blue in color from only the hematoxylin counterstain. The number of NF-κB positive nuclei was converted to percentage of all RPE nuclei in the sample area, and normalized to the untreated control group (No ATAC) or the 7.5-month-old group.

2.2.4 Western blot

RPE/Bruch's membrane (BM)/choroid tissues were isolated and pooled for animals in each of the four treatment groups (groups 1-4, N = 6) and in each age group of the naive animals (2.5, 7.5, and 11.5 months; N ≥ 3). To detect the MAC deposits, the tissue samples were homogenized in 200 μL of ice-cold MAC extraction buffer (50 mM Tris-HCl, pH 6.8; 150 mM NaCl; 0.1% SDS) containing protease inhibitor cocktail (Roche Diagnostics, Indianapolis IN). To preserve the MAC protein complex, 40 μg of total protein was mixed with equal volume of 2× non-reducing loading buffer, devoid of boiling, and directly subjected to 5-10% SDS-PAGE. Proteins were transferred to a PVDF membrane and incubated with a series of blocking buffers, primary antibody against MAC (Table 2-1), and HRP conjugated secondary antibody (R&D Systems, Minneapolis, MN). The enhanced chemiluminescence (ECL) method was used to detect the MAC protein bands from animal groups 1-4 and the naive animals at three different ages. The glyceraldehyde 3-phosphate dehydrogenase (GAPDH)-loading control blot was done similarly using a mouse GAPDH antibody (Table 2-1). All protein bands were subsequently quantified using Image J (NIH, Bethesda MD), and the ratio of MAC-to-GAPDH was calculated. The final relative intensity of MAC was normalized either to the youngest age group of 2.5 months or to the No ATAC control group.

To detect caspase-1 cleavage and NF-κB activation, the RPE/BM/choroid tissues were homogenized in 200 μL of ice-cold RIPA buffer (Thermo Scientific, Waltham, MA) containing protease inhibitor cocktail (Roche Diagnostics). Blotting procedures followed our established protocol.[102] For GAPDH, the same membrane was incubated in stripping buffer and then re-probed with the GAPDH antibody (Table 2-1). The protein band intensity of cleaved caspase-1

(20kD), phosphorylated NF-κB p65 subunit (65 KDa), phosphorylated NF-κB p50 subunit (50 KDa), and GAPDH (36kD) was individually measured using Image J and converted into ratios relative to GAPDH. The final relative intensity of cleaved caspase-1 p20 and phosphorylated NF-κB p65 was normalized to the No ATAC control group.

For western blot detection of Aβ, both fibrillar $A\beta_{1-40}$ preparation and the RIPA buffer-extracted RPE/BM/choroid tissue lysates were mixed with 2× non-reducing loading buffer, devoid of boiling, and directly subjected to 5-12% SDS-free PAGE separation. Electrophoresis was run using MES buffer (Invitrogen, pH 7.3 ~ 7.7), and proteins were transferred onto a 0.2 μm PVDF membrane. The anti-Aβ 6E10 antibody was used to detect the fibrillar $A\beta_{1-40}$ preparation, whereas the anti-Aβ 4G8 antibody was used for tissue lysates (Table 2-1). Aβ bands were developed by the ECL method. For the membrane containing tissue lysate proteins, it was stripped and re-processed for GAPDH detection. The intensity of high-molecular species Aβ (MW > 95 kDa) and GAPDH (36kD) was independently measured using Image J and converted into ratios of Aβ-to-GAPDH. The final relative intensity ratio of Aβ-to-GAPDH was normalized to the youngest age group of 2.5 month.

Antigen	Antibody	Dilution	Source	Applications
Membrane attack complex (MAC)	Mouse monoclonal (clone aE11)	1:1000 (WB)	Dako, Burlington, ON, Canada	Western blot
Membrane attack complex (MAC)	Rabbit polyclonal	1:500	BIoss, Woburn, MA	Immunohistochemistry
Interleukin-18 (IL-18)	Rabbit polyclonal	1:100	Santa Cruz Biotechnology, Dallas, TX	Immunohistochemistry
Amyloid-beta amino acid 17-24 ($A\beta_{17-24}$)	Mouse monoclonal anti-$A\beta_{17-24}$ (clone 4G8)	1:400 (IHC) 1:1000 (WB)	BioLegend, Dedham, MA	Immunohistochemistry Western blot
Phosphorylated NF-κB p65 (Ser 276)	Rabbit polyclonal	1:75 (IHC) 1:500 (WB)	Santa Cruz Biotechnology, Dallas, TX	Immunohistochemistry Western blot
Phosphorylated NF-κB p50 (Ser 337)	Rabbit polyclonal	1:500 (WB)	Santa Cruz Biotechnology, Dallas, TX	Western blot
Caspase-1	Mouse monoclonal	1:1000	R&D Systems, Minneapolis, MN	Western blot
Amyloid-beta amino acid 1-16 ($A\beta_{1-16}$)	Mouse monoclonal anti-$A\beta_{1-16}$ (clone 6E10)	1:2000	BioLegend, Dedham, MA	Western blot
GAPDH	Mouse monoclonal	1:10,000	EMD Millipore, Billerica, MA	Western blot

Table 2-1 List of primary antibodies used in Chapter 2

2.2.5 ELISA for Aβ

A chemiluminescent ELISA assay specific for the detection of Aβ x-40 isoform was used to quantify Aβ in the vitreous of rat eyes (BioLegend, Dedham, MA). 6-month-old (N = 4) and 11.5-month-old (N = 6) rats were sacrificed for vitreous collection. Vitreous samples were diluted with the HRP detection antibody at a ratio of 1:1. After 18 h of detection antibody incubation at 4 °C, the ELISA plate was then incubated with chemiluminescent substrates for 15s and imaged with a microplate reader (Synergy H1, BioTek, Winooski, VT). A non-linear 4-parameter regression model was used to generate the standard curve to calculate Aβ concentrations of all vitreous samples (Gen5 version 2.04.11, BioTek).

2.2.6 Suspension array for IL-1β and IL-18

An ELISA-based cytokine assay for the mature, secreted products of the inflammasome, IL-1β and IL-18, was carried out (Bio-Plex 200 System, Bio-Rad Laboratories, Hercules CA). Vitreous from rat eyes in groups 3-4 were pooled. Experiments were carried out following methods in our earlier publication.[102]

2.2.7 Statistical analyses

Non-parametric tests were used throughout the study. For the two group comparisons (Figures 2-1C-F, 2-2A, C, E, 2-3A-C, and 2-4A, B, E-G), a Mann-Whitney U test (one-tailed) was used. For the three group comparisons, a Kruskal-Wallis and post hoc Dunn's multiple comparisons test was used to determine differences among age groups (Figures 2-1A, B). All analyses were

conducted with GraphPad Prism version 6 (GraphPad Software, La Jolla, CA). Statistical significance was set at $p \leq 0.05$.

2.3 Results

2.3.1 Age-dependent increases of MAC, Aβ, and NF-κB in the RPE-choroid

In this chapter, the first question we asked is whether MAC deposits increase with normal aging and, if so, whether it is related to inflammasome activation in the RPE-choroid. A significant increase in MAC (MW > 580 kDa) was evident in the RPE-choroid homogenates of rats ranging in age from 2.5 to 11.5 months using western blot. The normalized MAC levels were 1.88-fold higher at 7.5 months and 2.75-fold higher at 11.5 months when compared to the samples obtained from 2.5-month-old rats (Figure 2-1A).

Aβ is a known pathological activator of complement cascade in AD.[103] Its ocular presence has been reported in drusen of postmortem eyes[52] and in rodent eyes.[63] To correlate Aβ accumulation with MAC formation, we semi-quantitatively compared the levels of high-molecular weight Aβ species (MW > 95 kDa) among the RPE-choroid homogenates from different ages. We found an age-dependent increase of high-molecular weight Aβ from 2.5 to 11.5 months (Figure 2-1B). Based on the knowledge that biosynthesized Aβ is present in both retina and the vitreous compartment of the eye,[104] we quantified the Aβ in rat vitreous samples at two ages. With increasing age, the vitreal Aβ concentration increased, by almost 80-fold, from 7.49 ± 5.16 pg/mL at 6 months to 599.10 ± 159.25 pg/mL at 11.5 months of age (Figure 2-1C).

To support these results, we also assessed MAC formation and Aβ accumulation in retinal cross sections by immunohistochemistry. We demonstrated that there are increasingly higher levels of immunoreactivity of both MAC and Aβ in the 11.5-month animals compared to the 7.5-month-old animals, particularly in the choroid and the basal side of RPE (Figure 2-1D, E, G, H).

NF-κB is a major transcription factor that responds to a variety of pro-inflammatory signals by nuclear translocalization to upregulate the expression of target genes. In this dissertation, we demonstrated that Aβ activates NF-κB, which can be specifically inhibited by NF-κB antagonists (e.g., vinpocetine or BAY 11-7082) (see Chapter 4).[102] In the present study, by using an antibody targeting the phosphorylated p65 subunit of the translocated NF-κB, we observed an increase in the percentage of RPE nuclei harboring the phosphorylated p65 subunit, mirroring the age-related increase we observed with both MAC and Aβ (Figure 2-1F, I).

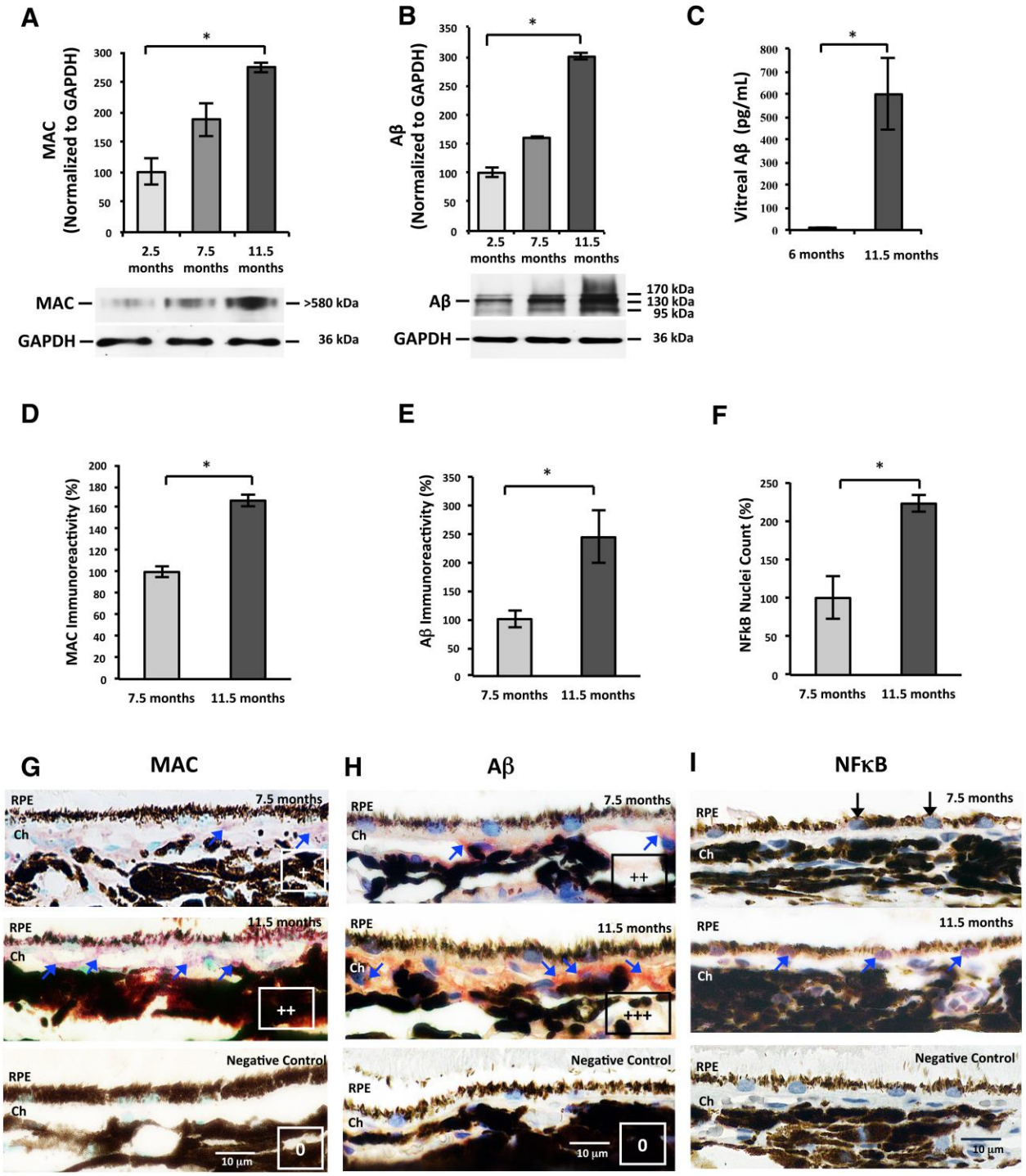

Figure 2-1 Age-dependent increases of ocular MAC, Aβ and NF-κB.

(A) Western blot analysis revealed increasing MAC levels in the rat RPE-choroid with age from 2.5 to 11.5 months old ($N \geq 3$, Kruskal-Wallis, $p \leq 0.05$). (B) Western blot analysis showed enhanced accumulation of high-molecular weight Aβ (MW > 95 kDa) in the rat RPE-choroid with age from 2.5 to 11.5 months old ($N \geq 3$, Kruskal-Wallis, $p \leq$

0.05). (C) ELISA measurements showed a dramatic increase in the soluble Aβ levels in the vitreous fluids of the 11.5 months old (599.1 pg/mL, N = 6) compared to the 6 months old group (7.5 pg/mL, N = 4) (Mann-Whitney, $p \leq 0.05$). (D-E) Analysis of MAC deposition (D) or Aβ (E) in rat RPE-choroid demonstrated a significant increase in immunoreactivity with increasing age, with data normalized to the younger age group of 7.5 months (N = 3, Mann-Whitney, $p \leq 0.05$). (F) NF-κB activation in RPE increased with age. The percentage of RPE cells with nuclear labeling of translocated NF-κB p65 subunit was higher in the retina of the 11.5 months old group compared to the 7.5 months old group (N = 3, Mann-Whitney, $p \leq 0.05$). (G) Representative micrographs of MAC immunoreactivity at both ages (7.5 and 11.5 months) showed MAC deposition on the basal side of RPE and in choroid. Immunoreactivity was processed with VIP, resulting in a purple color (blue arrows) and nuclei counterstained with Methyl Green. Background immunoreactivity (0) and semi-quantitative scoring of + and ++ are given for the following examples: 7.5 months old (+), 11.5 months old (++), and negative control (0). Note the dark brown choroidal melanocytes in the 11.5 months picture appeared surrounded by red haze due to bright field illumination. (H) Representative micrographs of Aβ immunoreactivity at both ages (7.5 and 11.5 months) showed positive immunolabeling on the basal side of RPE and in choroid. Immunoreactivity was processed with AEC, resulting in a red color (blue arrows) and nuclei counterstained as blue. Examples of semi-quantitative scores are given as follows: 7.5 months old (++), 11.5 months old (+++), and negative control (0). (I) Representative micrographs of the RPE nuclei from the 11.5 months old group showed more robust NF-κB p65 immunoreactivity than the 7.5 months old group. Positive NF-κB p65 immunolabeling is purple in RPE nuclei and indicated by blue arrows. RPE nuclei devoid of NF-κB p65 are blue and indicated by black arrows. Scale bars; 10 μm. RPE, retinal pigment epithelium; Ch, choroid.

2.3.2 ATAC did not affect local NF-κB activation in RPE

While ATAC inhibits complement cascade, it is unclear whether systemic administration of ATAC would reduce local inflammation in the eye. To test this, animals were treated with oral administration of ATAC in drinking water (60 mg / 100 mL) for 40 days. Animals readily

accepted drinking water laced with ATAC *ad libitum*, and no overt signs of side effects or toxicity were noted, consistent with our earlier studies in which ATAC was given in food.[98]

After 40 days, the average ATAC level, as measured by fluorescence spectroscopy, was 1.98 and 3.5 μg / 500 μL in the 7.5 and 11.5-month-old ATAC-treated rats, respectively. As expected, no appreciable amount of ATAC was evident in control rats at either age group (Figure 2-2A). A CH50 assay, which measures the amount of hemolysis in blood due to complement activation, has been used before as a surrogate marker for complement activity both clinically and in experimental studies.[98, 105] Our results showed that sera from the ATAC-treated animals displayed a significant three- to four-fold decrease in hemolysis relative to the sera of the control animals in both age groups studied, thus confirming that orally administered ATAC was present and effective at inhibiting complement activation in the sera of treated rats (Figure 2-2B). Next, we assessed the nuclear translocation of the p65 subunit in RPE after ATAC treatment. Intriguingly, systemic administration of ATAC did not change NF-κB p65 nuclear translocation when compared to control animals at 7.5 or 11.5 months old (Figure 2-2C, D). Further western blot analyses of phosphorylated NF-κB p65 and p50 subunits in 11.5-month-old rats supported this, and no significant difference in normalized band intensity was found between animals receiving ATAC or drinking water (Figure 2-2E, F).

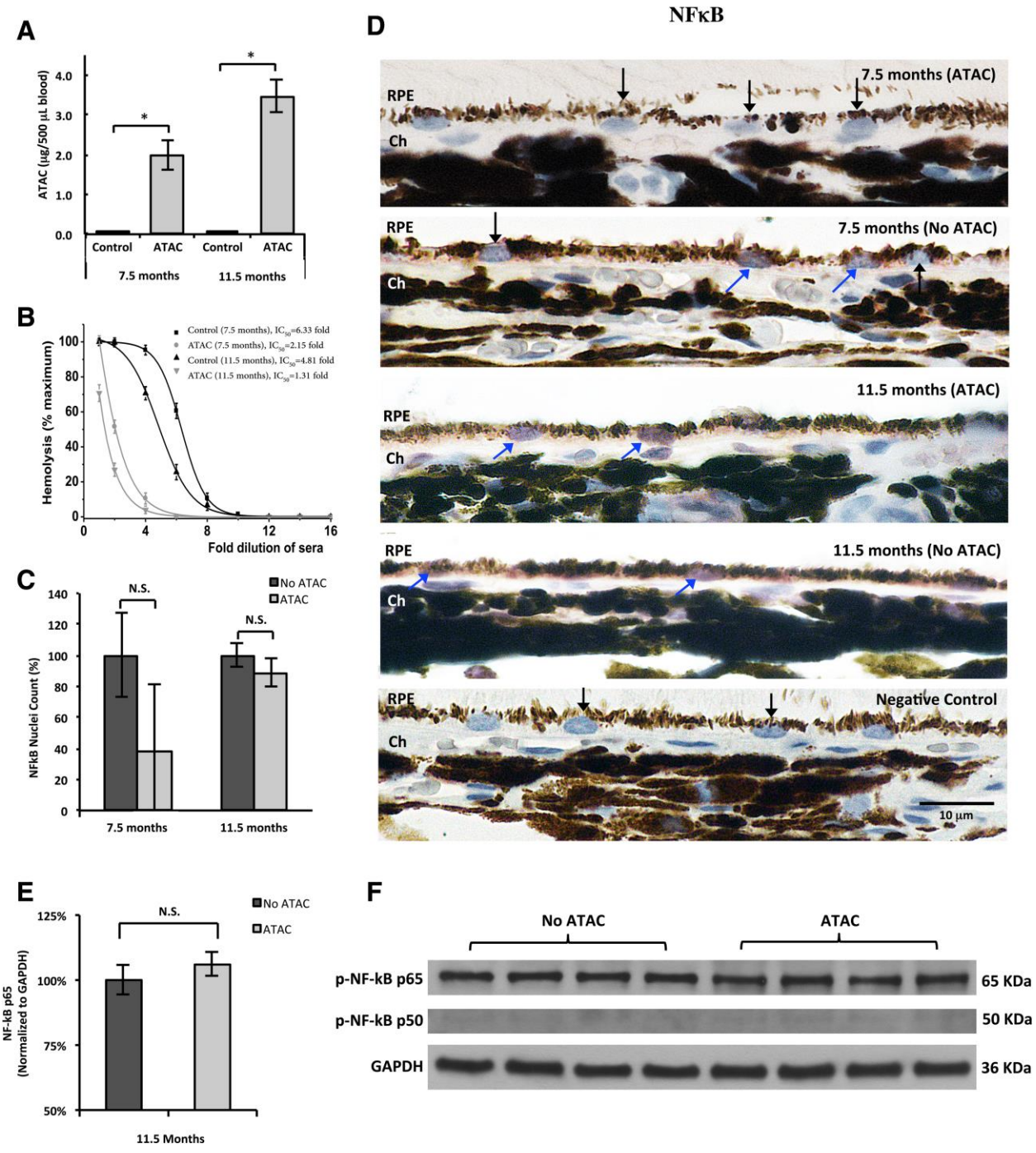

Figure 2-2 Systemic ATAC administration did not alter NF-κB activation in RPE.

(A) The amount of ATAC in blood was measured after 40 days of drug administration in 7.5-month-old (1.98 µg / 500 µL) and in 11.5-month-old (3.5 µg / 500 µL) animals. Animals treated with ATAC showed significantly higher ATAC blood concentrations than age-matched controls without ATAC treatment at both ages (N = 6, Mann-

Whitney, $p \leq 0.05$). (B) The degree of inhibition on total complement activation by ATAC was measured by a CH50 hemolysis assay. Dilutions of the sera containing different levels of ATAC were performed to calculate the half maximal inhibitory concentration (IC_{50}) for total complement activity. Higher IC_{50} values proportionally reflect higher levels of complement activity. Note that the IC_{50} levels are lower (i.e., curves shifted to the left) for ATAC-treated animals compared to untreated controls at both ages. (C) ATAC administration did not affect NF-κB activation in RPE at both ages of 7.5 and 11.5 months (N = 3, Mann-Whitney, $p > 0.05$). (D) Representative micrographs of NF-κB p65 immunoreactivity in RPE-choroid from each group in (C). RPE cells that demonstrate NF-κB p65 nuclear translocalization have purple nuclei and are marked by blue arrows. Unlabeled RPE nuclei are counterstained with hematoxylin (blue only) and are marked by black arrows. Scale bar; 10 μm. RPE, retinal pigment epithelium; Ch, choroid. (E, F) RPE-choroid tissue lysates from 11.5-month-old rats with ATAC administration contained the same amount of phosphorylated p65 subunit as in rats without ATAC in drinking water (N = 6, Mann-Whitney, $p > 0.05$). The level of phosphorylated p50, however, was extremely low in both groups.

2.3.3 ATAC reduced MAC deposition in the RPE-choroid

Our earlier studies showed that ATAC was effective at decreasing MAC in the central nervous system,[98, 99] and our next question was whether the observed systemic level of ATAC was sufficient to inhibit MAC formation locally in the eye. To answer this, ATAC-treated animals (7.5 and 11.5 months old) were sacrificed, and tissue lysate of RPE, choroid, and BM underwent western blot analysis. At both ages, animals treated with ATAC demonstrated less MAC deposits (MW > 580 kDa) in the RPE-choroid compared to non-ATAC-treated animals. Furthermore, ATAC treatment was more effective at suppressing MAC in the younger group (7.5 months old). This is intriguing, as the younger group demonstrated a lower ATAC concentration in sera (1.98 μg / 500 μL), but with a proportionally greater inhibition of MAC (50% inhibition) compared to the older group with 3.5 μg / 500 μL ATAC in sera, yet only 25% inhibition of MAC (Figure 2-2A and 2-3A, B). To better understand the distribution of MAC in the ocular compartments after

systemic ATAC, we assessed MAC in retinal cross sections by immunohistochemistry. MAC immunoreactivity was robust in the choroid and BM of non-ATAC-treated rats at both ages, and it was reduced by ATAC treatment at both ages (Figure 2-3C, D).

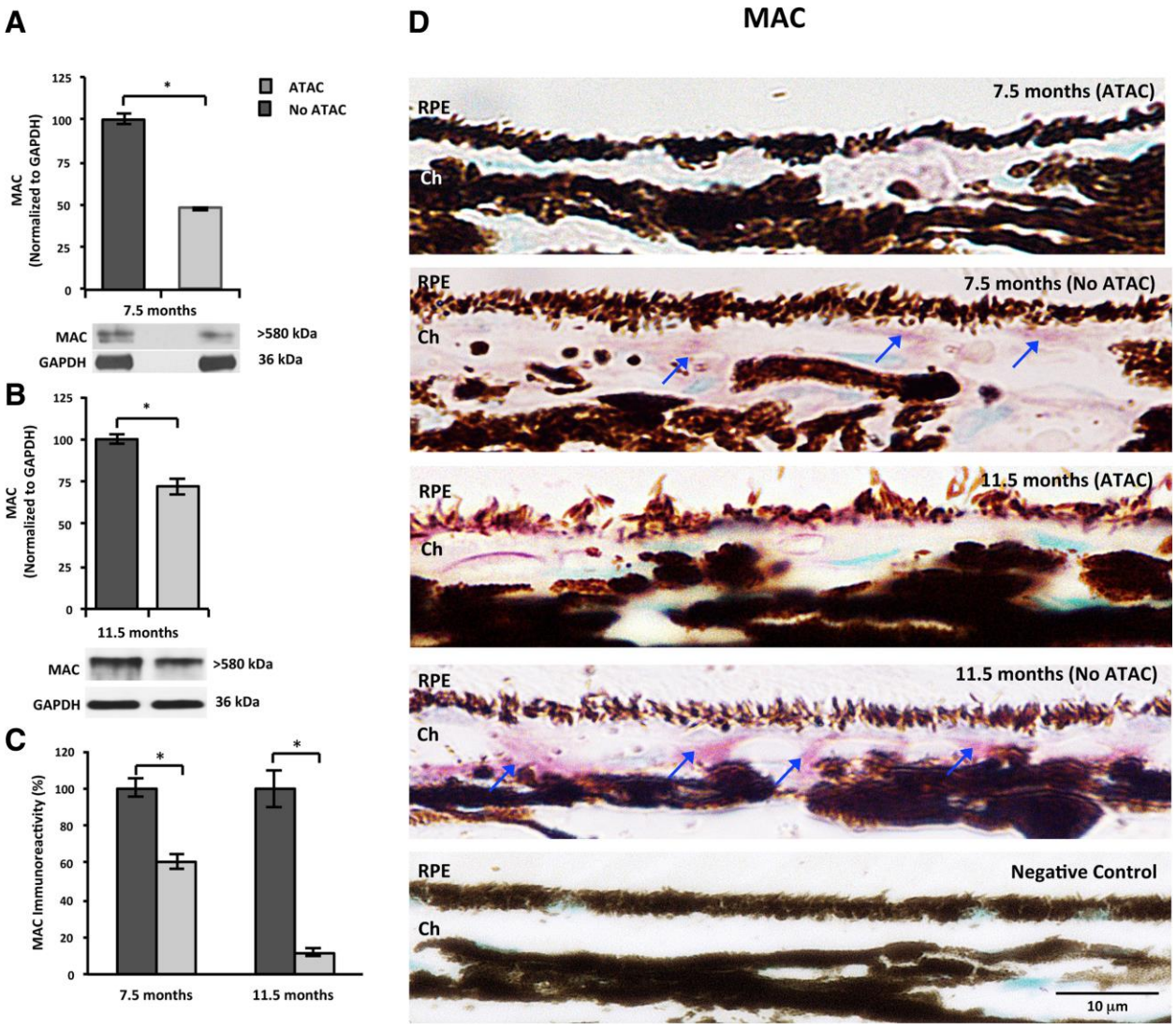

Figure 2-3 ATAC treatment suppresses MAC deposition in the RPE-choroid.

(A, B) At both ages of 7.5 months (A) and 11.5 months (B), western blot analysis showed that ATAC significantly reduced MAC deposits in rat RPE-choroid (N = 6, Mann-Whitney, $p \leq 0.05$). (C) At both ages, MAC immunoreactivity in the rat RPE-choroid was significantly lower in the ATAC-treated group compared to the age-

matched, No ATAC control group (N = 3, Mann-Whitney, $p \leq 0.05$). (D) Representative micrographs from each group in (c) showed MAC immunoreactivity on the basal side of RPE cells and in choroid. Blue arrows identify positive MAC deposits labeled with VIP chromogen (purple). Nuclei were counterstained as green. Scale bar; 10 μm. RPE, retinal pigment epithelium; Ch, choroid.

2.3.4 ATAC suppressed inflammasome activation in the RPE-choroid

Earlier studies in non-ocular systems suggest that MAC formation is a potential trigger for inflammasome activation.[48, 49] Here we used an inhibitor of MAC, ATAC, to suppress inflammasome activation in the RPE-choroid. To test whether MAC promotes inflammasome activation, we first examined the level of pro-caspase-1 (MW 45 kDa) cleavage in RPE-choroid homogenates using western blot. At both ages tested (7.5 and 11.5 months), ATAC successfully lowered cleaved caspase-1 (MW 20 kDa) by ~90 % (7.5 months old) and by ~50 % (11.5 months old), when compared to untreated controls (Figure 2-4A-C). Next, we assessed the levels of two mature products of inflammasome activation, IL-1β and IL-18. Compared to the ATAC group, we found that IL-18 immunoreactivity was higher in the untreated rat RPE-choroid. On closer visual examination, it was evident that the majority of the IL-18 immunolabeling was located to the basal side of RPE and at the RPE-choroid interface (Figure 2-4D, E). We next tested secreted levels of IL-1β and IL-18 in the vitreous by custom-made ELISA assays. Secreted levels of IL-1β and IL-18 were 3- and 2.5-fold lower in the vitreous of animals treated with ATAC, respectively, compared to the untreated age-matched controls (Figure 2-4F, G).

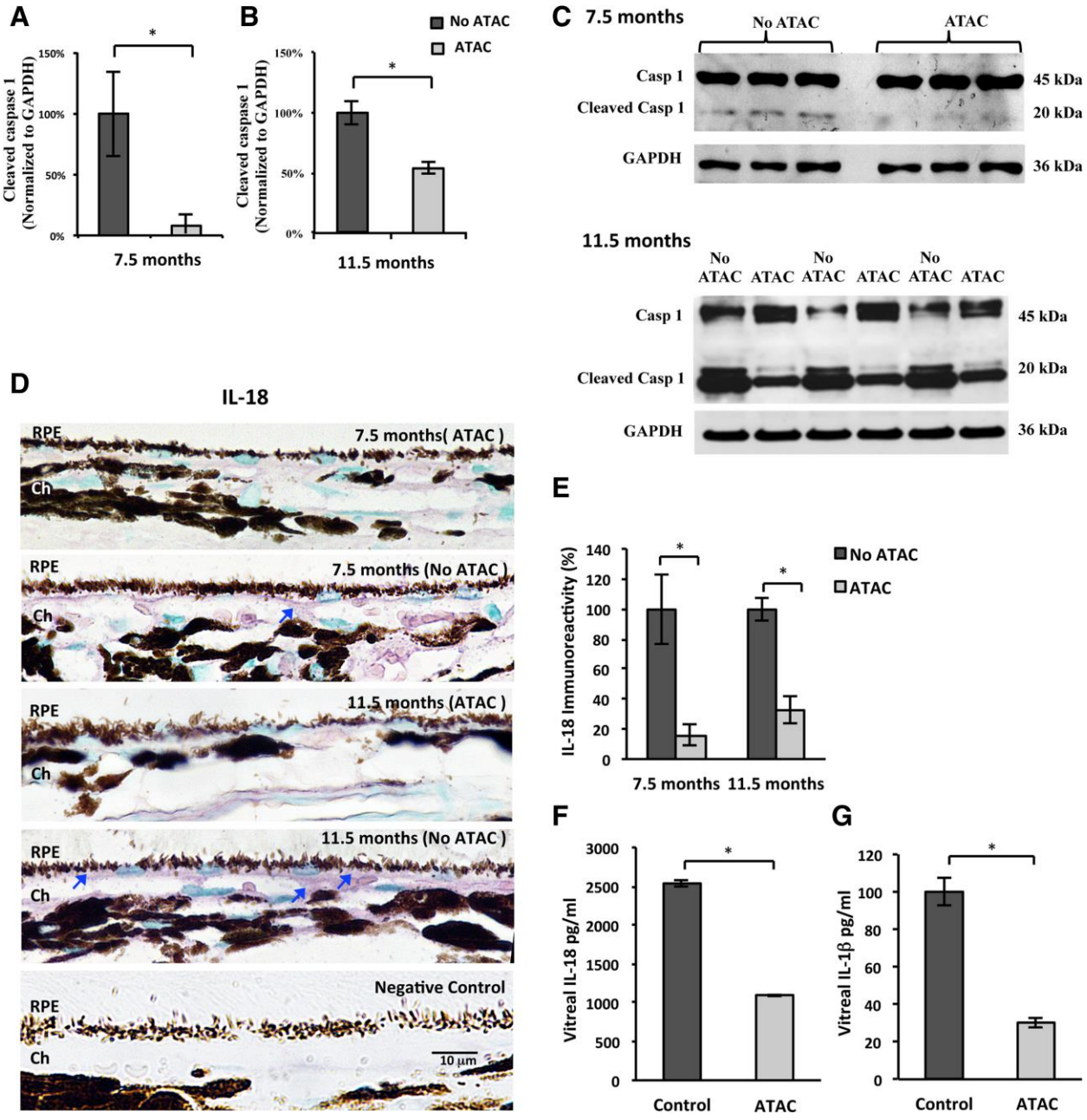

Figure 2-4 ATAC treatment inhibited inflammasome activation in the RPE-choroid.

(A-C) At both ages of 7.5 months (A) and 11.5 months (B), western blot analysis showed that ATAC significantly inhibited pro-caspase-1 (MW 45 kDa) cleavage into active caspase-1 (MW 20 kDa) in rat RPE-choroid (N = 6, Mann-Whitney, $p \leq 0.05$). Images of western blot demonstrate a concomitant increase in the pro-caspase-1 band and decrease in the active caspase-1 band after ATAC treatment in both age groups (C). (D) Representative micrographs

illustrate immunoreactivity for IL-18, a product of inflammasome activation, on the basal side of RPE cells and in choroid from treated and untreated animals at 7.5 and 11.5 months of age. Blue arrows indicate positive IL-18 labeling (VIP, purple). Scale bar; 10 μm. RPE, retinal pigment epithelium; Ch, choroid. (E) IL-18 immunoreactivity in the rat RPE-choroid was significantly downregulated by ATAC treatment. Labeling was normalized to 100% for the untreated animals in each age group (N = 3, Mann-Whitney, $p \leq 0.05$). (F, G) ELISA measurements of vitreous samples taken from treated and untreated control animals at 11.5 months of age. Note the dramatic reduction in secreted IL-18 (F) and IL-1β (G) concentrations after ATAC treatment (N = 6, Mann-Whitney, $p \leq 0.05$).

2.4 Discussion

With normal aging, the RPE-choroid complex undergoes many changes including drusen deposition, thickening of BM, and thinning of the choroid. The RPE also undergoes a number of age-associated changes, including loss of melanin granules, accumulation of lipofuscin, changes in pro-inflammatory cytokine secretion, and even cell death.[7, 106] However, the cellular mechanisms underlying these changes in the RPE-choroid remain largely unknown. Here, we provide a new perspective by investigating the relationship among aging, MAC formation, and inflammasome activation.

2.4.1 Aβ facilitates MAC formation and MAC-induced inflammasome activation in the RPE-choroid

In AD, Aβ is a known activator of the classic complement pathway.[107, 108] In the eye, it also co-localizes with complement factors in drusen, and demonstrates an age-associated increase.[50] We previously showed by pathway analysis (Ingenuity, GSEA) that the complement system is triggered by Aβ stimulation of RPE *in vitro*.[65] However, little has been done to assess the potential interaction between Aβ and the complement terminal product, MAC. Here we report

age-associated increases in MAC and Aβ in the RPE-choroid complex and soluble Aβ in the vitreous fluids (Figure 2-1). The observed age-associated MAC formation in rat RPE-choroid is consistent with our earlier findings of MAC deposition in BM and choroid of older postmortem human eyes.[91] MAC mediated inflammasome activation was shown previously in cells derived from bone marrow and lung epithelial cells *in vitro*.[48, 49] Our data support their findings and extend it to an ocular cell type, the RPE.

From our work, and those of others, it is plausible that the inhibition of MAC in the RPE-choroid will dampen inflammasome activation in RPE. We found that ATAC administration concomitantly prevented full-length caspase-1 from being cleaved into an enzymatically mature caspase-1 p20 subunit, the signature event of inflammasome activation in the same animals in which we observed a reduction in MAC levels (Figures 2-3 and 2-4). However, NF-κB activation, a primer for inflammasome activation, was not affected by ATAC treatment, demonstrated by statistically equivalent amounts of the phosphorylated p65 subunit in both retinal sections and RPE-choroid lysates (Figure 2-2). Intriguingly, the phosphorylated p50 subunit's level was extremely low in both ATAC and drinking-water-treated rats. Although the p50/p65 heterodimer is considered the primary form of NF-κB complex in a wide variety of cell types, there are other active NF-κB dimeric combinations that do not require either one or both of them.[109] All of these suggest that ATAC's inhibitory effects spare NF-κB activation that involves p65 or p50 and are specific for MAC. Hence, the significant reduction in inflammasome activation products, IL-18 and IL-1β, which we observed after ATAC treatment, is likely due to inefficient post-translational processing by mature caspase-1, rather than due to altered pro-IL-18 and pro-IL-1β production by NF-κB pathway (Figure 2-4). Whether and how the specific

inhibition of NF-κB pathway can in turn affect MAC formation remains elusive and is beyond the scope of this chapter. Although the literature suggests NF-κB signaling regulates multiple genes in the complement cascades, such as CFB, C3, and C4, our data indicates no effects on C5a production when NF-κB activation is blocked by vinpocetine *in vivo* (see Supplementary Figure 1), and thus, likely not affecting MAC formation as well.[102, 110-112]

2.4.2 Age-associated differences in MAC deposition and MAC inhibition by ATAC

Another interesting outcome of our study is the difference in ATAC efficacy in the two age groups tested. The younger rats had lower ATAC levels in blood (~2 μg / 500 μL) than the older rats (~3.5 μg / 500 μL) (Figure 2-2), yet there was a proportionally greater decrease in MAC, caspase-1 cleavage, and secreted IL-18 in the younger rats compared to the older group, suggesting that ATAC treatment was more efficacious in the younger group (Figures 2-3 and 2-4). The exact mechanism behind this finding is not clear. One possible explanation is that, with age, there is more Aβ accumulation in the rat eye, leading to more robust NF-κB activation (p65 nuclear translocalization) and more MAC deposition, which is not proportional to the increase in ATAC concentration, or its activity, and thus overwhelmed ATAC's suppressive effects leading to reduce efficacy in the older rats compared to that observed in younger rats (Figure 2-1).

2.5 Conclusion

In summary, we have shown an age-dependent increase in Aβ, MAC, and NF-κB in rat RPE-choroid. We have also demonstrated that Aβ, a drusen component, is an effective priming signal for NF-κB activation *in vitro* and *in vivo*[102] and promotes the NLRP3 inflammasome activation in the rat eye (see Chapter 3).[113] Suppression of MAC leads to a concomitant suppression of

NLRP3 inflammasome activation measured by caspase-1 cleavage and secretion of mature IL-18 and IL-1β as depicted in the schematic summary (Figure 2-5). An inherent limitation of this study is that rodents do not have a macula/fovea, and thus renders this animal model less useful as it does not reproduce "macular" disease. However, this model is useful to understand the basic, cellular changes in the retina that are associated with chronic inflammation, aging, and age-related retinal diseases. Our work from this chapter suggests that MAC-induced NLRP3 inflammasome activation may be an important cause of the chronic pro-inflammatory environment in the outer retina of a normal aging eye.

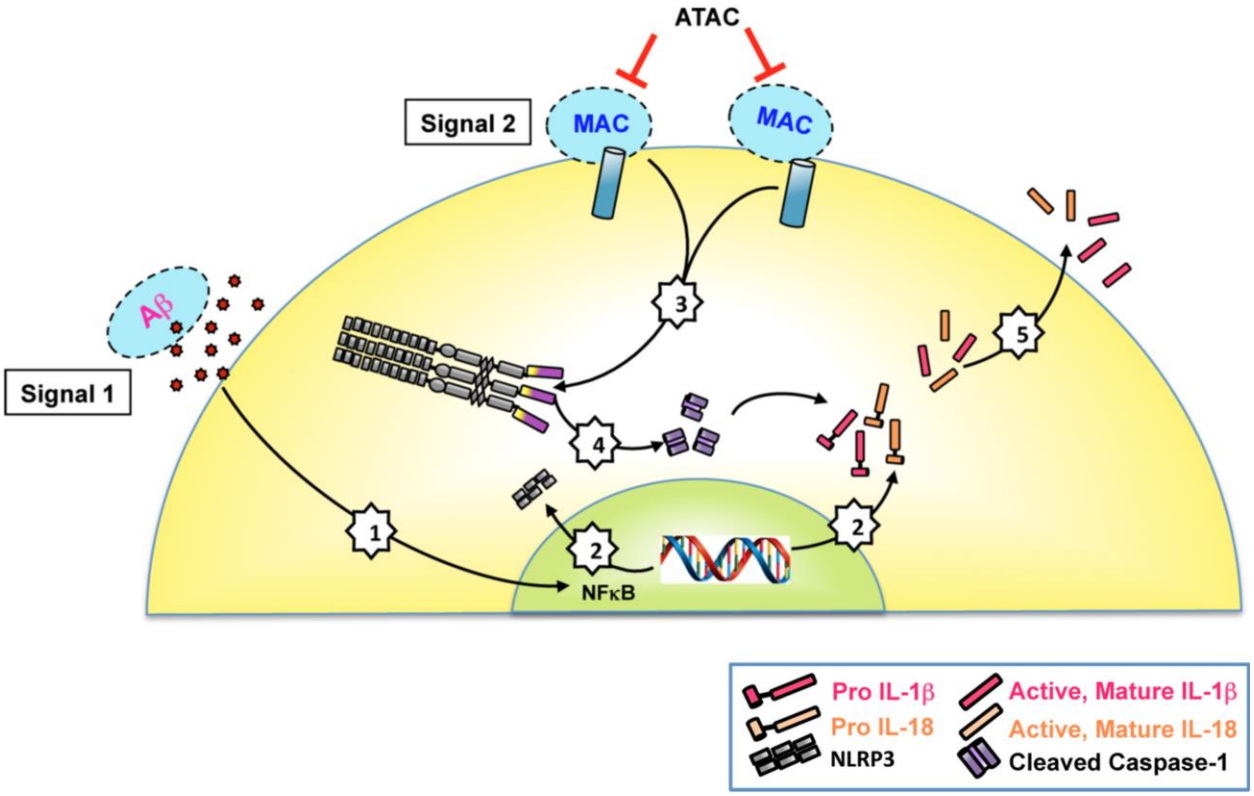

Figure 2-5 Proposed inflammasome activation mechanisms by Aβ and MAC in RPE-choroid

Age-associated changes in RPE-choroid include an increased accumulation of Aβ that acts as a "Signal 1" to activate the NF-κB pathway (1). The activated NF-κB pathway then upregulates the transcription of NLRP3, pro-IL-

18 and pro-IL-1β (2). Next, assembly and activation of the NLRP3 inflammasome is triggered by MAC deposition ("Signal 2") on the RPE cell membrane (3). NLRP3 activation results in pro-caspase-1 auto-cleavage (4). The cleaved caspase-1 then functions as a cytokine-processing enzyme to facilitate the production and secretion of active, mature IL-18 and IL-1β (5). ATAC compound works as a MAC inhibitor, suppressing MAC-induced inflammasome activation on RPE.

Chapter 3: Inflammatory mediators induced by amyloid beta in the retina and RPE *in vivo*: implications for inflammasome activation in age-related macular degeneration

3.1 Introduction

AMD is a multifactorial disease that is responsible for a significant proportion of visual impairment in the elderly in Western society.[13, 114] Early AMD is characterized by the presence of drusen, abnormal pigmentation of RPE[115, 116] and is associated with gradual vision loss.[117] In some cases early AMD will progress to a late, more advanced form that causes profound loss of central vision.[118] Little is known about the etiology of this disease or the processes that occur in the eye during the early stages of AMD. Identifying the molecular and cellular events that lead to symptomatic AMD and the development of treatment strategies that act at the early stages of the disease are therefore of high priority.[119]

One of the strongest predictors of AMD is the number and size of drusen.[117] Aβ, the peptide associated with neurodegenerative events in the brain in AD, is an important constituent of drusen (Figure 3-1).[50, 117] By analogy, the presence of Aβ in drusen raises the possibility that it may also contribute to neurodegenerative events in the retina in AMD.[120, 121] Study on donor eye tissue established a correlation between Aβ and GA.[62] A recent clinical trial addressing the safety and efficacy of anti-Aβ treatment for AMD has begun, further emphasizing the need to understand the specific mechanisms underlying the effect of Aβ in the eye.[119]

In contrast to past studies that used the more AD-specific, $A\beta_{1-42}$ peptide, we focused on the structurally similar $A\beta_{1-40}$ peptide in this study.[56] $A\beta_{1-40}$, the more common and less toxic form, is present in drusen[52, 122] and is thus a relevant candidate to consider for AMD (Figure 3-1). Using microarray analysis, Kurji et al.[65] identified genes in the immune response and inflammation pathways as being highly upregulated by RPE cells in response to $A\beta_{1-40}$ stimulation *in vitro*. There is emerging evidence that these pathways may be mediated by inflammasome activation.[123] Recent studies on AMD pathogenesis have concentrated on the activation of NLRP3 inflammasome in the RPE. However, important questions remain, such as whether inflammasome activation is involved in the retina's response to Aβ, and if exposure to inflammatory mediators such as IL-1β and IL-18 leads to AMD-like pathology.

To elucidate the effect of $A\beta_{1-40}$ *in vivo* and investigate the ensuing sequelae of inflammatory mediators on the retina and RPE in the context of early AMD, we performed intravitreal injection of $A\beta_{1-40}$ in a rodent model and studied the expression profile of key genes involved in the putative pathways of AMD pathogenesis, with a focus on inflammation and apoptosis. Intravitreal injection was chosen because it achieves the same effect of delivering peptide to outer retina/ RPE as subretinal injections without the associated retinal damage or detachment, which may itself cause inflammation and confound our results.[124, 125] We hypothesize that Aβ will stimulate inflammasome activation and over-expression of inflammatory mediators including cytokines, in the retina and RPE; such a response to Aβ may occur in the outer retina of pre-symptomatic AMD patients. Thus, treatments to minimize Aβ's effect in the eye may slow the progression of AMD, a strategy being investigated in clinical trials.[126]

3.2 Methods

3.2.1 Ethics statement

The postmortem donor eye study was approved by the Clinical Research Ethics Board at the University of British Columbia. Methods for securing human tissue were in compliance with the Declaration of Helsinki. The animal procedures were carried out according to the protocol reviewed and approved by the University of British Columbia Animal Care Committee and conformed to the Canadian Council on Animal Care guidelines. All animal studies were performed in accordance with the Resolution on the Use of Animals in Research of the Association of Research in Vision and Ophthalmology.

3.2.2 Donor eye tissue immunohistochemistry

Human eyes were obtained from the Eye Bank of British Columbia. Eye tissues were fixed in 10% formalin and embedded in paraffin to obtain 6 μm sections through the pupil and optic nerve axis. Sections were deparaffinized and rehydrated by standard procedures. After antigen retrieval in 70% formic acid for 18 min at room temperature (RT), sections were blocked with 3% H_2O_2 for 15 min and 3% goat serum for 40 min. Sections were incubated in primary antibody specifically against $A\beta_{1\text{-}40}$ (Cell Signaling Technology; Table 3-1) overnight at 4°C. Primary antibody omission or non-immune isotype antibodies were used as negative controls. Sections were then incubated in appropriate secondary antibodies and developed in avidin biotin peroxidase complex (ABC)-AEC system (Vector Laboratories).

Antigen	Primary Antibody	Type	Dilution	Specificity	Source and Catalog No. (Clone No.)
Amyloid-beta (Aβ) 1-40	Rabbit antihuman	Polyclonal	1:200	Recognizes human Aβ 1-40 isoform and crossreacts with mouse, rat, and monkey isoforms	Cell Signaling Technology, Beverly, MA; 9682
Amyloid-beta (Aβ)	Mouse antihuman	Monoclonal	1:500	Recognizes amino acid residues 17 to 24 of Aβ, crossreacts with mouse isoform	Covance, Princeton, NJ; SIG-39220 (4G8)
Interleukin-1 beta (IL-1β)	Goat antirat	Polyclonal	1:400	Detects rat IL-1β/IL-1F2 in cultured cells or tissue sections	R&D Systems, Inc., Minneapolis, MN; AF-501-NA
Interleukin-6 (IL-6)	Rabbit antirat	Polyclonal	1:400	Detects recombinant and native IL-6 secreted into body fluids and/or cell supernatants in rabbits, humans, mice, rats, and pigs	Abcam, Cambridge, UK; ab6672
OX-42 (CD11b/c equivalent antibody)	Mouse antirat	Monoclonal	1:300	Detects rat CD11 b/c in macrophages/dendritic cells with morphology of microglia in the brain	Cedarlane, Hornby, ON; CL042AP (MRC OX-42)
X-linked inhibitor of apoptosis protein-associated factor 1 (XAF1)	Rabbit antirat	Polyclonal	1:500	Detects cytoplasmic, mitochondrial, and nuclear XAF1 in rabbits, humans, mice, and rats	Abcam, Cambridge, UK; ab81353

Table 3-1 List of primary antibodies used in Chapter 3.

3.2.3 Aβ oligomerization

$A\beta_{1\text{-}40}$ (American Peptide, Sunnyvale CA) was prepared as previously described.[65] Briefly, lyophilized Aβ peptide was dissolved in hexafluoroisopropanol and agitated at RT for 48 h. Oligomerization was confirmed with atomic force microscopy and dot blot assay. Stock Aβ was diluted in phosphate buffered saline (PBS, pH 7.4) to yield a final concentration of 1.4 μg/μL. Aliquots of this solution were kept at -80°C until use. Human reverse peptide $A\beta_{40\text{-}1}$ (American Peptide, Sunnyvale CA) was prepared in an identical manner.

3.2.4 Animal model and treatment

Five month-old male Long-Evans rats (Charles River Laboratory, Wilmington MA) were raised on standard rodent diet and kept in enclosure with environmental enrichment and a 12 h light cycle. On Day 0, under inhalational anaesthesia, intravitreal injections were performed under a dissecting microscope using a 32-gauge Hamilton needle and syringe (Hamilton, Reno NV) to deliver 5 μL of oligomeric $A\beta_{1\text{-}40}$ peptide (7 μg) with 0.1 μL 10% sodium fluorescein as dye (Akorn, Buffalo Grove IL). This dosage yields an Aβ intravitreal concentration of approximately 30 μM, higher than that used in the *in vitro* experiment[65] and comparable to *in vivo* doses in other studies.[125, 127, 128] Age matched control animals received 5 μL intravitreal injection of reverse peptide $A\beta_{40\text{-}1}$ (1.4 μg/μL) or vehicle (PBS). After the procedure, animals were given oxygen and were monitored in a recovery enclosure until they resumed baseline activity level. Animals were kept for 1, 4, 14, and 49 days post-injection (N = 7 per treatment group) and euthanasia was performed with CO_2 inhalation. Eyes were immediately enucleated and frozen or preserved in 4% paraformaldehyde in DPBS (Invitrogen, Carlsbad CA).

3.2.5 Reverse transcription PCR (RT-PCR)

The anterior segment of the frozen eye was removed to expose the posterior eyecup. Separate samples of neuroretina or RPE-choroid were obtained from the eyecup by surgical dissection under dissecting microscope. Total RNA was isolated from tissue using RNAqueous-4PCR kit (Ambion, Austin TX). RNA quantity and quality were assessed using Nanodrop 2000c spectrophotometer (Fisher Thermo Scientific, Wilmington DE). 750ng of RNA from each tissue was reverse transcribed into cDNA using the High Capacity RNA-to-cDNA Master Mix (Invitrogen, Carlsbad CA). RT-PCR primer sequences are listed in Table 3-2. GAPDH served as endogenous control. All reactions were carried out on the Applied Biosystems 7500Fast SDS (Applied Biosystems, Carlsbad CA) using Power SYBR® Green (Applied Biosystems, Carlsbad CA). Each sample was repeated in triplicates with near-identical results. Cycling conditions were as follows: 95°C for 15 s, 58°C for 30 s, 60°C for 45 s, 40 cycles. Melting curve analysis was automatically performed immediately after amplification. Gene products were quantified relative to GAPDH using the $2^{-\Delta\Delta CT}$ method.

Gene	Forward Primer	Reverse Primer
IL-6	TCAACTCCATCTGCCCTTCAG	AAGGCAACTGGCTGGAAGTCT
TNF-α	AAATGGGCTCCCTCTCATCAGTTC	GCTTGGTGGTTTGCTACGAC
IL-1β	CACCTCTCAAGCAGAGCACAG	GGGTTCCATGGTGAAGTCAAC
IL-18	AGAAGGCTCTTGTGTCAAC	CTTCCTTTTGGCAAGCTAG
Caspase-1	AGAGAAGAGAGTCCTGAAC	TCTCTGAGGTCAACATCAG
NLRP3	CAGAAGGCATGTGAGAAG	ACAGGATCTTGCAGACTG
XAF1	GGAGAGGAGACAGCCTATG	CCTGGTGCTCATTTAGAA
VEGF	TGCAGACCAAAGAAAGATAGAAC	GGATCTTGGACAAACAAATGC
GAPDH	GAACATCATCCCTGCATCCA	CCAGTGAGCTTCCCGTTCA

Table 3-2 List of RT-PCR primer sequences used in Chapter 3 for rat tissues.

3.2.6 Retinal tissue immunohistochemistry

Rat paraffin tissue sections cut at a thickness of 4 μm were prepared through standard procedures described in our previous publication.[100] Sections of retina within 200 μm from the optic disc were known to be of even thickness regardless of embedding orientation[129] and thus were selected for processing.

To identify the localization of intravitreally injected $A\beta_{1\text{-}40}$ peptide, anti-Aβ antibody (4G8, Covance; Table 3-1) was applied to tissue sections for 1 h at RT and subsequently left overnight at 4ºC, following antigen retrieval in 70% formic acid and blocking steps (3% H_2O_2, 5% goat serum). Incubation in primary antibody was followed by standard biotinylated secondary antibody incubation. These sections were developed with VIP chromogen (Vector Laboratories) and counter-stained with Methyl Green (Vector Laboratories).

Immunohistochemistry was also performed to evaluate the product of selected upregulated genes in the retina. Sections first underwent antigen retrieval, removal of endogenous peroxidase and normal serum blocking by sequential incubation in protease K (20 μg/ml, pH 8.0, Sigma-Aldrich, St. Louis MO), 0.3% H_2O_2 and 3% normal horse serum. Sections were then incubated overnight at 4°C with monoclonal antibodies including IL-6, IL-1β, X-linked inhibitor of apoptosis protein associated factor 1 (XAF1), and CD11b/c, a cell surface marker for microglial cells (Table 3-1). After development with VIP chromogen, sections were photographed at ×20 and ×60 magnification using a brightfield microscope with a digital camera attachment (DS-Fi2 camera and DS-L3 monitor; Nikon, Tokyo Japan). Microscopic scoring was conducted by scanning the whole retinal sections under ×20 magnification in 1000 μm increments (diameter of the field) and by averaging the number of immunoreactive cells per increment. The final mean immunoreactive cell count was the averaged score of a minimum of 2-4 retinal sections per animal at each time point.

Retinal thickness was measured from the internal limiting membrane to the photoreceptor outer segments/RPE junction and the mean value was derived from measurements of 2-4 retinal sections per animal at each time point.

3.2.7 Suspension array assay for secreted cytokines

Rat vitreous was collected and aliquoted for cytokine analysis using suspension 23-plex cytokine arrays as described by the manufacturer (Bio-Rad Laboratories). The premade assays target the following cytokines: erythropoietin (EPO), granulocyte colony stimulating factor (G-CSF),

granulocyte macrophage colony stimulating factor (GM-CSF), chemokine (C-X-C motif) ligand 1 (GRO/KC), interferon-gamma (IFN-γ), IL-1α, IL-1β, IL-2, IL-4, IL-5, IL-6, IL-7, IL-10, IL-12p70, IL-13, IL-17, IL-18, macrophage colony stimulating factor (M-CSF), macrophage inflammatory protein 1alpha (MIP-1α), MIP-3α, regulated on activation, normal T cell expressed and secreted (RANTES), TNF-α and vascular endothelial growth factor (VEGF). 50 µL of cytokine standards, samples (pooled vitreous fluids) and blanks (dH_2O only) were incubated with 25 µL of anti-cytokine conjugated beads in 96-well filter plates for 30 min at RT with agitation (1100 rpm for 30 s, then 300 rpm for 30 min). Plates were subsequently washed three times by vacuum filtration with 100 µL of Bio-Plex wash buffer per well, using the Bio-Plex Pro™ Wash Station (Bio-Rad Laboratories). This was followed by the addition of 25 µL of diluted biotinylated detection antibody and further incubation with agitation at RT. After three filter washes (described above), 25 µL of streptavidin-phycoerythrin (SAPE) were added and the plates were incubated for 10 min at RT with agitation. Finally, plates were washed by vacuum filtration three times. Beads were subsequently re-suspended in 125 µl of Bio-Plex assay buffer, and vortexed for 30 s at 1100 rpm and further incubated for 2 min at 300 rpm. Standards, samples and blanks were analyzed using the Bio-Plex 200 Suspension Array System and subsequent raw median fluorescent intensity (MFI) data was captured and analyzed using Bio-Plex Manager software 4.1 (Bio-Rad Laboratories), using a standard high PMT setting.

3.2.8 Statistics analyses

Statistical analyses on RT-PCR and immunohistochemical studies were performed between $A\beta_{1-40}$ group and reverse peptide group and/or vehicle control group using Student's *t*-test with unequal variance. Suspension array data statistics was performed using the Bio-Plex Manager

software 4.1 (Bio-Rad Laboratories). Standard curves were developed using Brendon's 5 Point logistic regression analysis and a recovery range of 70-130% was established for the determination of a statistically valid standard curve.[130] RT-PCR and suspension array data are expressed as mean ± SE. Immunohistochemical data are expressed as mean ± SD with $p \leq 0.05$ set as threshold for statistical significance.

3.3 Results

3.3.1 $A\beta_{1\text{-}40}$ is a component of drusen

We first used a specific antibody to verify that $A\beta_{1\text{-}40}$, the more prevalent but less toxic form of Aβ peptide, is a component of human drusen (Figure 3-1A). Using non-immune isotype antibody yielded no $A\beta_{1\text{-}40}$ immunoreactivity (Figure 3-1B). This is consistent with previous studies of drusen composition.[50]

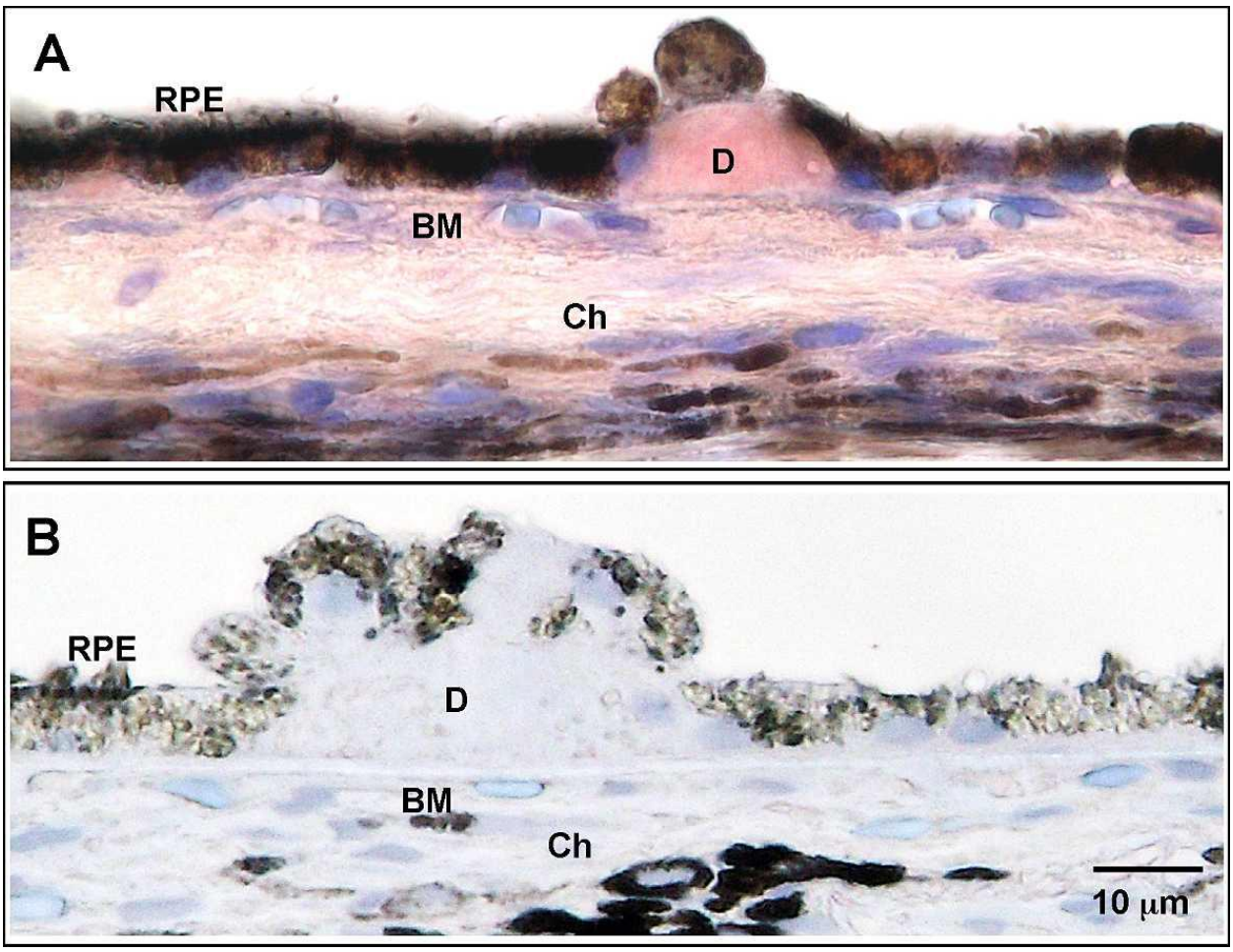

Figure 3-1 $A\beta_{1\text{-}40}$ in drusen.

Immunohistochemistry for $A\beta_{1\text{-}40}$ was developed in AEC (red) and counterstained with Mayer's hematoxylin (blue). (A) $A\beta_{1\text{-}40}$ in drusen of a 72-year-old non-GA female postmortem donor eye. (B) Negative control using non-immune rabbit IgG isotype antibody on the same donor eye section. RPE, retinal pigment epithelium; D, drusen; BM, Bruch's membrane; Ch, choroid. Scale bar: 10 μm.

3.3.2 Presence of $A\beta_{1\text{-}40}$ in all retinal layers after intravitreal injection

To confirm the effectiveness of intravitreal injection in delivering peptide to the outer retina, we probed the retinal tissue sections with 4G8 antibody that binds residue 17-24 in the human Aβ peptide. In $A\beta_{1\text{-}40}$-injected eyes, Aβ immunoreactivity was detected throughout retinal layers on

Day 1; the greatest intensity was localized to the photoreceptor outer segment (OS) while the RPE also demonstrated marked immunoreactivity (Figure 3-2A, G). This immunoreactive pattern was less intense on Day 4 (Figure 3-2D, I). Preferential accumulation of Aβ in the OS has been previously reported in both mice and humans.[63] These results were in keeping with previous reports[125] and verified the penetration of intravitreally-injected peptide through the retina and reaching the RPE. The reverse peptide $A\beta_{40\text{-}1}$ sections showed significantly less 4G8 immunoreactivity in the retina as expected (Figure 3-2B, E, H, J). We observed background levels of immunoreactivity in vehicle-injected eyes, confirming minimal non-specific binding of the antibody (Figure 3-2C, F).

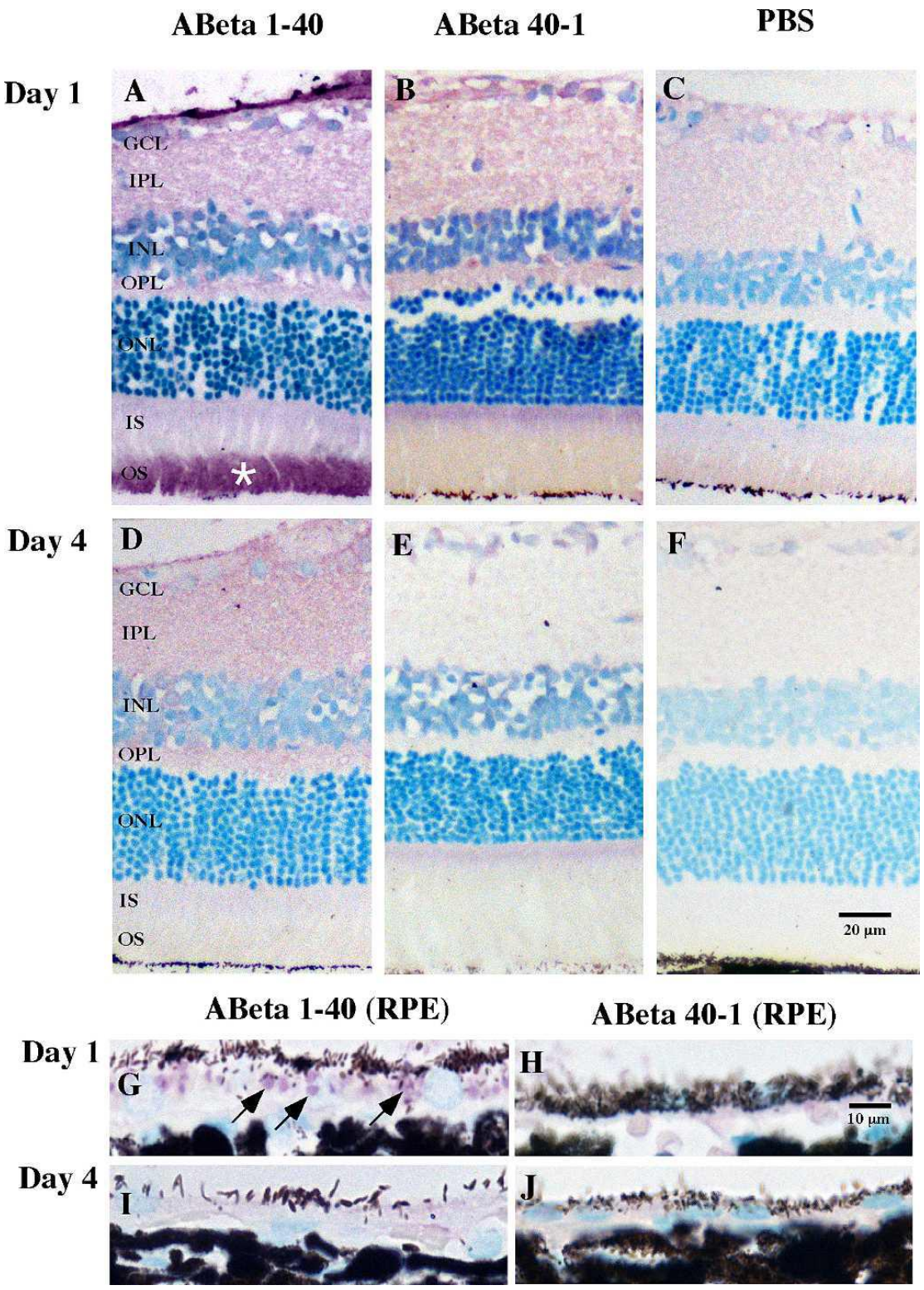

Figure 3-2 Localization of $A\beta_{1-40}$ or reverse peptide $A\beta_{40-1}$ demonstrated in retinal tissue on Days 1 and 4 following intravitreal injections.

Immunoreactivity for $A\beta_{1-40}$ and $A\beta_{40-1}$ was undertaken with 4G8 antibody, visualized with VIP chromogen (pink/purple), and counterstained with Methyl Green. VIP chromogen revealed immunoreactivity in the neuropil and extracellular compartments throughout all retinal layers on Day 1 and less on Day 4 in the Aβ group (A, D). Strong immunoreactivity was detected in the OS (star) in Aβ-injected eyes. Tissues from eyes receiving reverse peptide injection demonstrated significantly less immunoreactivity than the forward peptide group (B, E), as did the vehicle-injected eyes (C, F). Focusing on the RPE, there were discrete intracellular vesicles (arrows) possibly representing phagocytosed outer segment discs in the Aβ group compared to the reverse peptide group in Day 1 sections (G, H). Day 4 sections showed no vesicles but rather a diffuse and faint layer of VIP chromogen at the RPE in the Aβ group compared to the reverse peptide group (I, J). GCL, ganglion cell layer; IPL, inner plexiform layer; INL, inner nuclear layer; OPL, outer plexiform layer; ONL, outer nuclear layer; IS, inner segment; OS, outer segment. Scale bar: 20 μm (A–F), 10 μm (G–J).

3.3.3 Gene expression changes after $A\beta_{1-40}$ intravitreal injections

To assess whether the pro-inflammatory effect of Aβ on RPE extrapolates to an *in vivo* setting, we first screened for expression of inflammatory mediators by examining two cytokines. IL-6 is a known inducer of acute phase protein production and its serum level has been associated with progression of AMD.[131] In the Aβ group, there was significant upregulation of IL-6 gene on Days 1 and 4 compared to reverse peptide (Figure 3-3A, B). The RPE-choroid exhibited a greater fold change than the neuroretina, relative to the PBS vehicle control. No significant IL-6 upregulation was found in either tissue at later time points.

TNF-α is a prototypic cytokine with a potent effect on the retina and RPE.[124, 132] The Aβ group showed significantly higher levels of TNF-α mRNA than the reverse peptide in the neuroretina at all time points, with relatively greater response on Days 1 and 14 (Figure 3-3C). In contrast,

TNF-α in the RPE-choroid from the Aβ group was significantly upregulated on Day 1, increased further on Day 4, but was no longer significantly at Days 14 and 49 (Figure 3-3D).

Apoptosis is a putative mechanism of RPE and photoreceptor loss in AMD, but its exact trigger and onset remains unknown. XAF1, a pro-apoptotic gene, was markedly over-expressed in RPE stimulated by $A\beta_{1-40}$,[65] therefore it was examined here. Compared to reverse peptide and vehicle, Aβ caused significantly higher fold change in XAF1 expression in the neuroretina and RPE-choroid on Days 1 and 4 (Figure 3-3E, F). The magnitude of change was slightly greater in the RPE-choroid than in the neuroretina. No significant fold change in XAF1 expression was found on Days 14 and 49 in either tissue.

Given the central role of VEGF in stimulating choroidal neovascularization (CNV) in late AMD, we assessed the expression profile of VEGF. VEGF upregulation has been observed in RPE cells treated with $A\beta_{1-40}$[64] and *in vivo* after an intravitreal injection with $A\beta_{1-42}$.[127] Our results, however, showed no significant upregulation of VEGF in either neuroretina or RPE-choroid in the $A\beta_{1-40}$ group compared to reverse peptide throughout the time course of the study (Figure 3-3G, H). This is consistent with our earlier *in vitro* observations using $A\beta_{1-40}$.[65]

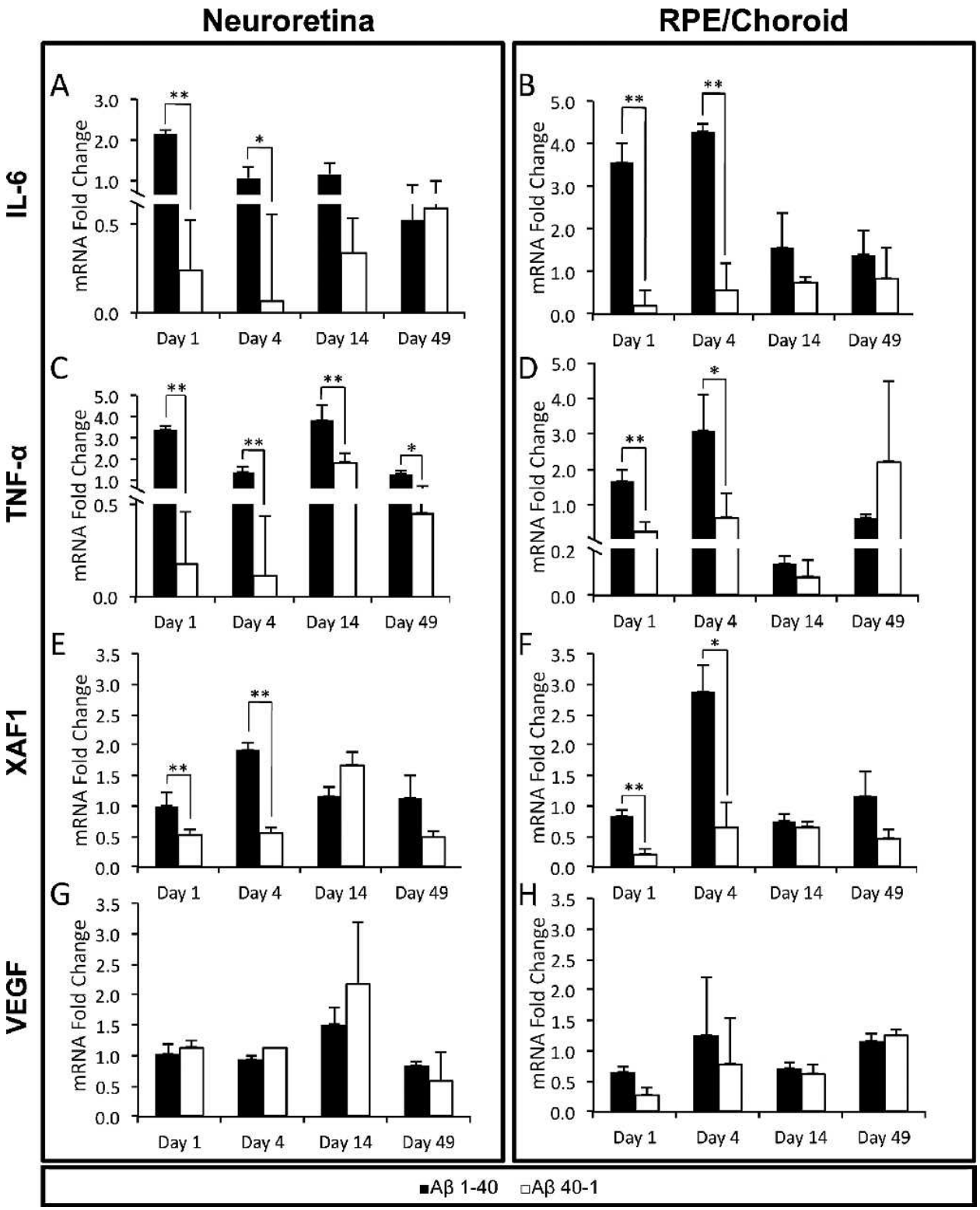

Figure 3-3 Reverse transcription PCR of selected genes in the RPE-choroid and neuroretina.

The relative mRNA quantity (normalized to endogenous control GAPDH and expressed as fold change over vehicle control PBS) in the $A\beta_{1-40}$ group was compared to that in the reverse peptide group. Genes were examined on Days 1, 4, 14, and 49 to capture both immediate and later changes after intravitreal injection at Day 0: (A, B) IL-6, (C, D) TNF-a, (E, F) XAF1, (G, H) VEGF. Error bars denote standard error. N = 7 per treatment group per time point, Student's *t*-test, $*p < 0.05$; $**p < 0.01$.

Recently, the inflammasome NLRP3 activation has been proposed as a potential mechanism promoting inflammation in AMD.[36] The increased levels of inflammatory cytokines in response to Aβ in our animals raised the possibility that NLRP3 could mediate cytokine upregulation in this setting. The expression profiles of IL-6 and TNF-α indicated that the strongest inflammatory response occurred on Days 1 and 4 post injection, therefore we sought evidence of inflammasome activation at these time points using IL-1β, IL-18, caspase-1 and NLRP3 genes. IL-1β and IL-18, two pro-inflammatory cytokines, are products of NLRP3 inflammasome processing[133] and IL-1β was markedly elevated in RPE upon $A\beta_{1-40}$ stimulation *in vitro*.[65] Caspase-1 is part of the NLRP3 inflammasome complex and is required for the cleavage of IL-1β and IL-18 pro-peptides[123]. In our study, IL-1β transcription was significantly elevated in the Aβ group on Day 1; the neuroretina showed a greater fold change than the RPE-choroid (Figure 3-4A, B). In contrast, IL-18 was not significantly upregulated on Day 1 in the Aβ group. Caspase-1 expression was significantly higher in the neuroretina but not RPE-choroid on Day 1 (Figure 3-4A). NLRP3 was markedly upregulated in the Aβ group, with neuroretina showing a greater response than RPE-choroid (Figure 3-4A, B). The trend of inflammasome marker was similar on Day 4. Of note is the significant upregulation of IL-18 at this later time point, with the RPE-choroid showing the largest fold increase (Figure 3-4C, D).

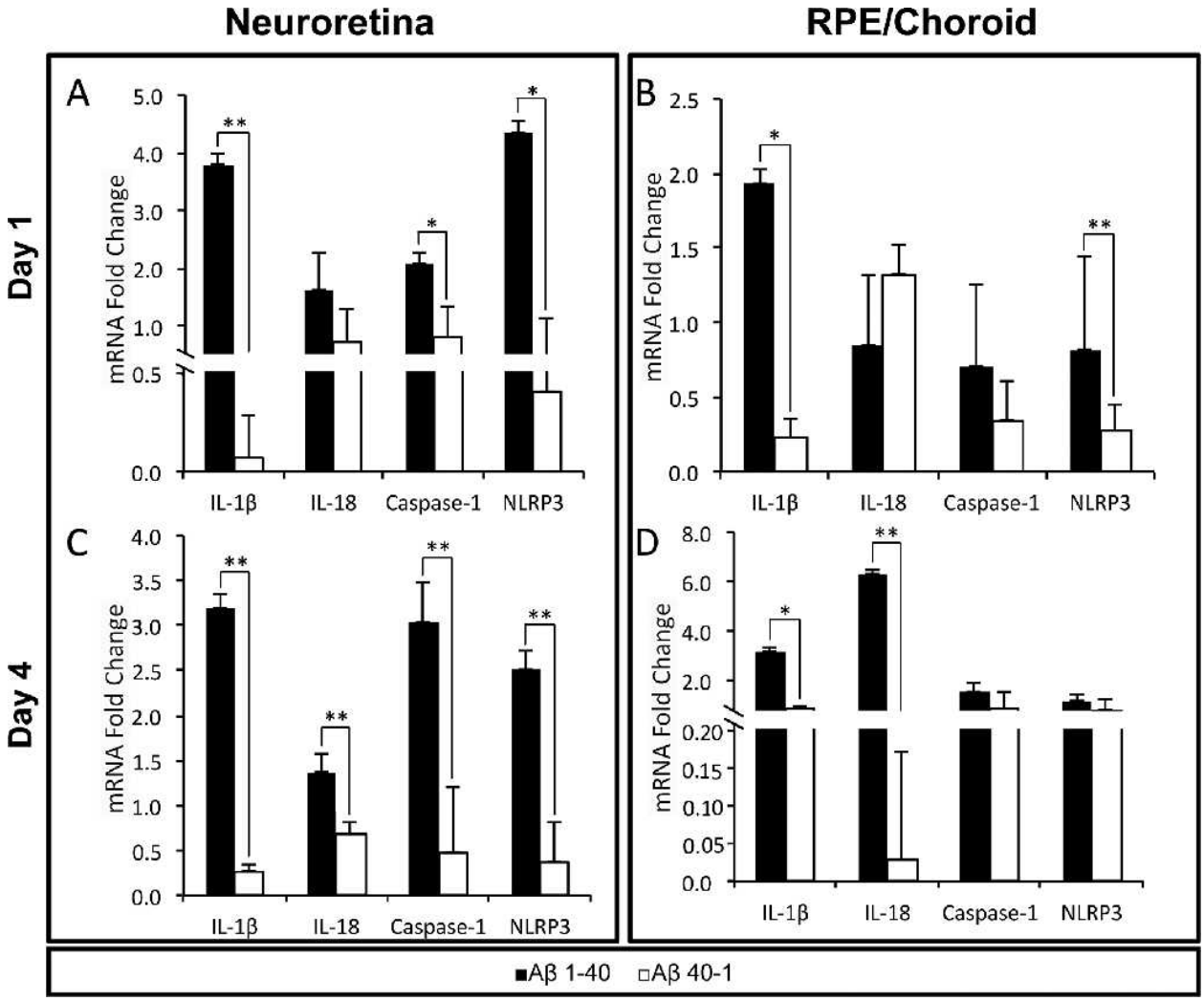

Figure 3-4 Inflammasome gene reverse transcription PCR data.

The relative mRNA quantity (normalized to endogenous control GAPDH and expressed as fold change over vehicle control PBS) in the $A\beta_{1\text{-}40}$ group was compared to that in the reverse peptide group. (A, B) Day 1, (C, D) Day 4. Error bars denote standard error. N = 7 per treatment group per time point, Student's *t*-test, $*p < 0.05$; $**p < 0.01$.

3.3.4 Cytokine levels in the retina and vitreous following $A\beta_{1\text{-}40}$ intravitreal injection

Based on the overexpression of inflammatory mediator genes in both neuroretina and RPE-choroid, we performed immunohistochemistry on retinal sections to further study the distribution of selected mediators. IL-6 immunoreactivity in the Aβ-injected eyes was distributed

predominantly in the GCL and INL (Figure 3-5A-C), but the RPE also demonstrated significantly greater immunoreactivity compared to reverse peptide group (Figure 3-5D, E). The overall number of IL-6 immunoreactive cells was greater in the Aβ group than in reverse peptide or vehicle control groups on Days 4 (Figure 3-5F), corresponding with the peak in IL-6 mRNA level (Figure 3-3A, B). This difference was diminished on Day 14 but still significant. By Day 49, however, there was no significant difference between the groups.

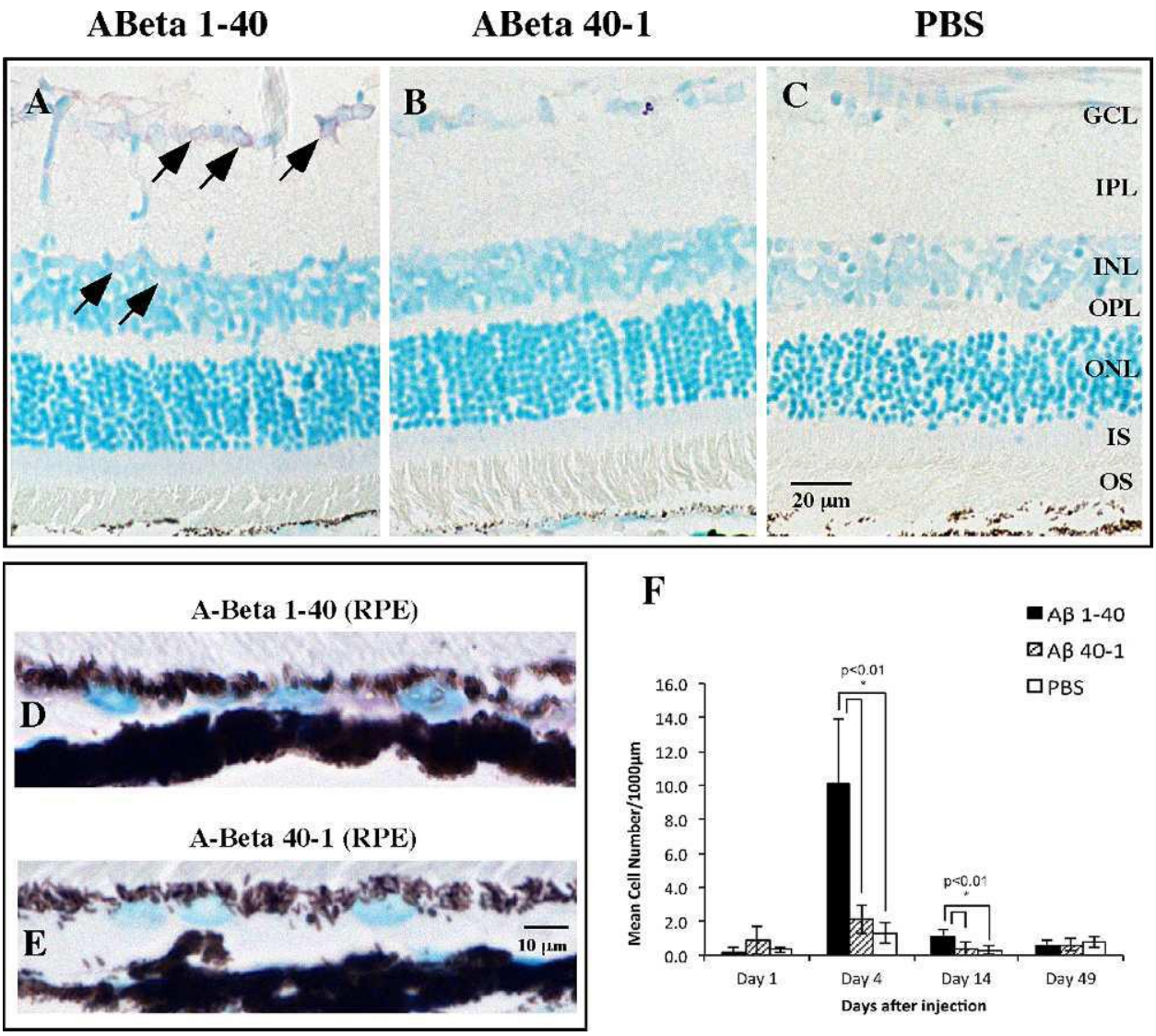

Figure 3-5 IL-6 immunoreactivity in the retina and RPE.

(A–C) Representative retinal micrographs of IL-6 immunoreactivity on Day 4. In the Aβ group, IL-6 immunoreactivity was mostly detected in cellular profiles in the GCL and INL (arrows). In contrast, the reverse peptide group showed very sparse IL-6 immunoreactivity, while the vehicle injection group identifies background level of IL-6 immunoreactivity. (D, E) The Aβ group also demonstrated more intense IL-6 immunoreactivity in the RPE than the reverse peptide group. (F) Bar graph of mean cell count of IL-6-immunoreactive cells at four time points, showing significantly greater IL-6 immunoreactivity in the Aβ group on Days 4 and 14 than in the reverse peptide or vehicle control group. Micrographs were examined at ×20 and ×60 magnification. Scale bar: 20 μm (A–C), 10 μm (D, E). Error bars denote standard deviation. N = 3, Student's *t*-test, $*p < 0.01$.

IL-1β immunoreactivity was primarily detected in the GCL and INL in the Aβ group with sparse immunoreactivity in the reverse peptide and vehicle control groups (Figure 3-6A-C). The RPE also demonstrated greater IL-1β immunoreactivity in the Aβ group than the reverse peptide group (Figure 3-6D, E). Comparing the cell counts among the groups, we noted more IL-1β immunoreactive cells in both Aβ group and reverse peptide group than in vehicle control on Days 1 and 4, but these differences did not reach significance threshold (Figure 3-6F). On Days 14 and 49, the Aβ group, compared to reverse peptide and vehicle control groups, had significantly more IL-1β immunoreactive cells.

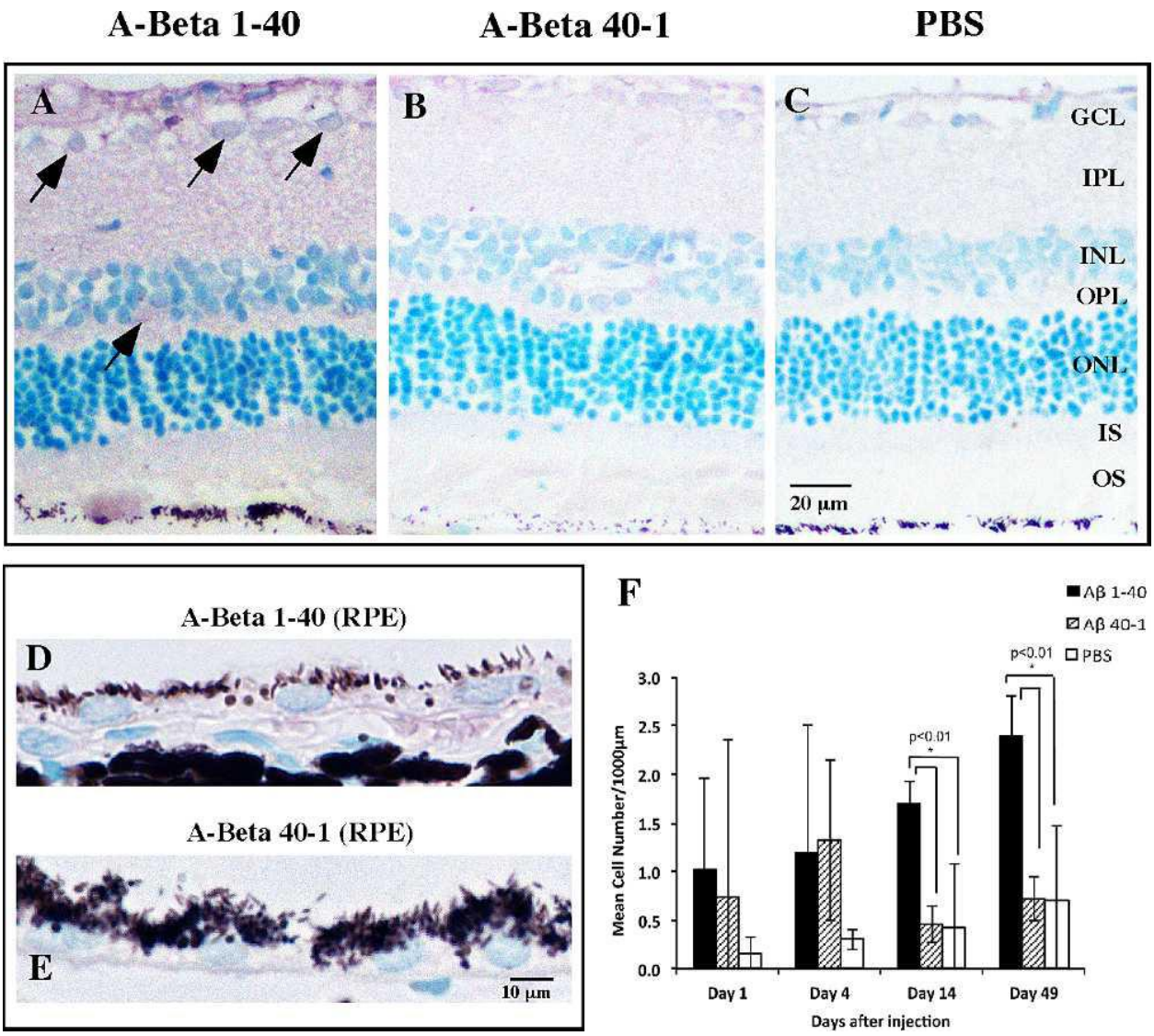

Figure 3-6 IL-1β immunoreactivity in the retina and RPE.

(A–C) Representative retinal micrographs of IL-1β immunoreactivity on Day 14. Marked IL-1β immunoreactivity was observed in the Aβ group and was predominantly localized to cellular profiles in GCL and INL (arrows) and in the neuropil IPL and OPL. Reverse peptide group demonstrated weak IL-1β immunoreactivity without any foci of distribution. Vehicle injection group demonstrated background IL-1β immunoreactivity. (D, E) Aβ group showed greater IL-1β immunoreactivity in the RPE than the reverse peptide group. (F) Bar graph of mean cell count of IL-1β-immunoreactive cells at four time points, showing significantly more IL-1β immunoreactivity in the Aβ group on Days 14 and 49 compared to the reverse peptide or control group. Micrographs were examined at ×20 and ×60

magnification. Scale bar: 20 μm (A–C), 10 μm (D, E). Error bars denote standard deviation. N = 3, Student's *t*-test, *$p < 0.01$.

Increased vitreal levels of inflammatory cytokines are present in patients with retinal pathologies including proliferative diabetic retinopathy[134] and central retinal vein occlusion.[135] Few studies have assessed the cytokines in the vitreous of AMD patients. In our study, elevated amount of IL-1β immunoreactivity in the retina exposed to Aβ prompted us to look further for evidence of cytokines in the vitreous in this model. Using ELISA-based assay, we found significantly higher levels of IL-1β and IL-18 in the vitreous of Aβ-injected eyes (13920±433 pg/ml, 1126±264 pg/ml respectively) than in reverse peptide controls (9803±280 pg/ml, 440±56 pg/ml respectively) (Figure 3-7). Of special note, MIP-3α, a lymphocyte and dendritic cell chemokine, showed the greatest increase in vitreal concentration in the Aβ group (759±54 pg/ml) compared to the reverse peptide group (199±21 pg/ml) (Figure 3-7). The levels of the other cytokine analytes included in the assay kit did not reach statistical significance and hence were not graphed.

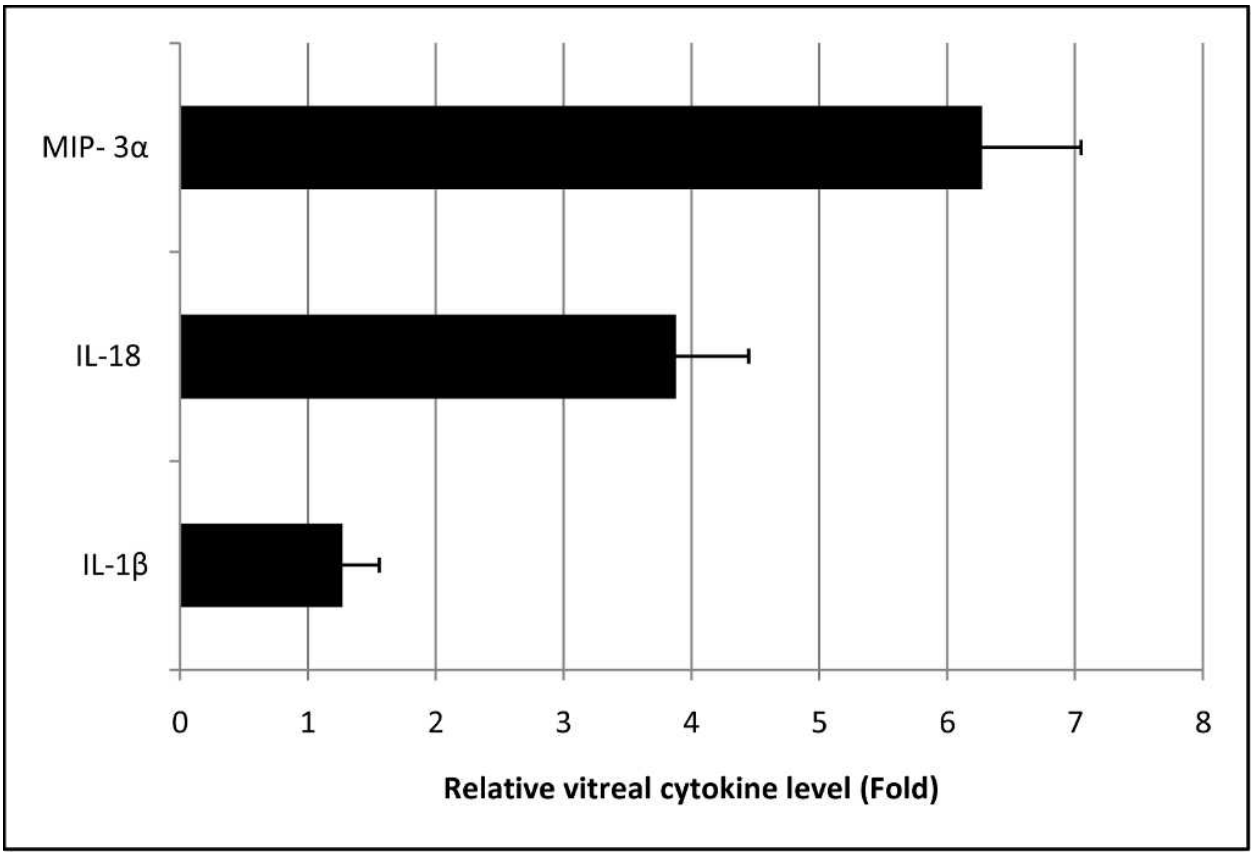

Figure 3-7 Day 14 vitreous cytokine suspension array assay.

Only statistically significant results (N = 7, Student's *t*-test, $p < 0.05$) are shown. Inflammasome product IL-1β was significantly elevated in Aβ-injected vitreous (13,920 ± 433 pg/mL) compared to reverse peptide-injected vitreous (9803 ± 280 pg/mL). Similarly, IL-18 showed significantly higher concentration in Aβ-injected vitreous (1126 ± 264 pg/mL) than in reverse peptide-injected vitreous (440 ± 56 pg/mL). MIP-3α showed the greatest difference between the Aβ group (759 ± 54 pg/mL) and the reverse peptide group (199 ± 21 pg/mL). Other cytokines including IL-6 and TNF-α did not reach threshold of significance ($p < 0.05$). Error bars denote standard error.

3.3.5 Microglia activation was significant at Day 1

Microglia are known to take up Aβ and generate an inflammatory response that affects RPE function;[136, 137] this has been proposed as a possible mechanism of AMD pathogenesis. To test this hypothesis we evaluated the microglial response to $A\beta_{1\text{-}40}$ using OX-42 antibody against

CD11b/c antigen, a cell surface marker representing total microglia (active and resting) (Figure 3-8A-C). The majority of CD11b/c positive cells were localized to the GCL and INL and some demonstrated evidence of activation based on their rounded morphology (Figure 3-8A inset). We observed a statistically significant but marginal increase in CD11b/c positive cells in the Aβ group compared to reverse peptide and vehicle control on Day 1 post injection (Figure 3-8D). No significant difference in microglial count was observed among the groups at other time points.

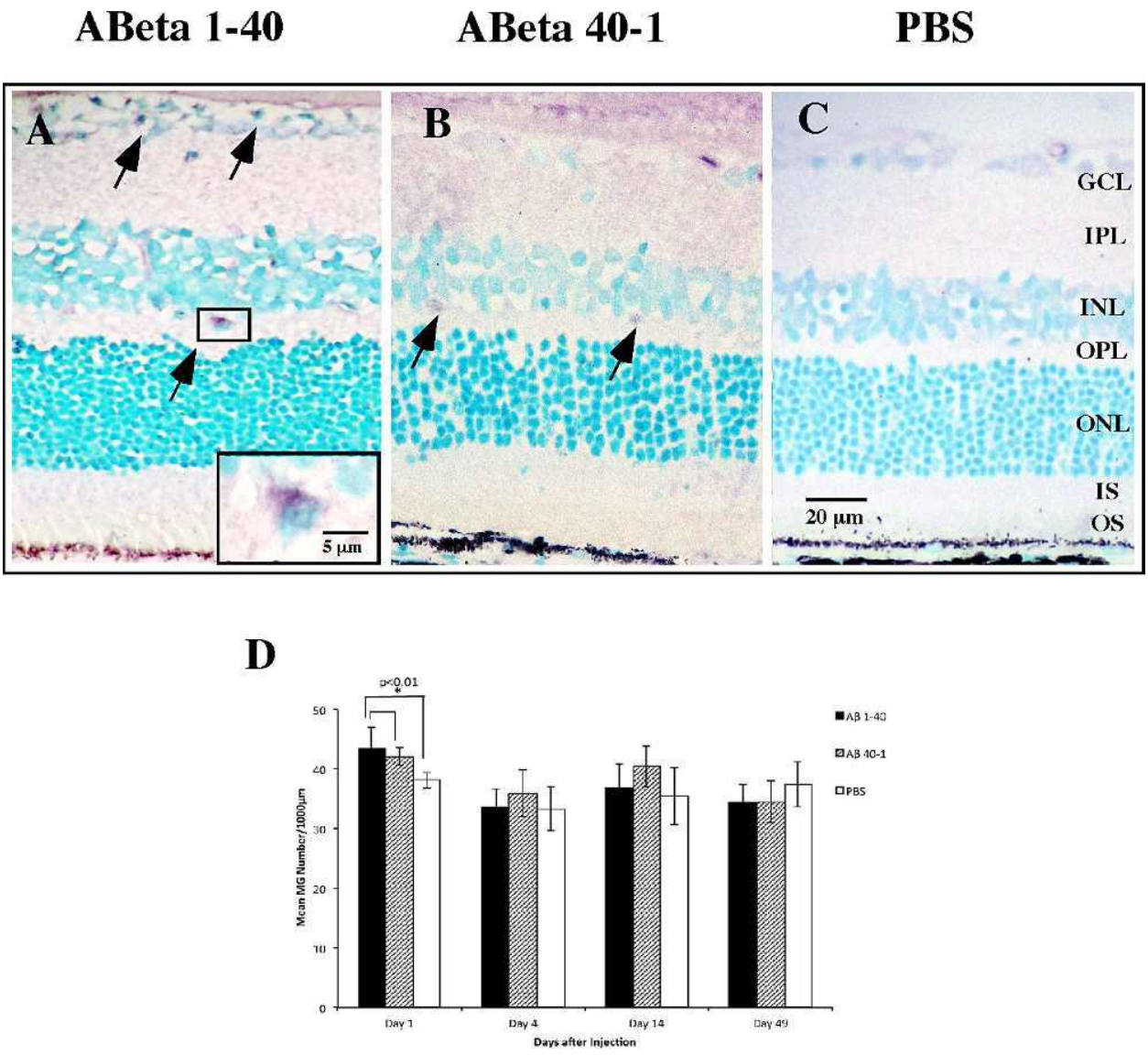

Figure 3-8 Microglia response to $A\beta_{1-40}$ stimulation.

Retinal sections were reacted with OX-42 antibody against cell surface marker CD11b/c, representative of total microglia. (A–C) Representative immunoreactivity pattern of CD11b/c labeling in the retinal sections at Day 1. Note that the Aβ section and the reverse peptide section both contained CD11b/c-positive cells within the GCL and INL (arrows), with the vehicle group demonstrating significantly lower CD11b/c immunoreactivity. Some CD11b/c-positive cells demonstrated rounded morphology and were intimately associated with cell bodies of retinal neurons (inset). (D) Bar graph of mean CD11b/c immunoreactivity profiles in three groups, with significance demonstrated at Day 1 between the $A\beta_{1-40}$ forward peptide group and the reverse peptide and vehicle control groups. Micrographs

were examined at ×20 and ×60 magnification. Scale bar: 20 μm; 5 μm (inset). Error bars: standard deviation. N = 3, Student's *t*-test, $*p < 0.01$.

3.3.6 Cell death and neovascularization were not associated with $A\beta_{1-40}$

GA represents a late stage of AMD and is characterized by extensive RPE and photoreceptor loss that is thought to occur via apoptosis. Cytokines including TNF-α have been linked to photoreceptor apoptosis,[124] therefore it is important to establish whether apoptosis is a feature in this model of early AMD. We first looked for protein expression of the pro-apoptotic factor XAF1. Despite upregulation of XAF1 gene, we did not detect higher XAF1 immunoreactivity in the retina in the Aβ group compared to controls (data not shown). Additional immunohistochemical analyses of the tumor suppressor gene p53 as well as terminal deoxynucleotidyl transferase dUTP nick end labeling (TUNEL) staining were undertaken, but no significant differences were observed between the groups (data not shown). To further evaluate retinal degeneration and preclude cell loss via non-apoptotic mechanisms,[138] we compared the neuroretinal thickness between Aβ-injected and control eyes. Neuroretinal thickness was preserved at all time points (Figure 3-9), and we did not observe any evidence of BM disruption or angiogenic activities.

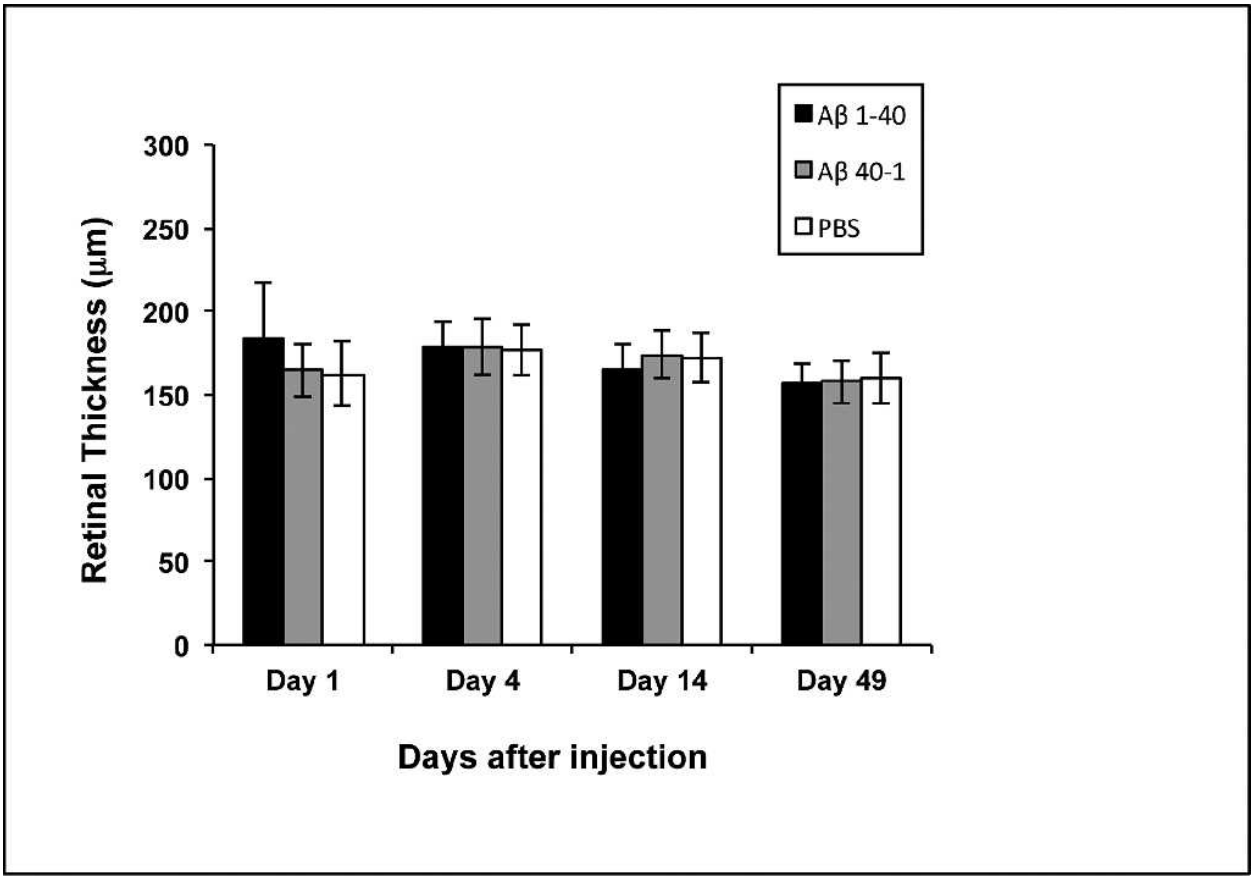

Figure 3-9 Retinal thickness measurements.

Retinal thickness was measured from internal limiting membrane to photoreceptor outer segment/RPE junction in parafoveal sections. No significant difference in retinal thickness was observed in any group throughout the experiment. Error bars denote standard deviation. N = 3, Student's *t*-test.

3.4 Discussion

A compelling role for local, chronic inflammation in the pathogenesis of AMD has been established by studies on drusen[117, 139] and gene polymorphisms.[140] Cytokines, key drivers of inflammation, have gained much interest for their potential role in AMD pathophysiology; for instance, high serum IL-6 level is found to be an independent predictor for the progression of AMD.[131] Analysis of post-mortem human eyes from AMD patients revealed elevated eotaxin

and IP-10,[141] as well as increased IL-1β immunoreactivity in association with large drusen.[101] Finding a trigger for cytokine expression is clearly important for targeted intervention, and we hypothesized that $A\beta_{1-40}$, the principal form of the Aβ peptide found in the eye[104] and in drusen,[52] may be responsible for promoting cytokine production and inflammatory pathways.[65] Our results demonstrated that intravitreal injection of $A\beta_{1-40}$ caused marked upregulation of cytokines in the RPE and neuroretina. This model is consistent with the early phases of age-related maculopathy according to Hageman et al.'s hypothesis[117] that suggests RPE dysfunction generates a pro-inflammatory milieu in early AMD pathogenesis.

3.4.1 RPE plays a major role in responding to Aβ

Our data suggests that both neuroretina and RPE-choroid upregulate inflammatory pathway genes in response to Aβ stimulation. Relative to the neuroretina, the RPE demonstrated comparable magnitude of gene expression changes despite fewer total cells, indicating a high sensitivity to Aβ stimulation. The RPE is chiefly responsible for the maintenance and homeostasis of the outer retina and photoreceptor, but it is also known to actively participate in immune response via cytokine production.[142, 143] In contrast, it is mostly glial cells,[144] and principally microglia, that secrete cytokines in the neuroretinal layers.[121, 137] Based on our immunohistochemistry data, the microglial response was minimal and transient in the Aβ group. Previous studies have induced marked microglial activation using intravitreal $A\beta_{1-42}$,[121, 125] likely due to the greater neurotoxicity associated with $A\beta_{1-42}$ compared to $A\beta_{1-40}$.[122] The increase in microglia we observed on Day 1 did not correlate with cytokine gene expression at other time points, nor was the magnitude of change large enough to convincingly demonstrate an association with the differential expression of inflammatory mediators seen. Combined with the

fact that Aβ induces RPE to upregulate inflammatory pathways *in vitro*[65], it is likely that the RPE, not microglia, is the predominant source of cytokine in this study. The choroid was considered as a potential portal for systemic cytokines entering the retina; however, given that the blood-retinal barrier was intact after intravitreal injections, it is unlikely that Aβ oligomers (dimer: 8.6 kDa) and cytokines (all larger than Aβ) were exchanged between the choroidal vasculature and the retina.

3.4.2 A role for NLRP3 inflammasome activation?

We observed a time-dependent over-expression of IL-6 and TNF-α in eyes treated with $A\beta_{1\text{-}40}$. IL-1β, a cytokine product of NLRP3 inflammasome, was concurrently upregulated on Days 1 and 4 in the neuroretina and RPE. IL-18 was also upregulated on Day 4. The associations between Aβ, NLRP3 inflammasome, and RPE have been described separately: Halle et al.[123] reported Aβ-induced NLRP3 inflammasome activation in microglia while Kauppinen et al.[145] showed NLRP3 inflammasome-dependent cytokine synthesis in human RPE under oxidative stress *in vitro*. The temporal pattern that emerged from our data is strongly suggestive of a role for NLRP3 inflammasome in response to Aβ in the eye, a novel finding. We propose that, upon Aβ exposure, NLRP3 inflammasome is initially activated in the RPE and neuroretina, as illustrated by the over-expression of NLRP3 gene on Day 1. The activation of NLRP3 inflammasome recruits caspase-1 and catalyzes the formation of IL-1β initially, followed shortly by IL-18. IL-1β in turn stimulates the RPE in an autocrine manner,[146] causing over-expression of TNF-α and IL-6 to further propagate a local pro-inflammatory state.[147] This novel association highlights the key function of NLRP3 inflammasome in coordinating cytokine expression in the eye. In our model, cytokine expression mostly diminished to baseline levels by 14 days post-

injection. This observation presumably reflects clearance of Aβ, as microglia are known to remove Aβ from the retina.[121] Interestingly, we observed high TNF-α mRNA level and IL-1β immunoreactivity on Days 14 and 49 that might indicate some degree of persistent inflammatory pathway activation in the eye. Whether this represents the establishment of chronic inflammation is unclear and should be investigated in a future study that extends the observation period beyond the 49 days studied here. We demonstrated that $A\beta_{1-40}$ stimulates cytokine production in healthy RPE and retina and establishes a pro-inflammatory environment in the posterior segment of the rodent eye. It can be inferred that accumulation of Aβ in drusen may generate an increasing level of cytokines that primes the outer retina for subsequent damage, prior to the onset of clinical evidence of AMD.

Cytokines are integral to the host's immune defense, but their imbalances are often implicated in diseases. TNF-α, IL-6, and IL-1β are also elevated in retinal detachment,[124] proliferative vitreoretinopathy,[146] and ischemia.[148] These cytokines also play an important part in the pathophysiology of AMD based on evidence from clinical and epidemiological studies.[131] For instance, cytokines are known to stimulate chemotaxis and our vitreous assay revealed an elevated level of chemokine MIP-3α (Figure 3-7). MIP-3α mediates migration of dendritic cells and lymphocytes via CCR6 receptor as part of mucosal defense against microbes.[149] Human ARPE-19 produces MIP-3α in response to IL-17A.[150] RPE has also been known to increase production of IL-8, another chemokine, when stimulated by $A\beta_{1-40}$.[65] In light of these observations, chemotaxis may constitute an important part of a response to Aβ in the eye and warrants further investigations.

To the best of our knowledge, our study showed, for the first time, that IL-18 is upregulated in the retina, RPE, and vitreous following Aβ stimulation. IL-18 is thought to be involved in late stages of AMD. Doyle et al.[43] showed that IL-18 inhibits angiogenesis in CNV, while Tarallo et al.[36] reported that IL-18 promotes RPE death in dry AMD. Neither event was observed in this study, but our model only assessed the effects up to 49 days following a single Aβ injection. It is likely that multiple Aβ injections and follow-up beyond 49 days may better simulate a chronic, local pro-inflammatory environment thought to be present in the retina of patients with early AMD and thus helpful to define the role of IL-18 in AMD.

3.4.3 Cell loss is not a feature of this model of early AMD

There is an established connection between inflammation and apoptosis. Both IL-1β and TNF-α are known to increase expression of apoptotic factors in the RPE.[151-153] Apoptosis has been proposed as a mechanism contributing to degenerative events in AMD.[154] The present study saw a significant upregulation of the XAF1 gene by RPE-choroid in Aβ-injected eyes (Figure 3-3E, F), in keeping with our previous *in vitro* observations[65]. XAF1 directly activates caspase-dependent apoptosis in conjunction with TNF-α.[154, 155] Surprisingly, there was no significant change in the immunoreactivity of XAF1 in the retinal tissue sections. Such mismatch between XAF1 mRNA and protein was previously reported in other tissues.[156] We suspect that anti-apoptotic processes might have interfered with the synthesis of XAF1 protein. Absence of significant p53 or TUNEL immunoreactivity and preservation of retinal thickness in Aβ-injected eyes strongly suggest that cell death is not a feature of the present study. This is in contrast to intravitreal $A\beta_{1-42}$-induced retinal neuron degeneration in AD models.[127, 128] The difference is likely due to the inherently-greater neurotoxicity of $A\beta_{1-42}$ compared to $A\beta_{1-40}$.[122] On the other

hand, existing animal models of AMD capture many features of late disease: Malek et al.[157] demonstrated drusen-like deposits, RPE changes and CNV in the apoE4-HFC diet mouse model. Both *Ccl2/Cx3cr1* double knockout mouse model and *Ccl2*- or *Ccr2*- knockout mouse model produced subretinal deposits and RPE/photoreceptor atrophy[158-160]. However, these models do not directly or independently rely on a local, pro-inflammatory retinal environment thought to be present in pre-symptomatic AMD. Using intravitreal $A\beta_{1-40}$ injection, we induced a pro-inflammatory response in the healthy retina without causing cell loss. This model creates the opportunity to study how inflammatory cytokines affect the homeostasis of the outer retina and to evaluate the effectiveness of interventions that control the pro-inflammatory environment, hypothesized to be one of the earliest changes associated with the etiology of AMD.

3.5 Conclusion

This chapter's study verified the pro-inflammatory effects of drusen component $A\beta_{1-40}$ *in vivo* in the rat retina. Cytokine genes including IL-6, TNF-α, IL-1β, and IL-18 are upregulated by the RPE and neuroretina after Aβ stimulation. The activation of NLRP3 inflammasome may play a central part in mediating this response and is thus a potential novel target for AMD treatment. $A\beta_{1-40}$ is likely to be an important contributor to AMD by promoting the release of cytokines and establishing a background level of chronic, local inflammation that promotes dysfunction of cells of outer retina including the RPE. The absence of retinal cell apoptosis in this model makes it suitable for studying the early pro-inflammatory events that may prime the retina towards AMD development. Our results are useful for future studies that require an *in vivo* platform for testing therapeutics that target and suppress inflammasome activation and cytokine production in the retina. Current literature on the use of anti-inflammatory agents in AMD derives from studies

that focus on late stages of the disease,[161] however our study prompts a closer look at the possible benefit of such approach in early AMD with the goal to minimize disease progression and prevent vision loss.

Chapter 4: Vinpocetine inhibits amyloid beta induced activation of NF-kB, NLRP3 inflammasome and cytokine production in retinal pigment epithelial cells

4.1 Introduction

AMD is a leading cause of visual impairment among the elderly in developed countries.[13] Advanced AMD accounts for the majority of vision loss and manifests as CNV (wet form) or GA (dry form). Chronic, subclinical inflammation in the outer retina is thought to promote AMD pathogenesis long before symptom onset.[20, 117] Extracellular deposits beneath the RPE, known as drusen, are hallmarks of AMD and contain protein and lipid components capable of stimulating inflammation.[117, 139] Aβ, a peptide found in senile plaques in the brain in AD, is a constituent of drusen and is believed to contribute to the inflammatory state in the outer retina.[50, 51]

Aβ is a physiologic peptide that exists in two forms: the 1-42 form is associated with AD plaques while the 1-40 form is more prevalent in the eye and drusen.[52, 104] $A\beta_{1\text{-}40}$ activates inflammatory/immune response pathways but not acute toxicity in RPE cells, in keeping with the insidious onset of AMD.[65] More recently, the pro-inflammatory effect of $A\beta_{1\text{-}40}$ was verified *in vivo* using an intravitreal injection model that demonstrated upregulation of NLRP3 inflammasome associated products (IL-1β, IL-18), cytokines (IL-6, TNF-α), and increased microglia activation.[113] The NLRP3 inflammasome is an intracellular multi-protein complex that recruits and cleaves caspase-1 when activated; this inflammasome complex with activated caspase-1 in turn cleaves IL-1β and IL-18 pro-peptides into their mature forms.[36, 123, 133] A host

of diverse molecules have been identified as activation signals, including PAMPs (e.g. pore-forming toxins), DAMPs (e.g. ATP, crystals), and other proteins such as Aβ.[38, 162, 163] Aβ is being investigated as a potential target for dry AMD,[164] however, concomitant suppression of inflammation, specifically the inflammasome, may be a novel approach in attenuating the stimulus that underlies the early development of AMD and preventing its progression to vision-threatening late stages.

Vinpocetine is a modified vinca alkaloid extracted from the periwinkle plant, widely used as dietary supplement in Europe and Asia for cognitive impairment and cerebrovascular diseases.[165, 166] Recent evidence demonstrates that it possesses an anti-inflammatory property via the suppression of NF-κB activation in a variety of cell types.[167] Compared to traditional steroids and non-steroidal anti-inflammatory drugs (NSAIDs), vinpocetine has no known significant side effects, thus making it an attractive alternate anti-inflammatory agent for long term use. The role of NF-κB in ocular tissue has not been studied in the context of AMD, but it is believed that NF-κB pathways supply the necessary signals to prime the NLRP3 inflammasome complex for activation as well as the production of pro-peptides that are substrates for the inflammasome.[33, 168] As a potent pro-inflammatory transcription factor, NF-κB is classically activated in response to cellular insult by TNF-α[169] via intermediate kinases and in turn, regulates the expression of cytokines including TNF-α.[170] TNF-α is upregulated by the RPE and retina in the presence of Aβ[113] and is capable of causing damage to photoreceptor cells.[124] Therefore, further investigation into the effect of NF-κB inhibition on the expression of inflammatory mediators is essential towards a better understanding of AMD pathogenesis and therapy.

We aimed to characterize the response of NF-κB to Aβ stimulation in the eye and examine the effect of vinpocetine on NLRP3 inflammasome activation and pro-inflammatory cytokine expression. We focused on the RPE cells in particular because they are the key homeostatic regulator in the outer retina and their dysfunction is hypothesized to be one of the first steps in the development of AMD. Targeting the NF-κB pathways may suppress early events associated with inflammasome activation, and provide an avenue for future treatment strategies for chronic inflammatory retinal diseases such as AMD.

4.2 Methods

4.2.1 Peptide and vinpocetine preparation

$A\beta_{1\text{-}40}$ oligomeric peptide (American Peptide, Sunnyvale CA) was prepared according to previously described methods[171] and stored in 1.4 μg/μL aliquots. Vinpocetine was purchased from AK Scientific Inc (Union City, CA). Vinpocetine was dissolved in dimethyl sulfoxide (DMSO) as vehicle at a stock concentration of 5 mg/ml and diluted to the desired concentration based on published figures for *in vitro*[172] and *in vivo* activity.[167]

4.2.2 Establishment of ARPE-19/NF-κB-luciferase reporter cell line

To measure NF-κB activation, an NF-κB specific reporter expression plasmid was constructed: the NF-κB specific promoter was composed of six tandem NF-κB consensus binding sites and a minimal CMV promoter fragment. Following the NF-κB specific promoter is a luciferase reporter gene. The entire NF-κB reporter unit was cloned into a eukaryotic expression vector pcDNA3.1(+). ARPE-19 cells (ATCC® CRL-2302™) at passage 4 were seeded in a 6-well plate

and cultured for 24 h. At the time of transfection, cell confluence was approximately 80%. The ARPE-19 cells were transfected by 2 μg of NF-κB-luciferase expression plasmid using 4 μL of FuGene HD transfection reagent (Roche Applied Science, Indianapolis IN). The transfected cells were subcultured in diluted cell concentration and selected by G418 (1 mg/mL) in culture medium for four weeks. The monoclonal stable reporter cells resistant to G418 selection were expanded and tested for the response to recombinant human TNF-α (rhTNF-α) stimulation. The monoclonal stable cells with the best response to rhTNF-α stimulation were used for subsequent experiments.

4.2.3 *In vitro* evaluation of NF-κB activation and the effect of vinpocetine

To verify the inhibitory effect of vinpocetine on NF-κB in ocular cell type, we compared vinpocetine to BAY11-7082, a classic inhibitor of NF-κB.[173] ARPE-19/ NF-κB reporter cells were seeded in a 24-well plate and cultured overnight. The reporter cells were washed twice with PBS and pretreated with vinpocetine (50 μM) or BAY11-7082 (10 μM) in Dulbecco's modified essential medium (DMEM)/F12 without serum at 37°C in 5% CO_2 for 1 h, followed by addition of the known NF-κB stimulus TNF-α (2.5 ng/mL) into the medium above and cultured for 8 h.

To assess the effect of vinpocetine on RPE's response to Aβ, three treatments were prepared: $A\beta_{1\text{-}40}$ (1 μM) containing 2.5% DMSO, vinpocetine (50 μM) containing 2.5% DMSO, and 1 μM $A\beta_{1\text{-}40}$ combined with 50 μM vinpocetine containing 2.5% DMSO. 2.5% DMSO served as vehicle control. All treatments were prepared in DMEM/F12 medium without serum. Reporter cells were incubated with each treatment at 37ºC in 5% CO_2 for 8 h. The transcriptional level of the luciferase-NF-κB tandem protein is a sensitive surrogate indicator of NF-κB activation

state,[174, 175] therefore NF-κB activation was quantified by luciferase mRNA level via RT-PCR. Total RNA was isolated from tissue using RNAqueous-4PCR kit (Ambion, Austin TX) and reverse transcribed into cDNA using the High Capacity RNA-to-cDNA Master Mix (Invitrogen, Carlsbad CA). 130 ng total RNA from each treatment group was used with the following luciferase primers: forward: TCACAGAATCGTCGTATGC; reverse: CGTGATGGAATGGAACAAC. RT-PCR was carried out on the 7500Fast SDS (Applied Biosystems, Carlsbad CA) with the following cycling conditions: 95ºC for 30 s, 50ºC for 30 s, 72ºC for 45 s, 40 cycles. Melting curve analysis was automatically performed immediately after amplification. Each treatment group was compared to vehicle control and the results were expressed in mRNA fold change normalized to the housekeeping gene GAPDH, using the $2^{-\Delta\Delta CT}$ method.

4.2.4 Animal treatment studies

Animal procedures were carried out according to the protocol reviewed and approved by the University of British Columbia Animal Care Committee and conformed to the Canadian Council on Animal Care guidelines. All animal studies were performed in accordance with the Resolution on the Use of Animals in Research of the Association of Research in Vision and Ophthalmology. Five and half month-old female Long-Evans rats (Charles River Laboratory, Wilmington MA) weighing an average of 450 g were used. Animals were raised on standard rodent diet and housed with environmental enrichment in 12 h light/dark cycle. Anesthesia was induced with 5% halothane in 70/30 mixtures of N_2O and oxygen, and maintained with 1.5% halothane throughout surgical procedures. On Day 0, a single intraocular injection of $A\beta_{1\text{-}40}$ (7 μg) was performed on all animals according to described procedures.[113] Treatment group received vinpocetine

containing 100% DMSO (N=13) at a dosage of 15 mg/kg body weight, and control group received the same converted volume of 100% DMSO (N=13), as intraperitoneal (IP) injection 1 h prior to the intraocular injections, and then repeated daily for three subsequent days. Animals were sacrificed on Day 4 and eyes were immediately enucleated and frozen (for western blot and vitreous analysis) or fixed in 4% paraformaldehyde in DPBS (Invitrogen, Carlsbad CA) for 48-72 h prior to tissue processing for immunohistochemistry.

4.2.5 Immunohistochemistry

Fixed eye tissues were embedded in paraffin, oriented in the sagittal plane and cut at 4 μm thickness through the axis defined by the pupil and the optic nerve per established protocol.[100] Antibodies against NF-κB p65 subunit, IL-1β, IL-18, TNF-α, NLRP3, and caspase-1 were used to stain the paraffin sections. Antibody dilution and specifications are listed in Table 4-1. Sections were deparaffinized and rehydrated by standard procedures. All sections underwent antigen retrieval in proteinase K solution (20 μg/ml, pH 8.0; Sigma Aldrich, St. Louis, MO) for 10 min at RT except for NF-κB. NF-κB sections underwent antigen retrieval in 10mM sodium citrate buffer and microwave heating for 20 min at high power (800W). Sections were then washed 3 times in PBS (pH 7.4), treated with 0.3% H_2O_2 for 15 min, and blocked for 20 min with 3% normal serum diluted in 0.3% Triton-X (TX)-100-PBS solution to minimize non-specific staining. Tissue sections were then incubated in specific primary antibodies diluted in serum and PBS with 0.3% TX-100 for 1 h at RT and then overnight at 4°C. Negative controls were obtained by treating the sections with a non-reactive IgG isotype at the same concentration in place of the primary antibody incubation. After incubation in the primary antibodies, sections were thoroughly washed and incubated in secondary antibodies for 30 min at RT and rinsed 3

times in PBS, followed by incubation in ABC solution (Vector Laboratories) according to the manufacturer's protocol. Next, sections were developed in Vector® VIP or AEC (Vector Laboratories) chromogenic reactions for 2-5 min. Sections developed in VIP (purple labeling) were counterstained with Methyl Green (Vector Laboratories) for 1 min at RT then rinsed, dehydrated and coverslipped with Permount (Thermo Fisher Scientific, Waltham, MA) for light microscopy. Sections developed in AEC (red labeling) were counterstained with Mayer's Hematoxylin (Sigma Aldrich, St. Louis, MO) for 1 min at RT and then rinsed and coverslipped with aqueous mounting medium VectaMount (Vector Laboratories).

Sections from each animal in the two groups (Aβ + vehicle and Aβ + vinpocetine, N=5 per group) were processed at the same time to allow direct comparisons of chromogenic intensity. Four sections were examined per animal for each antibody in a masked fashion. Within each section, an intact, 1500 μm linear strip of retina centered on the optic nerve was evaluated with a ×40 objective lens (Eclipse 80i; Nikon, Tokyo, Japan). As NF-κB translocates to the nucleus when the NF-κB pathway is activated, we counted immunoreactive NF-κB nuclei in the RPE layer. Both positively labeled nuclei and non-labeled nuclei were counted in each 1500 μm field, and mean percentages of labeled nuclei (compared to total nuclei) were obtained.

Semi-quantitative analysis for caspase-1, NLRP3, IL-18, IL-1β and TNF-α was carried out in a masked manner. Within each 1500 μm field, the RPE, BM, and choroid were analyzed. Immunostaining intensity was scored from 0 to 3. A score of 0 indicates no detectable staining above background as determined by comparison with the negative control sections. The most intense immunoreactivity was classified as a score of 3. For intermediate intensity levels, a score

of 1 was given to samples with the weakest immunolabeling, while a score of 2 represented intermediate immunolabeling. Examples of semi-quantitative scoring are shown on Figures 4-2, 4-3. The mean semi-quantitative score of Aβ + vinpocetine was normalized to that obtained from Aβ + vehicle, which was set at 100% (Figure 4-2, 4-3).

4.2.6 Western blot

Western blot was employed to further distinguish the proportion of active and inactive caspase-1 in the treatment groups. Vehicle and vinpocetine treated rat retina-RPE-choroid tissues were isolated microsurgically and immersed in 200 μL of ice-cold RIPA buffer (Thermo Scientific, Rockford IL) containing protease inhibitor cocktail (Roche Diagnostics, Indianapolis IN). The tissues were completely homogenized using rotor-stator homogenizer and supernatant was obtained by centrifugation at 14,800 g for 10 min at 4°C. Total protein concentration was quantitated using BCA Protein Assay kit (Thermo Scientific, Rockford IL). Protein samples were treated in reducing conditions (2x SDS loading buffer with 2% β-mercaptoethanol) and boiled at 100°C for 5 min. The treated samples were directly subjected to 5-12.5% SDS-PAGE. 50 μg of total protein was loaded in each lane. N=5 for SDS-PAGE from each group. The gel was transferred to a PVDF membrane and the membrane was blocked in blocking buffer (PBS containing 5% skim milk and 0.2% Tween-20) at RT for 1 h. The membrane was then incubated in blocking buffer containing 1:1,000 diluted primary mouse antibody against caspase-1 (R&D Systems, Minneapolis MN) at 4°C for overnight. Finally, the membrane was incubated in blocking buffer containing 1:1,000 diluted secondary anti-mouse antibody conjugated with HRP (R&D systems, Minneapolis MN) at RT for 2 h. Standard enhanced chemiluminescence (ECL) method (Thermo Scientific, Rockford IL) was used to detect the intensity of full length (45 kD)

and cleaved (20 kD) caspase-1 protein bands from vehicle and vinpocetine treated samples. For the purpose of GAPDH detection as loading control, the same membrane from the caspase-1 study was stripped in stripping buffer (Tris-HCl, pH 6.8: 1 mM, SDS: 1%, β-mercaptoethanol: 1%) at RT for overnight. The above blotting method was repeated with a 1:10,000 diluted primary mouse antibody against GAPDH (EMD Millipore, Billerica MA). The intensity of cleaved caspase 1 (20 kD) and GAPDH (36 kD) protein bands was measured using ImageJ (NIH, Bethesda MD). The final relative intensity of cleaved caspase-1 was normalized with respect to the corresponding GAPDH intensity.

Antigen	Type	Dilution	Specificity	Source and catalog no.
Phosphorylated NF-κB p65	Rabbit Polyclonal	1:75	Detects Ser 276 residue in phosphorylated NF-κB p65 of mouse, rat and human origin.	Santa Cruz Biotechnology, Dallas, TX; sc-101749
Interleukin-1 beta (IL-1β)	Goat Polyclonal	1:400	Detects rat IL-1 β/IL-1F2 in cultured cells or tissue sections	R&D Systems, Minneapolis, MN; AF-501-NA
Interleukin-18 (IL-18)	Rabbit Polyclonal	1:100	Detects IL-18 of mouse, rat and human origin.	Santa Cruz Biotechnology, Dallas, TX; sc-7954
NLR family, pyrin domain containing 3 (NLRP3)	Goat Polyclonal	1:1000	Recognizes the C-terminus of human NLRP3. Cross-reacts with rat.	AbD Serotec (Bio-Rad), Hercules, CA; AHP1774
Caspase-1	Rabbit Monoclonal	1:300	Recognizes human caspase-1 amino acid 250 to C-terminus (both pro-peptide and cleaved peptide). Cross-reacts with rat and mouse.	Abcam, Cambridge, UK; ab108362
Tumor necrosis factor-alpha (TNF-α)	Rabbit Polyclonal	1:1000	Detects TNF-α existing in forms of Type II membrane protein and extracellular soluble protein in human, mouse and rat.	Abcam, Cambridge, UK; ab66579
Caspase-1 (WB)	Mouse Monoclonal	1:1000	Recognizes P20 subunit of human caspase-1. Cross-reacts with rat and mouse.	R&D Systems, Minneapolis, MN; MAB6215
GAPDH (WB)	Mouse Monoclonal	1:10,000	Recognizes 36 kD monomeric subunit of rabbit GAPDH. Cross-reacts with rat.	EMD Millipore, Billerica, MA; CB1001

Table 4-1 List of primary antibodies used in Chapter 4.

4.2.7 Suspension array assay

An ELISA-based cytokine assay was carried out using the Bio-Plex 200 System (Bio-Rad Laboratories). As part of the *in vivo* experiment, rat vitreous was collected during dissection and aliquoted (N=8). Samples, standards and blanks were prepared according to manufacturer's instructions. Signals were generated using biotinylated detection antibody and SAPE. Raw MFI data was captured and analyzed using Bio-Plex Manager software 4.1 (Bio-Rad Laboratories), under a standard high photomultiplier tube setting. Vitreous cytokine concentrations were determined in pg/mL. Normalized fold change was calculated as a ratio of cytokine concentrations in the Aβ+vinpocetine group over Aβ + vehicle group. The negative reciprocal of this result is plotted, i.e. fold change less than -1 indicates higher cytokine concentration in the vehicle group than vinpocetine group.

4.2.8 Statistical analyses

For the *in vitro* NF-κB activation study, comparisons were made between vehicle control and the vinpocetine treatment groups, respectively. In addition, the Aβ only group was compared to Aβ + vinpocetine group. Similarly, the TNF-α only group was compared to TNF-α+BAY and TNF-α + vinpocetine groups. Statistical analysis of results of RT-PCR studies was performed using one-tailed Student's *t*-test (GraphPad Software) and significance level at $p \leq 0.05$.

Statistical analysis for semi-quantitative data from IL-1β, IL-18, TNF-α, NLRP3, and caspase-1 immunohistochemistry in the *in vivo* studies was undertaken using the non-parametric Mann-Whitney *U* test, with significance set at $p \leq 0.05$ (GraphPad Software). The statistical analysis

for NF-κB p65 subunit was performed on the cell counts of positively labeled relative to unlabeled nuclei in the RPE layer. Student's *t*-test was used to determine the significance, which was set at $p \leq 0.05$.

Western blot data of full length and cleaved forms of caspase-1 were analyzed by first normalizing the 20 kD band intensity to that of the GAPDH band, and then comparing between Aβ + vehicle and Aβ + vinpocetine groups. Mann-Whitney *U* test was used to determine the statistical significance, which was set at $p \leq 0.05$.

Suspension array data was obtained via the Bio-Plex Manager software 4.1 (Bio-Rad Laboratories). The cytokine concentration in the Aβ + vinpocetine group was compared to that of the Aβ + vehicle group and a Mann-Whitney *U* test was used to determine the statistical significance, with $p \leq 0.05$ considered significant.

4.3 Results

4.3.1 NF-κB activation is induced by Aβ and suppressed by vinpocetine *in vitro*

The mechanism of NF-κB inhibition by vinpocetine has been examined in blood and epithelial cell types[167] but not in an ocular cell type. To investigate NF-κB activation, we transfected ARPE-19 with an NF-κB-luciferase plasmid, selected and established a reporter cell line. When challenged by TNF-α, a known stimulator of NF-κB, ARPE-19/NF-κB reporter cells demonstrated a robust NF-κB response (Figure 4-1A), consistent with the nature of RPE as an active cell with pro-inflammatory capabilities. Vinpocetine markedly suppressed this response,

as did BAY11-7082, a classic NF-κB inhibitor (Figure 4-1A), suggesting that ARPE-19 is susceptible to vinpocetine, and vinpocetine is as effective as BAY11-7082.

Given that NF-κB is readily activated in ARPE-19 cells, we next investigated whether NF-κB is involved in Aβ-mediated inflammatory pathway. ARPE-19/NF-κB reporter cells treated with 1 μM Aβ showed a 1.92 ± 0.25 fold increase (mean ± SD, $p<0.01$) in NF-κB activation (Figure 4-1A) compared to DMSO control group. In contrast, the group treated with both Aβ and vinpocetine showed significantly reduced NF-κB activation relative to the Aβ-alone group (0.91 ± 0.21 fold, $p<0.05$), to a level comparable to that of the control group. Treatment of RPE cells with 50 μM vinpocetine without Aβ decreased the level of NF-κB activation below control (0.49 ± 0.05 fold, $p<0.01$) (Figure 4-1A). This likely reflects the inhibition of constitutive NF-κB activation that is present in ARPE-19/NF-κB reporter cells.

4.3.2 NF-κB activation is induced by Aβ and suppressed by vinpocetine *in vivo*

Next, we followed up the cell culture study by assessing the activation of NF-κB *in vivo* using rats that received intraocular Aβ and IP injection of either vinpocetine or vehicle. Intraocular injection has been shown to effectively deliver Aβ peptide to the outer retina and RPE in earlier studies without the confounding effect of mechanical disturbances to the RPE layer due to subretinal delivery.[113] Parenteral route for vinpocetine administration was chosen due to its good blood-brain (and hence blood-ocular) penetration, and poor oral bioavailability.[176] Using a primary antibody against the phosphorylated p65 subunit of NF-κB, we probed the RPE layer in retinal cross section. NF-κB is sequestered in the cytoplasm in the inactive state and translocates into the nucleus when activated by phosphorylation. The nuclear presence of the p65 subunit

therefore is an indicator of NF-κB activation. The control group receiving intravitreal Aβ and a vehicle IP injection (Aβ + vehicle) demonstrated intense NF-κB labeling within the RPE nucleus (arrows, Figure 4-1B, left bottom). In contrast, the treatment group that received intravitreal Aβ and a vinpocetine IP injection (Aβ + vinpo) showed a predominance of nuclei without intranuclear NF-κB immunolabeling (Figure 4-1B, left top). The absence of nuclear translocation indicates a lack of NF-κB activation in the RPE in the vinpocetine treated animals. Quantitative analysis revealed that vinpocetine treatment reduced the number of NF-κB positive RPE nuclei by 50% (Figure 4-1B, right). Similar effects of vinpocetine treatment have been noted in microglia,[177] vascular smooth muscle cells, umbilical vein endothelial cells and lung epithelial cells.[167]

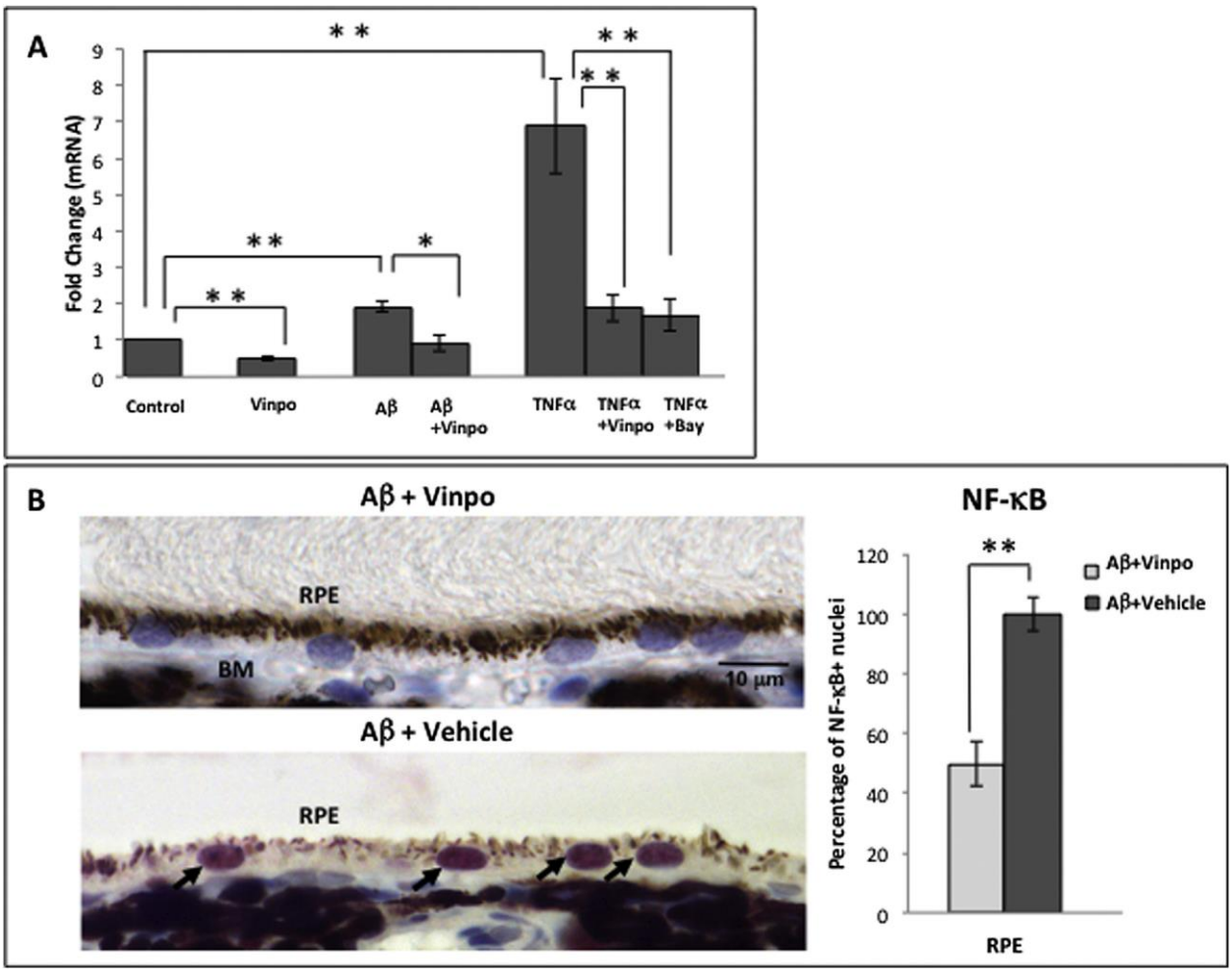

Figure 4-1 NF-κB activation is stimulated by Aβ and inhibited by vinpocetine in the RPE.

(A) ARPE-19/NF-κB-luciferase reporter cells were first challenged with TNF-α to determine NF-κB activation in this cell type, and if this response is susceptible to inhibition. Data are presented as mRNA fold change normalized to control conditions. TNF-α (2.5 ng/mL) stimulation resulted in a 7-fold increase in NF-κB activation in ARPE-19 reporter cells. An established NF-κB inhibitor, BAY11-7082 (10 mM), suppressed NF-kB activation by more than 3 fold. Vinpocetine (50 mM) also inhibited TNF-α-induced NF-κB activation by more than 3 fold. Stimulation with Aβ (1 mM) resulted in a nearly-2 fold increase in NF-κB activation and co-treatment with vinpocetine (50 mM) diminished this NF-κB activation. Treatment with vinpocetine alone reduced NF-κB activation level to less than that of control. Data are represented as the mean and error bars denote standard deviation (SD). Statistical analysis was performed using a one-tailed Student's *t*-test, *$p < 0.05$, **$p < 0.01$ (N = 3). (B) Adult rats received an intravitreal injection of 5 μL at 1.4 μg/μL $A\beta_{1\text{-}40}$ (oligomeric form) and an intraperitoneal injection of either vinpocetine (15

mg/kg) or vehicle (2.5% DMSO). Immunohistochemistry was used to highlight NF-κB labeling intensity and nuclear translocation of NF-κB in the RPE. The Aβ + vehicle group demonstrated intense red AEC labeling of NF-κB concentrated in the RPE nucleus (arrows), while Aβ + vinpo group displays minimal NF-κB immunoreactivity. Tissue sections were counterstained with hematoxylin resulting in blue nuclei, and the combination of blue counterstain with red AEC chromogen results in purple nuclei signifying activated NF-κB in the Aβ + vehicle retina. Note that Aβ + vinpo retina illustrated blue (not purple) nuclei, identifying lack of nuclear translocation of NF-κB. Scale bar: 10 μm. Total number of RPE nuclei and NF-κB immunopositive nuclei were counted in 4 retinal cross sections per animal (N = 5 per group). Histogram represents the mean and error bars denote standard error of mean (SEM). Statistical analysis was performed using Mann-Whitney *U* test, $*p < 0.05$, $**p < 0.01$.

4.3.3 Vinpocetine reduced the expression of NLRP3-related genes and pro-inflammatory cytokines *in vivo*

The NLRP3 inflammasome is a critical cellular apparatus for the detection of noxious stimuli, including Aβ, and the subsequent production of mature pro-inflammatory cytokines to defend against cellular insults.[123, 162] NF-κB has been proposed as a prerequisite priming mechanism for inflammasome activation.[33, 168] Based on the premise that NLRP3 inflammasome activation relies on NF-κB, we evaluated whether vinpocetine can inhibit inflammasome and its ability to produce cytokines.

We first assessed for the expression of cytosolic protein caspase-1 in retinal tissues. Caspase-1 is synthesized as a pro-peptide and must be cleaved in the inflammasome complex to become the active species. Analysis of retinal sections in the Aβ + vinpo group revealed that vinpocetine reduced total caspase-1 immunoreactivity (both cleaved and full length caspase-1) by more than 50% in the RPE (Figure 4-2A). We next examined NLRP3 protein within RPE cytoplasm.

Following vinpocetine treatment, there was a dramatic decrease of 80% in NLRP3 immunolabeling intensity compared to vehicle treatment (Figure 4-2B, left). Inspection of the RPE layer revealed relatively weak immunoreactivity in the Aβ + vinpo group compared to the conspicuous cytoplasmic labeling of NLRP3 in the Aβ + vehicle group (Figure 4-2B, right).

IL-18 and IL-1β are end products of NLRP3 inflammasome activation and are secreted by the RPE. BM and the choroid were included in the analysis of secreted cytokines given their close proximity to the RPE and role in progressive AMD changes. IL-18 immunoreactivity in the Aβ + vinpo group was greatly reduced in the RPE, choroid, and BM (Figure 4-2C, left). Immunohistological sections of the Aβ + vehicle group showed prominent IL-18 labeling intracellularly in the RPE and in the choroidal cells and in BM (Figure 4-2C). The immunolabeling pattern of IL-1β closely mirrored that of IL-18; vinpocetine treatment significantly decreased immunohistochemical levels of IL-1β in the RPE and choroid (Figure 4-2D). Lower level of these cytokines within the cellular cytoplasm and in the extracellular matrix suggests suppression of both the pro-peptides and the secreted mature protein products in animals treated with vinpocetine.

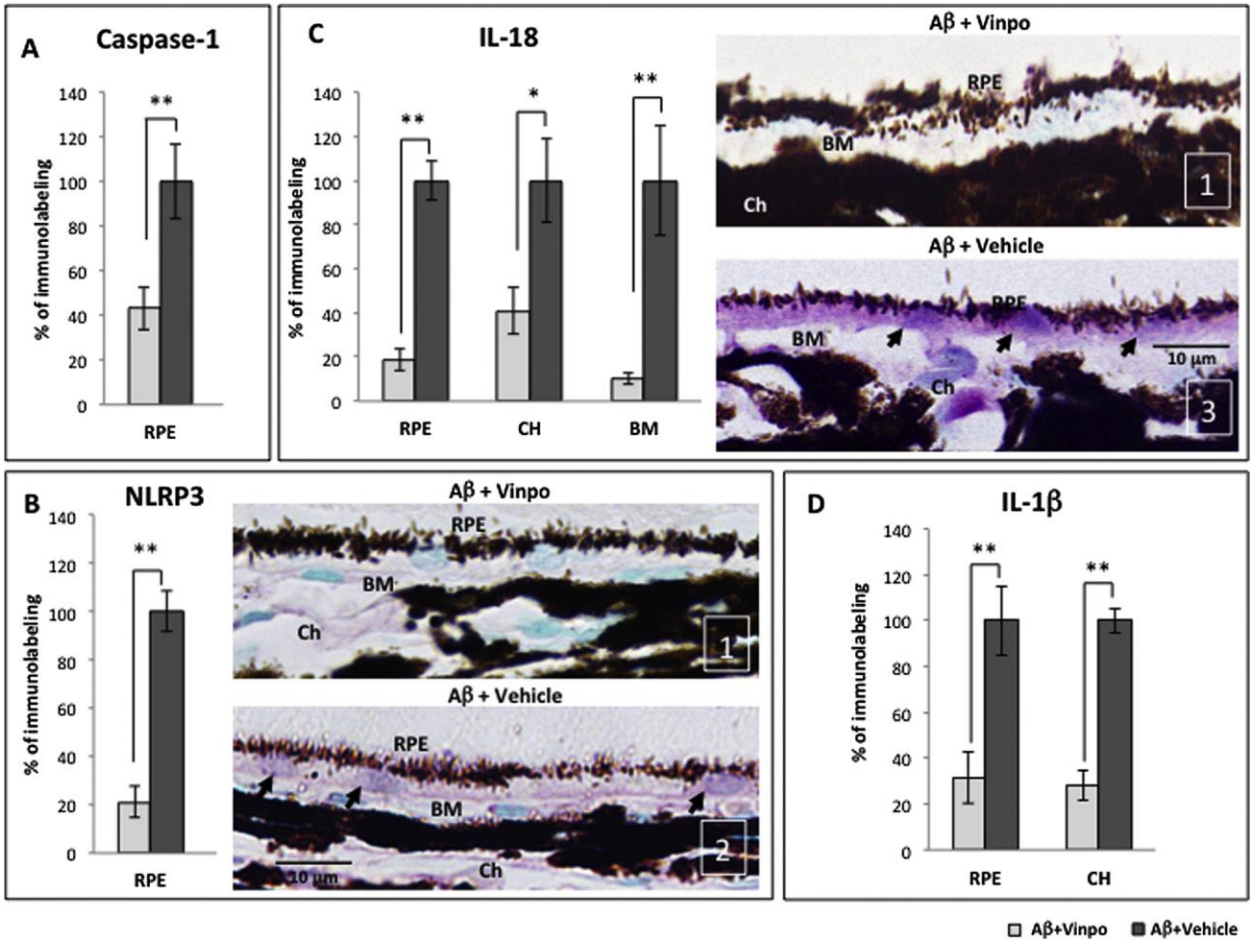

Figure 4-2 Vinpocetine reduced the expression of NLRP3-related components and pro-inflammatory cytokine products *in vivo*.

(A) Immunoreactivity of total caspase-1 (pro-peptide and cleaved forms) is reduced by vinpocetine in the RPE of Aβ-treated animals (Aβ + vinpo), compared to the vehicle group (Aβ + vehicle). The semi-quantitative immunoreactivity score in Aβ + vinpo rats was normalized to that obtained from the Aβ + vehicle group which was set at 100% in all graphs. (B) Vinpocetine suppressed the amount of NLRP3 protein in the RPE of Aβ-treated animals compared to the vehicle group. Representative pictures from Aβ + vinpo rats and Aβ + vehicle rats are shown (right). Positive immunoreactivity of RPE (arrows) is purple due to VIP chromogen. Nuclei appear green due to counterstaining with Methyl Green. Representative semi-quantitative scoring is shown in the lower right corner of the micrograph (white) and indicates immunoreactivity intensity, from 1 (weakest) to 3 (most intense). (C) Vinpocetine caused a 60-80% decrease in IL-18 level in the outer retina (RPE, BM and choroid) compared to the

vehicle group. Representative micrographs reveal prominent IL-18 immunoreactivity within the RPE (purple, arrows) in Aβ + vehicle animals. In contrast, the cross section from Aβ + vinpo animals exhibited minimal IL-18 immunoreactivity. (D) The immunoreactivity of IL-1b in the RPE and choroid was suppressed by vinpocetine in Aβ-injected eyes. Scale bar: 10 μm. Immunoreactivity was scored in 4 retinal cross sections per animal (N = 5 per group). Histogram represents mean and SEM. Statistical analysis was performed using a Mann-Whitney *U* test, $*p < 0.05$, $**p < 0.01$.

4.3.4 Vinpocetine decreased TNF-α expression

The NLRP3 inflammasome is one of many pro-inflammatory pathways regulated by NF-κB. *In vivo* stimulation of RPE with Aβ also provoked increased expression of TNF-α, a powerful cytokine associated with NF-κB signaling[170] but not dependent on inflammasome processes. TNF-α has important ocular effects, thus we assessed the effect of vinpocetine on Aβ-induced TNF-α expression. Immunohistochemistry results demonstrated that vinpocetine significantly inhibited the production of TNF-α to less than 50% of the vehicle control level in the RPE, choroid and BM (Figure 4-3A). Immunohistochemistry demonstrated intense TNF-α labeling in the RPE cytoplasm, the cytoplasm of choroidal cells and in the extracellular matrix including BM (Figure 4-3C). Sections from the vinpocetine treatment group demonstrated significantly less TNF-α immunoreactivity in the outer retinal layers (Figure 4-3B). This observation supports the inhibitory effect of vinpocetine on non-inflammasome associated NF-κB pathways, in keeping with its putative mechanism of action.

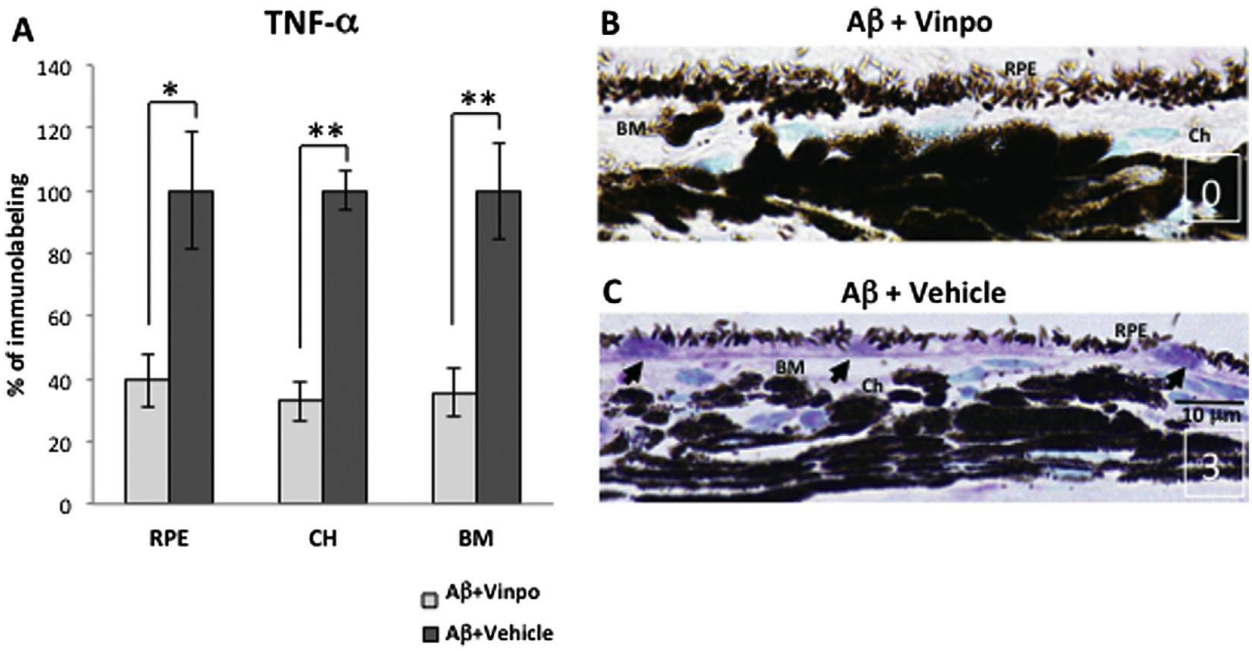

Figure 4-3 Vinpocetine decreased non-inflammasome-related cytokine TNF-α expression.

(A) Vinpocetine significantly reduced the immunoreactivity of TNF-α in the RPE, choroid (CH) and Bruch's membrane (BM) by approximately 60%. (B, C) Representative micrographs from Aβ + vinpo rats and Aβ + vehicle rats are displayed. The positive immunoreactivity is shown in purple due to the VIP chromogen. The nuclei appear green due to the counterstaining with Methyl Green. Representative semi-quantitative scoring is shown in the lower right corner of the micrographs (white) and indicates immunoreactivity intensity, with "0" indicating background levels (observed in control cross sections in which the primary antibody was replace with a non-specific IgG), and "3" indicating the highest immunoreactivity intensity level. Intense TNF-α labeling was seen in the RPE cytoplasm, the cytoplasm of choroidal cells and in the extracellular matrix including BM from Aβ + vehicle animals (C), while the immunoreactivity in Aβ + vinpo eye demonstrated significantly less TNF-α immunoreactivity in the outer retinal layers (B). Scale bar: 10 µm. Immunoreactivity was scored in 4 retinal cross sections per animal (N = 5 per group). Histogram represents the mean and SEM. Statistical analysis was performed using a Mann-Whitney *U* test, *$p < 0.05$, **$p < 0.01$.

4.3.5 Western blot verifies suppression of caspase-1 activation

Quantitative analysis of NF-κB translocation to the RPE nucleus and the semi-quantitative analysis of cytokines in immunohistochemical studies point to a strong inhibitory effect of vinpocetine on NF-κB and its downstream pathways in the outer retina. However, because retinal immunohistochemistry could not distinguish between the pro- and cleaved forms of caspase-1, it was not clear if inflammasome activation was suppressed by vinpocetine treatment. To further study this, western blot was performed on cell lysates from retinal tissues obtained from Aβ + vinpo and Aβ + vehicle treated rats. Cleaved caspase-1 bands (20 kD) were significantly reduced in the vinpocetine treatment group, indicating suppression of inflammasome activation (Figure 4-4A). Normalizing the 20 kD band luminescence to the housekeeping gene GADPH eliminates potential difference in amount of total protein loaded. The cleaved caspase-1 protein is dramatically diminished by 86% compared to the vehicle treated group (p<0.05, Figure 4-4B).

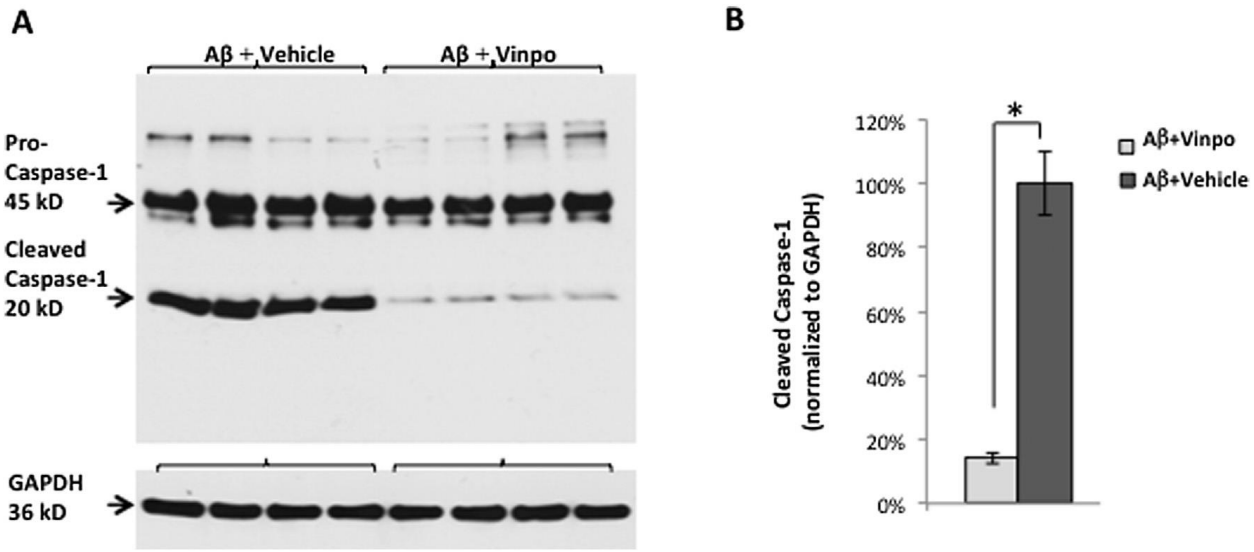

Figure 4-4 Western blot of caspase-1 shows a significant reduction in the cleaved portion of the peptide in the vinpocetine-treated group.

(A) Protein lysate (including neuroretina, RPE and choroid) from Aβ + vehicle group shows intense bands at 45 kD and 20 kD, corresponding to the uncleaved (pro-peptide) and cleaved (active) forms of caspase-1, respectively. Vinpocetine markedly reduced the 20 kD band intensity consistent with a decrease in caspsase-1 activation. GAPDH (36 kD) was used to visualize protein loading levels. (B) Standard ECL method was used to quantify the 20 kD band luminescence normalized to that of GAPDH. The cleaved (active) caspase-1 peptide is reduced by greater than 80% in the Aβ + vinpo group compared to the Aβ + vehicle group (N = 5 per group). Histogram represents the mean and SEM. Statistical analysis was performed using a Mann-Whitney *U* test, $*p < 0.05$.

4.3.6 Vinpocetine led to decreased intravitreal cytokine concentration

The over-expression of pro-inflammatory cytokines generated by Aβ is not only present locally in the outer retina but also evident in the vitreous.[113] Here we measured the effect of vinpocetine on secreted cytokines in the vitreous. The levels of cytokine in the vitreous from animals that received Aβ and vinpocetine was compared with those that received Aβ and vehicle and the results normalized as fold change. IL-1β (-3.00±0.15 fold) and IL-18 (-2.54±0.35 fold), mature secreted products associated with NLRP3 inflammasome activation, were all statistically significantly lowered in vitreous from the Aβ + vinpo group, consistent with immunohistochemical results demonstrating a lowering of these cytokines by vinpocetine treatment. Three other cytokines and chemokines demonstrated statistically significant and greater than 2.0 fold reduction by vinpocetine: MIP-3α (-5.39±0.23 fold), IL-6 (-4.74±0.58 fold), IL-1α (-4.19±0.41 fold), and TNF-α (-2.12±0.19 fold) (Figure 4-5). These cytokines represent NF-κB activation products and chemokines that are produced by RPE, and immune cells such as lymphocytes and microglia, and function in different arms of the immune response pathway.[150, 178, 179]

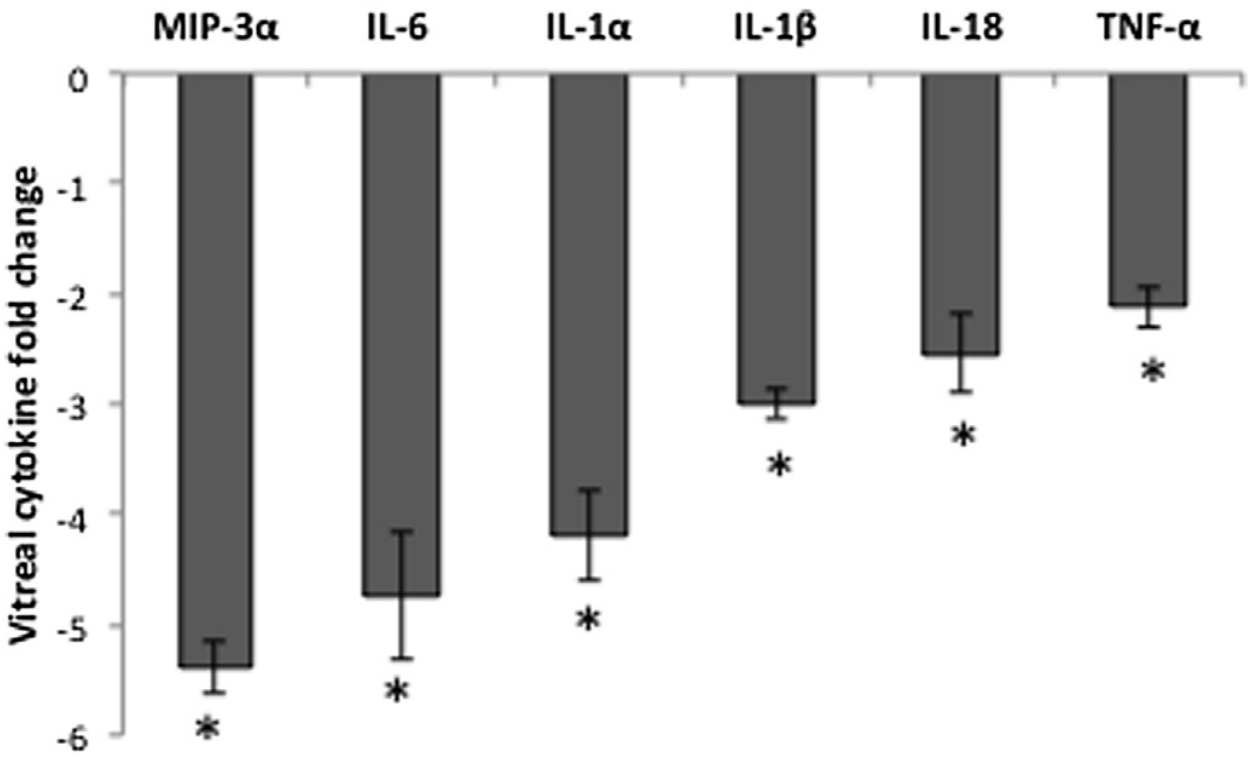

Figure 4-5 Vinpocetine reduces secreted cytokines in the vitreous after Aβ injection

Vitreous from vinpocetine and vehicle-treated animals (N = 8 per group) were pooled, and assayed using an ELISA based suspension array. Fold change was obtained by dividing the concentration of cytokine (in pg/mL) in the vehicle group by that of the vinpocetine group; negative sign denotes a downregulation due to vinpocetine treatment. Concentrations of secreted MIP-3α, IL-6, IL-1α, IL-1β, IL-18, and TNF-α were reduced by at least 2-fold in the Aβ + vinpo group. Histogram represents the mean and SEM comparisons of the Aβ + vinpo and Aβ + vehicle. Statistical analysis was performed using a Mann-Whitney *U* test, $*p < 0.05$.

4.4 Discussion

New evidence is emerging to support the role of specific inflammatory mechanisms in response to drusen components and how these pathways may contribute to the development of AMD. Although the majority of disease burden from vision loss derives from the advanced forms of AMD, it is known that drusen accumulation starts decades earlier and may promote a chronic

state of parainflammation in the outer retina.[92, 117, 180] Therefore, effective early AMD intervention necessitates the understanding of these inflammatory events and towards the identification of valid cellular targets. The present study focuses on a novel therapeutic agent, vinpocetine, in an animal model of the subclinical stages of AMD, and expands on our earlier findings by further exploring the pro-inflammatory effect of a drusen component, Aβ, on the RPE. In this model, a single intravitreal injection of a drusen component, Aβ, results in an pro-inflammatory milieu and inflammasome activation in the outer retina that emulates features that are hypothesized to exist in early AMD, without inducing features of late AMD such as cell death (GA) or angiogenesis (CNV).[113] By using an intravitreal, rather than a subretinal delivery, unnecessary complications due to mechanical disruption of the RPE layer are avoided in this model.

NF-κB is an important transcription factor that facilitates a wide range of cellular processes pertaining to inflammation, immune response, cell survival and proliferation. Given that inflammation is considered a driving force behind the development of AMD, it is logical to consider NF-κB as a potential key mediator of pathogenesis. Indeed, our results support that Aβ, a physiologic peptide in drusen, stimulates NF-κB activation in the RPE (Figure 4-1). NF-κB is constitutively expressed by the RPE and is activated by diverse signals such as monocytes co-culture,[132] TNF-α, IL-17A,[181] and *Alu* RNA.[34] Vinpocetine was highly effective at suppressing Aβ-induced NF-κB activation in the RPE both *in vitro* and *in vivo*. Vinpocetine (trade name Cavinton®) is a dietary supplement widely used in Europe and Asia for prevention against stroke and memory loss[182] due to its vasoactive and neuroprotective properties. More recently it was shown to inhibit NF-κB associated inflammatory pathway by inactivating IKK.[167] IKK normally

phosphorylates the inhibitory IκB molecule, which then releases NF-κB to enter the nucleus. Thus, by inactivating IKK, vinpocetine in effect would keep NF-κB sequestered in the cytoplasm. Our results demonstrated that vinpocetine inhibited NF-κB activation and nuclear translocation *in vitro* and *in vivo*, in keeping with the aforementioned mechanism (Figure 4-1). These results suggest that NF-κB plays an active role in the pro-inflammatory state induced by drusen components in the outer retina and is suppressed by vinpocetine.

NLRP3 inflammasome is implicated in a growing list of conditions including sepsis, gout, diabetes mellitus and atherosclerosis.[183] Numerous studies have established a role for NLRP3 inflammasome in promoting inflammation and RPE damage in response to factors associated with macular degeneration such as lysosomal destabilization,[32] oxidative stress,[145] and *Alu* RNA.[36] The present study highlights drusen component Aβ as an important stimulus for inflammasome activation in the RPE, in keeping with similar observation of Aβ's effect in microglia.[123]

Although vinpocetine is not known to directly interfere with NLRP3 inflammasome assembly or activation, it effectually suppressed inflammasome activation and the production of cytokines in our study (Figure 4-2), presumably in a NF-κB-dependent manner. The NLRP3 inflammasome is tightly regulated and its activation requires two signals.[162] NF-κB is an essential priming signal that promotes the expression of inflammasome components as well as that of the substrates IL-1β and IL-18.[33] Aβ oligomers and other misfolded proteins can serve as the second, activating signal that triggers inflammasome assembly.[162] By preventing NF-κB activation, vinpocetine inhibits the expression of downstream pathways. Our data demonstrated a decrease in the synthesis of

NLRP3 protein, which logically should lead to less inflammasome complex assembly and the recruitment of caspase-1. Without being incorporated into the NLRP3 complex, pro-caspase-1 cannot be cleaved and remains in its full-length form (Figure 4-4). Consequently, NLRP3 inflammasome overall is inactive and there is less IL-1β and IL-18 being secreted locally (Figures 4-2C, D). We noted that there was no marked difference in the intensity of pro-caspase-1 band on Western blot between vinpocetine and vehicle groups (Figure 4-4), which appeared to indicate that the expression of pro-caspase-1 is not inhibited by vinpocetine. Immunohistochemistry of caspase-1 showed significant decrease in total caspase-1 labeling, but it is rather unlikely that cleaved peptide accounted for the entirety of the 50% difference between vinpocetine and vehicle groups (Figure 4-2A). One explanation would be that western blot included the retina and choroid tissue which would have contributed more pro-caspase-1 protein to the lysate sample. Because the total cellular mass of choroid and retina is orders of magnitude greater than that of the RPE, even a small quantity of caspase-1 protein in any individual cell would obliterate the difference in pro-caspase-1 band intensity on western blot.

In addition to blocking inflammasome activation, vinpocetine has a suppressive effect on a multitude of cytokines due to the central position of NF-κB in the immune-response cascade. We determined that vinpocetine decreases the intracellular labeling (Figure 4-2) of IL-18 and IL-1β in the RPE and secreted in the vitreous (Figure 4-5), indicating a reduction in the pro-peptides and further disabling of the NLRP3 inflammasome pathway. NF-κB inhibition also impaired the secretion of non-inflammasome related cytokines in the vitreous, including TNF-α (Figure 4-3), IL-6, IL-1α, and MIP-3α (Figure 4-5). TNF-α propagates NF-κB activation and its presence in the outer retina has been shown to facilitate photoreceptor death.[124] IL-6 is a powerful cytokine

that mediates inflammatory response in a variety of disease states and is implicated in the progression of AMD.[131] IL-1α is a homolog of IL-1β but is cleaved by the protease calpain instead of caspase-1,[184] although more recent evidence suggests there is a partial association between IL-1α and NLRP3 inflammasome.[185] MIP-3α exerts chemotaxic effect on lymphocytes and was highly elevated in the vitreous post-intravitreal Aβ injections in rats.[113] Taken together, these affected cytokines may act on different aspects of the inflammatory pathway in all cells of the retina.

Among the limitations of the present study, the time course of this study did not allow us to delineate the effect of a chronic inflammatory cytokine exposure on RPE physiology or any potential benefit of vinpocetine long term (i.e. greater than 4 days). As such, further studies with an expanded time frame are needed to assess the utility of vinpocetine in early AMD. While this study demonstrated that vinpocetine inhibited Aβ-induced NF-κB activation, additional questions remain: (1) The pathway by which Aβ activates NF-κB remains under investigation; recent evidence suggests that receptor for advanced glycation endproduct (RAGE) and Toll-like receptor 4 (TLR4) are involved in Aβ recognition and subsequent NF-κB signaling.[186, 187] (2) Used as the vehicle to dissolve vinpocetine in this study, DMSO has been shown previously to have profound anti-inflammatory effects and can suppress NF-κB activation.[188] To separate vinpocetine's anti-inflammatory effects from DMSO's potential influence *in vitro*, we chose the DMSO-treated ARPE-19/NF-κB reporter cells as the control group and compared all other groups to it. However, in the *in vivo* study, comparisons were drawn between the Aβ + vehicle (i.e. DMSO) group and the Aβ + vinpocetine group that contained the same amount of DMSO. One limitation of this animal study design is the lack of a treatment naïve group (i.e. the Aβ

injection only group), which could have helped evaluate DMSO's anti-inflammatory effects *in vivo*. (3) NF-κB is a non-specific transcription factor that is not only involved in chronic inflammation related to degenerative changes but also important in acute inflammatory response to cellular insults such as infection or injury, as well as in wound healing. Complete inhibition of this crucial transcription factor may affect other cellular processes with unforeseen consequences. However, given vinpocetine is presently used as a dietary supplement in Europe and Asia,[182] a clinical evaluation of these populations may provide the answer to the long term sequelae of an NF-κB inhibitor.

4.5 Conclusion

In our earlier study, we found that the transcription factor NF-κB is implicated in RPE's response to Aβ by providing the priming signal for NLRP3 inflammasome activation and the synthesis of pro-inflammatory cytokines. Systemic vinpocetine, a well-tolerated anti-inflammatory agent, inhibited NF-kB activation in the RPE as well as NF-κB-dependent processes including inflammasome activation and cytokine production. NF-κB is a key upstream regulator of the inflammatory pathways that is not only activated by Aβ but is likely involved in the RPE's response to other pathological, age-related stimuli and drusen components such as carboxyethylpyrrole (CEP) and advanced glycation endproduct (AGE).[180] NF-κB inhibition may be a useful approach to control the chronic inflammation that is believed to drive the degenerative processes in early AMD, but more studies are needed to ascertain other cellular changes that may be affected by long-term inhibition of this important transcription factor.

Chapter 5: Evidence for the activation of pyroptotic and apoptotic pathways in RPE cells associated with NLRP3 inflammasome in the rodent eye

5.1 Introduction

Age-related macular degeneration (AMD) is a neurodegenerative disease that strikes the macula, causing irreversible blindness to people over the age of 50 in industrialized countries. The global prevalence of AMD has created a substantial economic and social burden with a projected estimate of 196 million people living with AMD in 2020.[189] Clearly, better eye-care strategies need to be designed to provide health care services to those in need. Clinically, AMD can be predicted by a severity scale that is a function of drusen deposition and pigment abnormalities.[190] The accumulation of drusen both in size and in number has become a hallmark of AMD progression. As it progresses, AMD transitions from early benign stages into advanced vision-threatening stages, presenting with either choroidal neovascularization (CNV, wet form) and/or geographic atrophy (GA, dry form). Although CNV is the severe subtype of the advanced AMD, it is clinically managed using the anti-vascular endothelial growth factor (VEGF) therapy.[191] However, there is no effective treatment to slow down the more prevalent dry form, which makes up approximately 90% of all AMD cases. Retinal pigment epithelium (RPE) cell death and secondary photoreceptor degeneration are two signature changes that lead to central vision loss in GA, the advanced stage of dry AMD. Hence, it is paramount to understand the fundamental mechanisms underlying these devastating impacts to the retina, especially the ones that undermine RPE health.

Despite the lack of consensus on the exact cell death pathway(s) involved, there have been three candidate cell death mechanisms proposed to underlie RPE atrophy in GA, including necrosis, apoptosis, and pyroptosis.[36, 69, 70] Necrosis is a classic form of RPE cell death in GA, which was reported in earlier clinical-pathological studies by Sarks et al.,[69] and also in basic research projects with ultrastructural and histochemical data.[117] Apoptotic RPE cell death, on the other hand, has gained substantial support from the literature in recent years. Using postmortem human eyes, Kaneko and colleagues identified the activation of caspase-3 in the RPE layer of GA eyes, but not in normal control eyes.[70] Moreover, Dunaief et al. demonstrated statistically significant differences in the number of terminal deoxynucleotidyl transferase dUTP nick end-labeling (TUNEL) positive retinal cells in postmortem retinas with AMD, compared to normal controls.[154] The third proposed mechanism of RPE death is pyroptosis, which is an inflammatory form of programmed cell death.[192] The cornerstone of pyroptosis is the activation of an intracellular multi-protein complex named the inflammasome. NLR family pyrin domain containing 3 (NLRP3) inflammasome is the most widely studied machinery, and consists of NLRP3, active caspase-1 and a bridging adaptor, apoptosis-associated speck-like protein containing a carboxy-terminal CARD (ASC). For the NLRP3 inflammasome to function, it requires sequential treatment of two types of pathological stimuli, (1) a priming signal to activate nuclear factor kappa B (NF-κB) and upregulate the transcription of NLRP3 and interleukin (IL)-1β precursor protein; (2) an activation signal to trigger the inflammasome assembly for the production of two pro-inflammatory cytokines, IL-1β and IL-18. The relationship between NLRP3 inflammasome and AMD pathology has been an attractive subject in the field and current knowledge on this subject is reviewed elsewhere in detail.[193] Although all three cell death

pathways described above seems to govern RPE cell fate in GA to some extent, it is still unclear whether these mechanisms act independently or in synergy.

Earlier work, including ours, demonstrated that components found in drusen, (e.g. amyloid beta, complement cascade products, etc) increase in the aged retina.[63, 171] Previously, we have established a rat intraocular injection model to mimic the increasing amyloid beta (Aβ) load associated with drusen in human eyes.[113] We demonstrated that drusen component, Aβ, triggers a short lasting pro-inflammatory response in RPE via the activation of NF-κB and NLRP3 inflammasome,[65, 113] which can be specifically abolished by vinpocetine (an NF-κB inhibitor).[194] Intriguingly, RPE cell loss is not a feature of the short lasting pro-inflammation associated with the acute Aβ intravitreal model[113]. In the present study, we extended the duration of outer retina pro-inflammation by making sequential Aβ injections, in order to better model the chronic pro-inflammatory events and associated cell death underlying the pathogenesis of the dry form of AMD.

5.2 Methods

5.2.1 Preparation of oligomeric Aβ

The lyophilized, synthetic $A\beta_{1–40}$ peptide (hereafter referred to as "Aβ") in the HCl salt form was purchased from American Peptide (Sunnyvale CA). We chose $A\beta_{1-40}$ peptide over its structurally similar but more toxic, Alzheimer's disease-specific, form of $A\beta_{1–42}$ peptide based on earlier studies that demonstrated the presence of $A\beta_{1–40}$ in drusen deposits in postmortem human eyes.[113] Oligomeric Aβ was prepared according to published protocols.[195, 196] Briefly, the

synthetic Aβ peptide was first reconstituted in 1,1,1,3,3,3-hexafluoro-2-propanol (HFIP, Sigma Aldrich, St. Louis MO) and evaporated by speed vacuum, resulting in thin transparent Aβ peptide film. The Aβ peptide film was then reconstituted in 100% DMSO (Sigma Aldrich) to a concentration of 1 mM, and further diluted in pre-warmed PBS (pH 7.4) to produce the Aβ injection solution of 323 μM, equivalent to 1.4 μg/μL. The injection solution was subsequently incubated at 37 °C for 48 h to form the oligomeric Aβ. Confirmation of successful oligomeric Aβ formation was achieved by western blot (WB) using our published protocols.[171] Reverse $A\beta_{40\text{-}1}$ peptide (hereafter referred to as "control") served as a sequence control for Aβ and was prepared in the same fashion. The absence of 6E10 antibody positive bands in the control solution indicated proper preparation (Supplementary Figure 2).

5.2.2 Animals

All animal procedures were approved by the Animal Care Committee of the University of British Columbia, conformed to the guidelines of the Canadian Council on Animal Care and in accordance with the Resolution on the Use of Animals in Research of the Association of Research in Vision and Ophthalmology. Efforts were made to ensure animal welfare and minimize their pain, distress and discomfort whenever possible. Adult female Long-Evans rats at the age of 4.5 month (Charles River, Wilmington MA) were randomly divided into two groups. Group 1 (N = 16) comprised rats receiving intravitreal injections of Aβ (5 μL at 1.4 μg/μL as previously published[113]) once every 4 days for a total of 3 injections in 8 days. Group 2 (N = 16) rats received intravitreal injections of the control solution the same way as described for Group 1. All rats were sacrificed on the 14^{th} day after initial injection. Eyes were immediately

enucleated and frozen for WB, PCR and ELISA or fixed in 4% paraformaldehyde diluted in DPBS (Invitrogen, Carlsbad CA) for 48-72 h prior to paraffin embedding.

5.2.3 Immunohistochemistry (caspase-1, IL-18, NF-κB, active caspase-3)

Paraffin-embedded rat eye tissues were processed following established protocols.[113] Sections from both the Aβ and the control groups were processed simultaneously in an effort to minimize variability in immunoreactivity conditions (N = 3 per group). Primary antibodies recognizing total caspase-1, IL-18, NF-κB and active caspase-3 are described in Table 5-1. Non-specific isotype IgGs (Sigma Aldrich) matching the species of primary antibodies are used on negative control tissue sections. For visualization, the slides were developed using the Vector® AEC substrate kit (Vector Laboratories) and counterstained with Mayer's Hematoxylin (Sigma Aldrich) for the nuclei. Sections processed simultaneously were analyzed and scored so as to avoid differences in immunolabeling due to conditions such as temperature, stock of antibody, etc. Caspase-1, IL-18 and active caspase-3 immunoreactivity was scored in a masked fashion and semi-quantitatively based on a 0-3 point scale. A score of 0 indicates no detectable staining above the background level as compared to the negative control sections, whereas a score of 1, 2, or 3 suggests weak, intermediate, and robust intensity of the immunoreactivity, respectively. The immunoreactivity scores of caspase-1, IL-18 and active caspase-3 were averaged and normalized to the control group.

To detect NF-κB translocalization, an antibody recognizing the phosphorylated Ser 276 locus on NF-κB p65 subunit was used (Table 5-1). Immunoreactivity was measured quantitatively, in a masked fashion, using a ×60 objective lens and ×10 eyepieces. Positive RPE nuclei were

identified as containing both the red AEC chromogen and blue hematoxylin counterstain, thus resulting in a purple appearance distinct from the unlabeled RPE nuclei that were blue in color due to the hematoxylin counterstain alone. The number of NF-κB positive nuclei was converted to percentage of all RPE nuclei in the sample area, and normalized to the control group.

5.2.4 Suspension array for vitreal cytokines

An ELISA-based cytokine assay for vitreal cytokines was carried out (Bio-Plex 200 System, Bio-Rad Laboratories). Vitreous from rat eyes in the same group (either Aβ or control) were pooled (N = 7). Experiments were carried out following methods in our earlier publication.[194]

5.2.5 Western blot

To determine the level of X-linked inhibitor of apoptosis (XIAP), whole retina tissues (including neuroretina, RPE, bruch's membrane and choroid) from each of the two injection groups were used (N = 5). To investigate IL-18 secretion and gasdermin D (GSDMD) cleavage, RPE-choroid tissues from each of the two injection groups were dissected out and pooled to use ($N \geq 3$). Tissues were homogenized in ice-cold RIPA buffer (Thermo Fisher Scientific, Waltham, MA) containing protease inhibitor cocktail (Roche Diagnostics, Indianapolis IN). Protein lysates were run under reducing conditions and established blotting procedures were followed. Detailed information on the primary antibodies used in western blotting can be found in Table 5-1[171]. As an internal loading control, GAPDH was detected either on the stripped membrane or using freshly thawed protein lysates (Table 5-1). The protein band intensity of XIAP (57 kDa), IL-18 (18 kDa), pro-GSDMD (53 kDa), N-GSDMD (30 kDa) and GAPDH (36 kD) was individually measured using Image J (NIH, Bethesda MD) and converted into ratios relative to GAPDH. The

final relative intensity of XIAP, IL-18, pro-GSDMD, or N-GSDMD was normalized to the control group.

Antigen	Antibody	Dilution	Source	Applications
Amyloid-beta amino acid 1-16 ($A\beta_{1-16}$)	Mouse monoclonal anti-$A\beta_{1-16}$ (clone 6E10)	1:2,000	BioLegend, Dedham MA	Western blot
Caspase-1	Rabbit Monoclonal	1:300	Abcam, Cambridge, UK	Immunohistochemistry
Phosphorylated NF-κB p65 (Ser 276)	Rabbit polyclonal	1:75	Santa Cruz Biotechnology, Dallas TX	Immunohistochemistry
Interleukin-18 (IL-18)	Rabbit polyclonal	1:100 1:1000	Santa Cruz Biotechnology, Dallas TX	Immunohistochemistry Western blot
Active caspase-3 (aCasp-3)	Rabbit monoclonal	1:1000	Cell Signaling Technology, Beverly MA	Immunohistochemistry
X-linked inhibitor of apoptosis (XIAP)	Mouse monoclonal	1:1000	BD Transduction Laboratories, San Jose CA	Western blot
Gasdermin D (GSDMD)	Mouse monoclonal	1:100	Santa Cruz Biotechnology, Dallas TX	Western blot
GAPDH	Mouse monoclonal	1:10,000	EMD Millipore, Billerica, MA	Western blot

Table 5-1 List of primary antibodies used in Chapter 5.

5.2.6 Reverse transcription PCR (RT-PCR)

Total RNA of RPE-choroid was isolated from pooled rat eye tissues ($N \geq 3$) using ultRNA Column Purification kit (Applied Biological Materials, Richmond BC, Canada). 200 ng total RNA from each injection group was reverse transcribed into cDNA using the High-Capacity cDNA Reverse Transcription kit (Applied Biosystems, Carlsbad CA). RT-PCR was carried out

on the 7500 Fast Real-time PCR System (Applied Biosystems) using the following cycling conditions: 95°C for 30 s, 50°C for 30 s, 72°C for 30 s, 40 cycles. RT-PCR primer sequences can be found in Table 5-2. Melting curve analysis was automatically performed right after the cycles' completion. The results were expressed as mRNA fold-change relative to the control group after normalization to the reference gene, GAPDH, using the $2^{-\Delta\Delta CT}$ method.

Rat Gene	Forward Primer (5'-3')	Reverse Primer (5'-3')
X-linked inhibitor of apoptosis (XIAP)	CACACAGTCTACATCTCCT	CTACAACCTGTCCAGTTCT
Glyceraldehyde 3-phosphate dehydrogenase (GAPDH)	CTCTTGTGACAAAGTGGAC	CCATTTGATGTTAGCGGGA

Table 5-2 List of RT-PCR primer sequences used in Chapter 5 for rat tissues.

5.2.7 RPE morphological assessment

To evaluate the morphological changes of RPE cells due to induced inflammasome activity, we developed a custom Photoshop algorithm to measure the area of a set length of RPE monolayer based on RPE pigmentation. For each animal group, a total of 9 sections from each animal were used for the analysis. All RPE micrographs were taken under ×60 magnification and subsequently cropped into 12cm x 2cm rectangular areas for further processing. Next, choroidal pigments were manually removed and the RPE-only areas were selected by applying "fuzziness". Then the pixel count for the cropped area was obtained. The RPE area measurement was expressed as number of pixels. This measure was equivalent to, but more accurate than measuring the thickness of the RPE monolayer.

5.2.8 Statistical analyses

Data are presented as Mean ± SD. Non-parametric tests were used throughout the study except the vitreal cytokine levels and RT-PCR were analyzed by one-tailed Student's *t*-test. For the non-parametric comparisons between the two groups (Aβ vs control), one-tailed Mann-Whitney *U* tests were used. All analyses were conducted with GraphPad Prism version 6 (GraphPad Software). Statistical significance was set at $p \leq 0.05$.

5.3 Results

5.3.1 Pro-inflammatory cytokine secretion in vitreous

To understand the overall inflammatory status in the rat eyes, we collected and examined the vitreous samples using an ELISA-based cytokine profile assay. We found monocytes chemoattractant protein 1 (MCP-1), chemokine (C-X-C motif) ligand 1 (GRO/KC), vascular endothelial growth factor (VEGF) and macrophage inflammatory protein 3 alpha (MIP-3α) were increased more than 50% in the Aβ injected eyes compared to those in the reverse Aβ injected (hereafter referred to as "control") eyes (Figure 5-1). A smaller, but significant, increase was associated with vitreal IL-1β, a mature secreted product following NLRP3 inflammasome activation, which led us to look at the inflammasome activity in Aβ injected rat eyes.

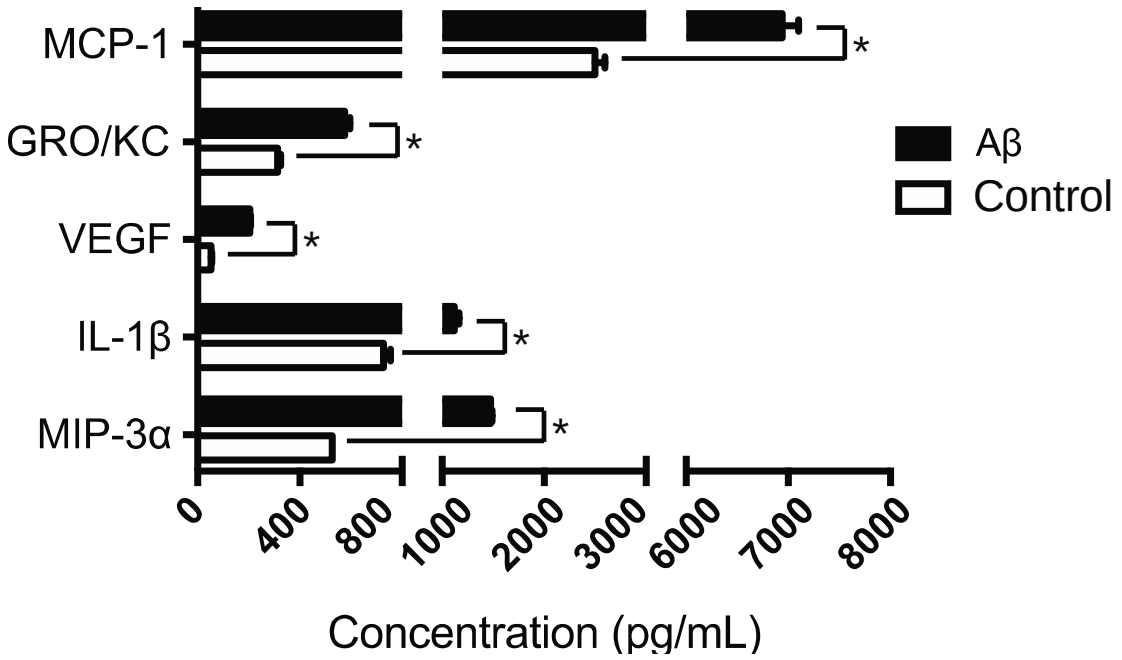

Figure 5-1 Vitreal cytokine secretion following sequential intraocular injections.

An ELISA-based rat cytokine assay was used to measure the vitreal cytokines levels. Cytokines with significant increase in the Aβ treated eyes compared to the controls were graphed. Sequential injections of Aβ led to a robust increase in chemokines (MCP-1, MIP-3α, GRO/KC), inflammasome product (IL-1β) and growth factor (VEGF). N = 7, Student's *t*-test, *$p<0.05$.

5.3.2 NLRP3 inflammasome activation by multiple Aβ injections

NLRP3 inflammasome activation is achieved by a sequential stimulation of a priming signal and an activation signal. To examine inflammasome activation in RPE, we first looked at the nuclear translocalization of NF-κB, a signature event of NF-κB activation. Using an antibody specifically targeting the phosphorylated p65 subunit of NF-κB, we found strong immunoreactivity in the nuclei of RPE cells in Aβ injected eyes compared to control eyes (Figure 5-2A-C). Next, we immunolabelled caspase-1 in the RPE layer of both Aβ-injected and control eyes, revealing that caspase-1 immunoreactivity was enhanced by 77% compared to the control eyes (Figure 5-3A).

Consistent with the elevation of IL-1β in the vitreous, we found the other inflammasome activation product, IL-18, was also upregulated, showing more than 6-fold higher immunoreactivity in the RPE layer of Aβ injected eyes (Figure 5-3B, C) and a 58% increase of IL-18 band intensity in protein lysates from the Aβ injected eyes, compared to the control eyes (Figure 5-3D, E).

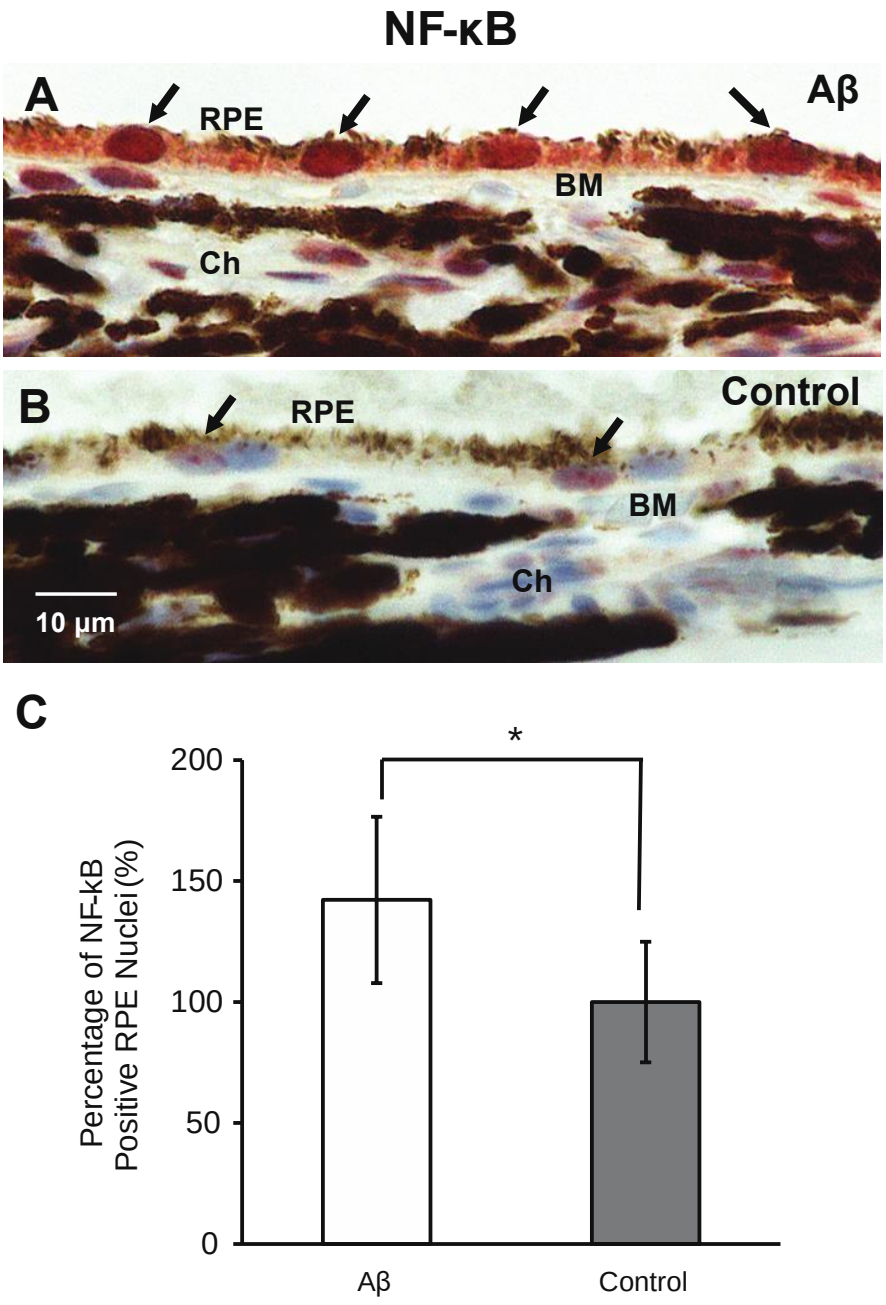

Figure 5-2 Activation of NF-kB pathway in retinal pigment epithelium (RPE).

(A-C) In retinal cross sections, injections of Aβ enhanced the nuclear translocalization of NF-κB phosphorylated p65 subunit in RPE (garnet red, arrows, A), compared to the light purple RPE nuclei in the control group (arrows, B). By counting the number of RPE nuclei with garnet red (AEC) labeling, there was a ~50% increase in the positive RPE nuclei over the control group (C). BM, Bruch's membrane; Ch, choroid. Scale bar: 10 μm. N = 3, Mann-Whitney, *p<0.05.

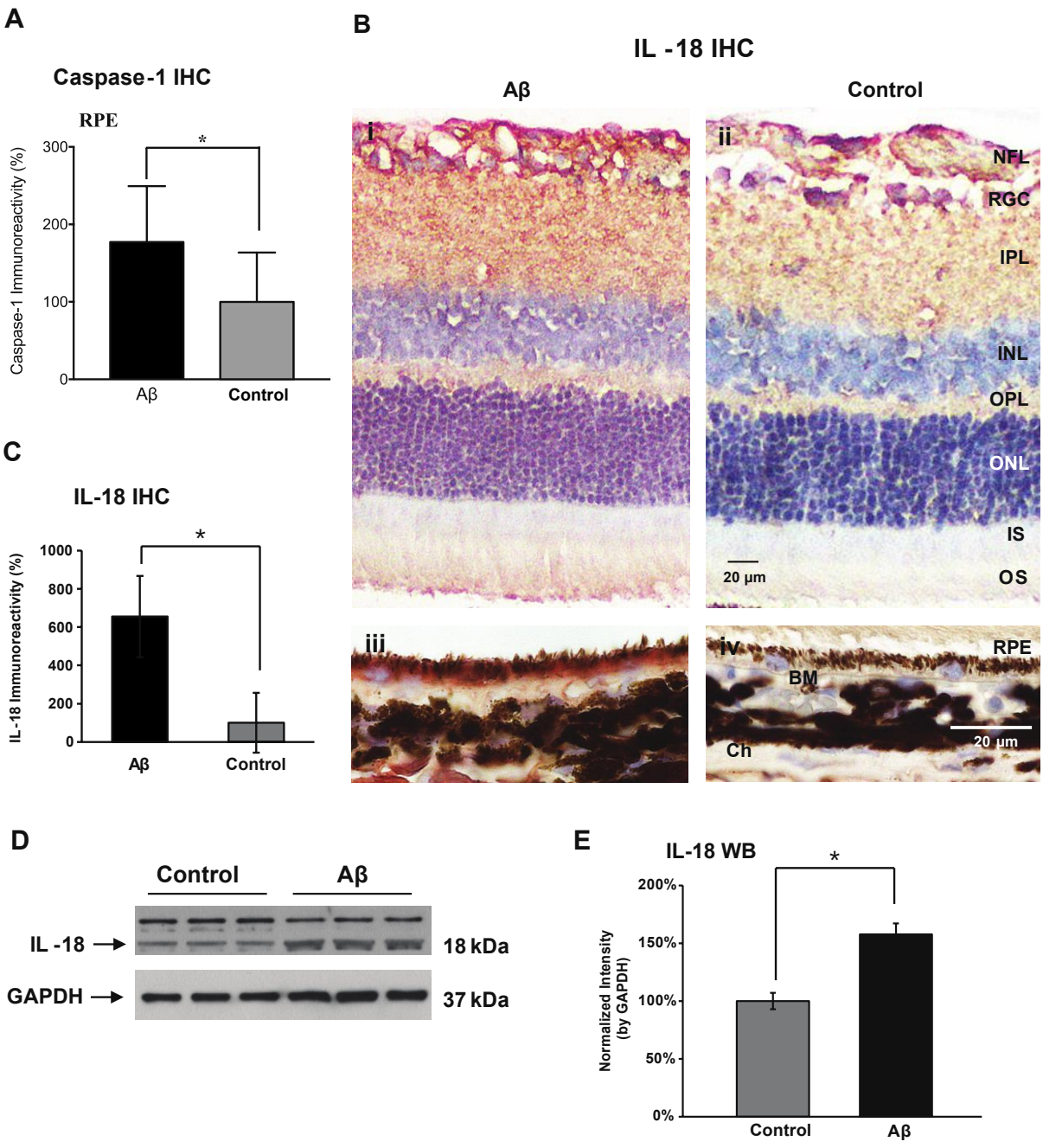

Figure 5-3 Sequential Aβ injections promote NLRP3 inflammasome activation.

(A) Immunoreactivity of total caspase-1 showed a 77% increase in RPE of the Aβ injected eyes compared to the control group. (B-C) The Aβ injected animals had a 6-fold higher IL-18 immunoreactivity than the control group (C). Representative micrographs exhibit an overall more intense IL-18 labeling (AEC, red, panel i & ii), particularly

in the RPE layer (iii & iv) (C). NFL, nerve fiber layer; RGC, retinal ganglion cells; IPL, inner plexiform layer; INL, inner nuclear layer; OPL, outer plexiform layer; ONL, outer nuclear layer; IS, inner segments; OS, outer segments; RPE, retinal pigment epithelium; BM, Bruch's membrane; Ch, choroid. Scale bars: 20 μm. (D-E) IL-18 western blotting showed a 58% increase of band intensity (MW = 18 kDa) in Aβ injected animals compared to the controls. $N \geq 3$, Mann-Whitney, $*p \leq 0.05$.

5.3.3 Cell death pathways triggered by Aβ injections

To study the forms of RPE cell death often seen in late AMD, especially GA, we next analyzed morphological changes in RPE after Aβ injections. We observed the presence of vacuolated RPE cells in cross sections of Aβ injected eyes (indicated by asterisks, Figure 5-4A-C). Using a custom Photoshop algorithm, we first applied a pigment threshold to identify the area occupied by RPE within a standard 12 cm x 2 cm boxed area centered on the RPE monolayer. Next, the number of pixels within the pigment threshold of that area was obtained as an index of the area measurement occupied by the RPE. Higher pixel values indicated thicker RPE monolayers. By comparing the Aβ-injected to the control groups, we observed a 2-fold increase in the number of pixels, suggesting a significant area increase in the RPE, presumably due to swelling of the RPE cells (Figure 5-4D).

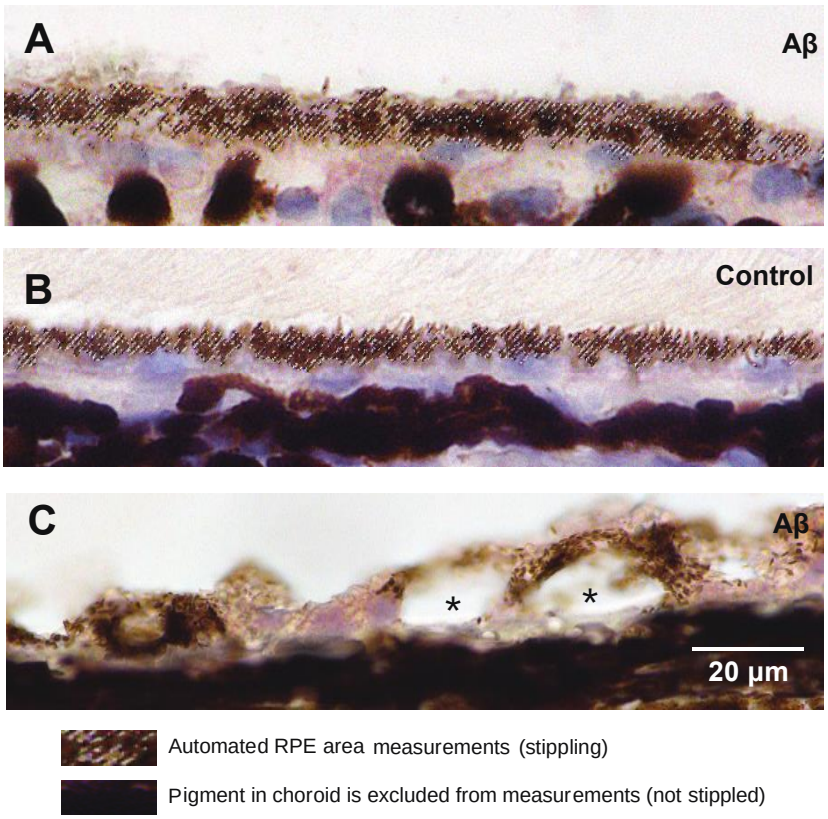

Figure 5-4 RPE morphological changes following sequential Aβ injections.

(A) Sequential Aβ injections caused RPE swelling, which was quantified by RPE area measurements using a custom Photoshop algorithm identifying the stippled area of RPE pigment. (B) Animals' receiving sequential control solution injections possessed thinner RPE layer compared to the Aβ group, indicated by the stippled area of RPE pigment. (C) Vacuolated RPE cells (asterisks) were observed only in animals receiving Aβ injections. (D) The number of pixels is a surrogate marker for RPE area measurement, which showed about 2-fold increase in Aβ group compared to the control group. N = 3, Mann-Whitney, *p<0.05.

To understand what caused the RPE to enlarge or swell, we prepared RPE-choroid tissue homogenates from both injection groups and tested them for GSDMD, a protein executing pyroptosis and whose proteolytic cleavage is triggered by both canonical and non-canonical inflammasome activation in immune cells.[197-199] The cleaved GSDMD N-terminal fragment (N-GSDMD) at 30 kDa was increased, while the uncleaved pro-GSDMD full-length protein at 53 kDa was decreased, in the Aβ group compared to the control group (Figure 5-5).

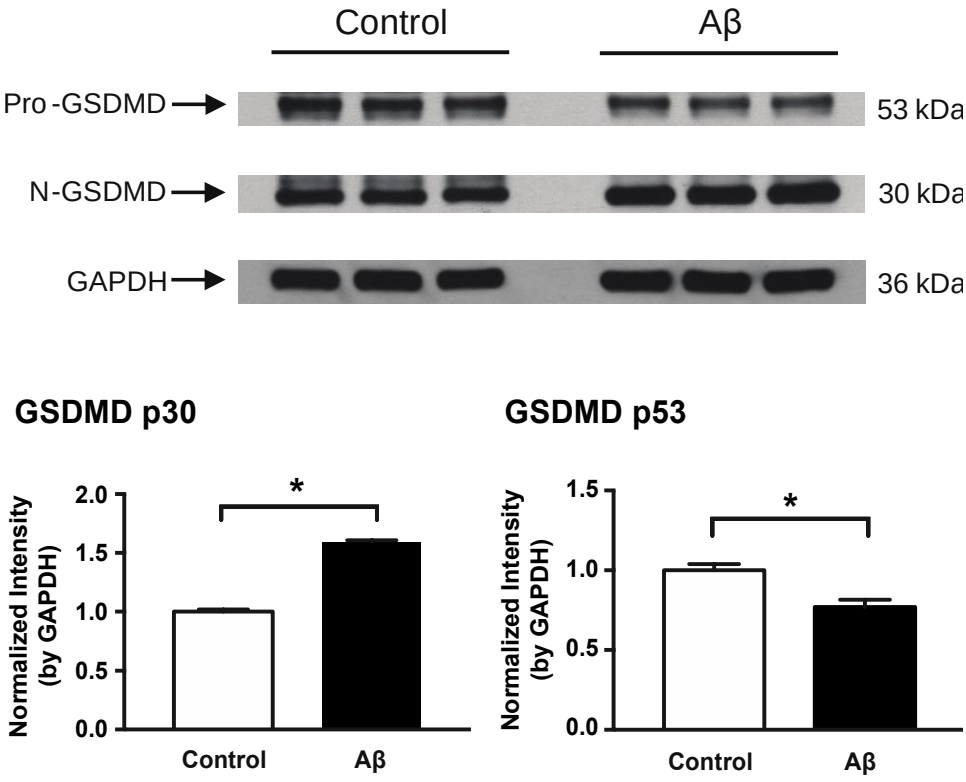

Figure 5-5 Activation of GSDMD mediated pyroptosis in response to Aβ stimulation.

RPE-choroid protein lysates from animals receiving either Aβ or control injections were probed with a GSDMD antibody. Compared to the control samples, Aβ significantly promoted the proteolytic cleavage of pro-GSDMD (53 kDa) into N-terminal GSDMD fragment (N-GSDMD, 30 kDa), a signature event indicating the activation of the pyroptotic pathway. GAPDH served as a loading control (36 kDa). $N \geq 3$, Mann-Whitney, $*p<0.05$.

Finally, we also tested for apoptosis involvement using caspase-3 activation as a surrogate marker. By immunohistochemistry, we found 2.5- to 4.5-fold higher immunoreactivity levels of active caspase-3 in photoreceptor inner segments and RPE of the Aβ group, respectively, compared to the control group (Figure 5-6A, B). Two examples of active caspase-3 immunoreactivity from both Aβ injected and control eyes were provided to demonstrate the enhanced red AEC labeling in photoreceptor inner segments and RPE from Aβ injected eyes (Figure 5-6C). To further support this finding, we measured the mRNA and protein levels of X-chromosome linked inhibitor of apoptosis (XIAP), a classic anti-apoptosis factor. At the transcriptional level, there was a 10-fold reduction in the Aβ group compared to the controls (Figure 5-7A). Consistent with the mRNA data, there was a 33% reduction in XIAP protein compared to the control group (Figure 5-7B, C).

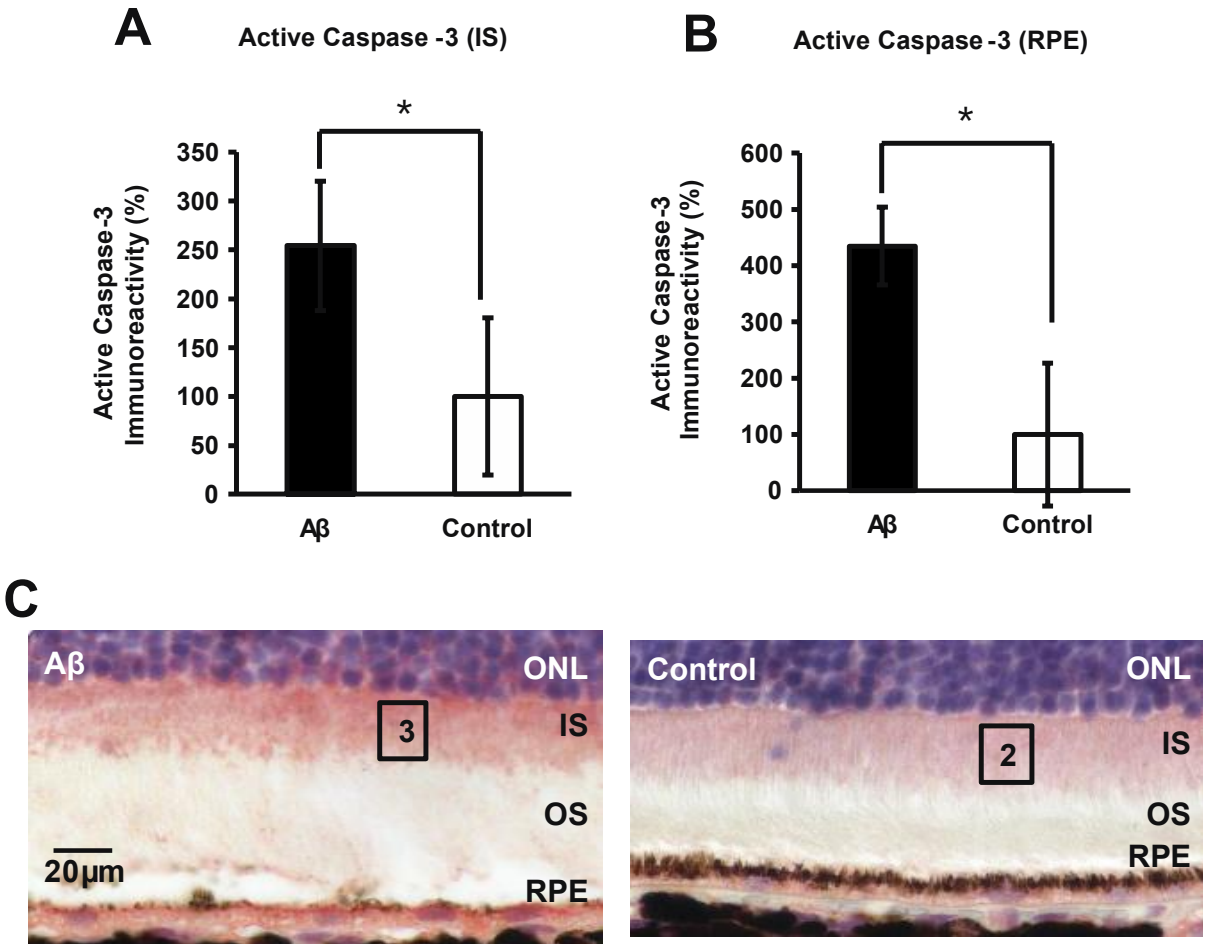

Figure 5-6 Caspase-3 activation in the outer retina of Aβ stimulated eyes.

(A-B) Immunoreactivity of active/cleaved caspase-3 was 2.5-fold and 4.5-fold higher in the Aβ injected eyes for photoreceptors inner segments (IS) and RPE, respectively, compared to the control eyes. N = 3, Mann-Whitney, **p*<0.05. (C) Representative micrographs illustrated examples of the semi-quantitative grading of active caspase-3's immunoreactivity in both Aβ injected and control animals. Robust caspase-3 immunoreactivity in the IS was seen in the Aβ injected retina, whereas weak and intermediate caspase-3 immunoreactivity was seen in the control eyes. ONL, outer nuclear layer; OS, outer segments. Scale bar: 20 µm.

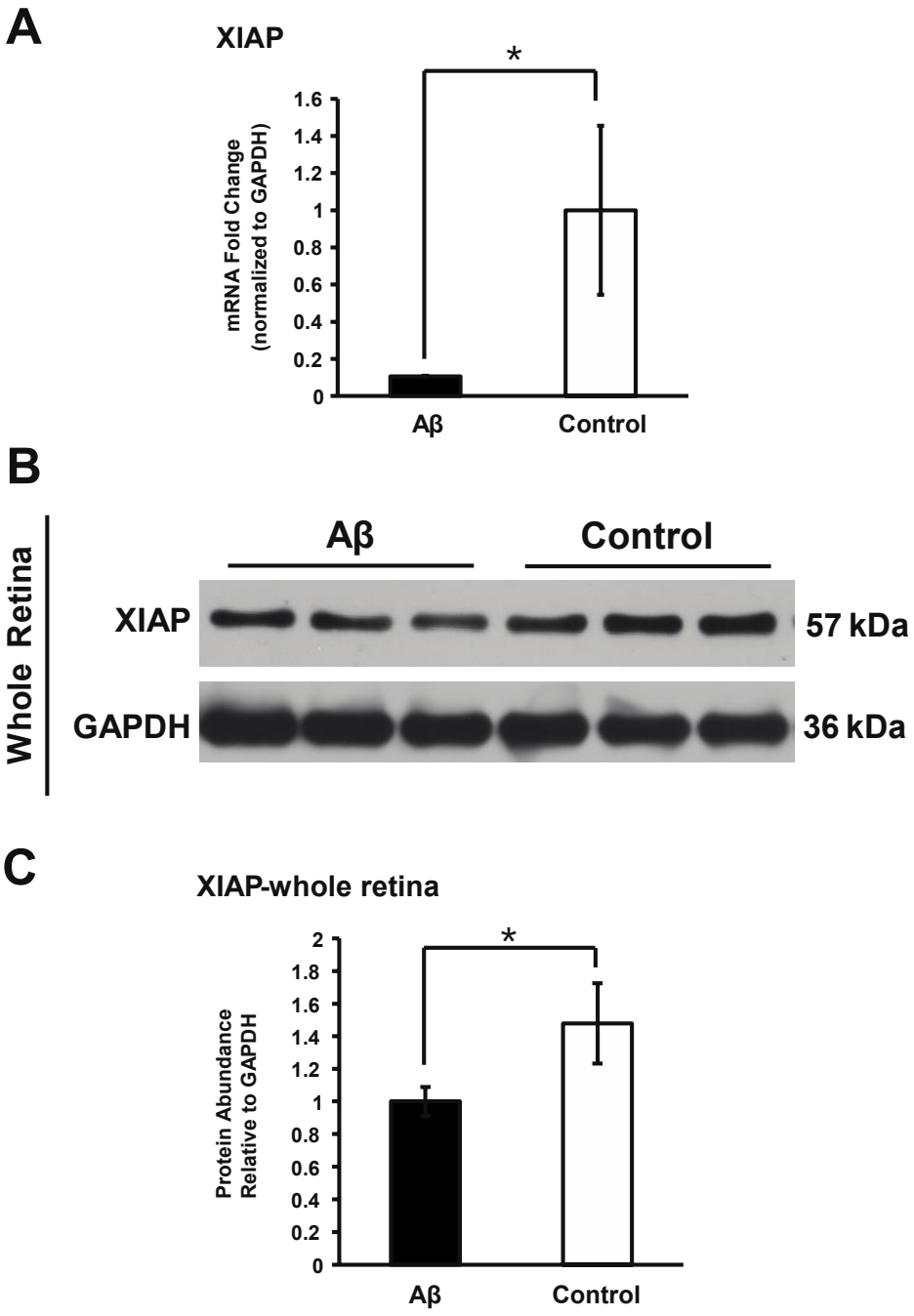

Figure 5-7 Decline of XIAP gene expression levels in Aβ stimulated eyes.

(A) Reverse transcriptional PCR revealed a 90% reduction of XIAP mRNA in Aβ stimulated eyes compared to controls. N ≥ 3, Student's *t*-test, * $p<0.05$. (B-C) In whole retina protein lysates, there was a significant 33% decrease of the XIAP protein level in Aβ stimulated eyes compared to reverse Aβ controls. N = 5, Mann-Whitney, *$p<0.05$.

5.4 Discussion

In late stage AMD, RPE cells die, yet the cell death pathways responsible remain a mystery. Based on pathological specimens of AMD donor eyes, atrophic RPE cells were thought to die from a necrotic cell death pathway, in which hypopigmented RPE cells filled with membrane-bound melanolipofuscin were eliminated, resulting in increased pigmentation and cell body enlargement in adjacent RPE cells.[69] More recently, reports from Kaneko et al.[70] and Tarallo et al.[36] highlight other cell death mechanisms (such as apoptosis and pyroptosis) that also likely contribute to atrophic RPE demise. However, the question remains as to what factors initiate the cell death cascades in AMD. In this study, using an animal model in which we mimic pro-inflammation due to chronic exposure to a drusen component, Aβ, we assessed the level of involvement of the pyroptotic and apoptotic pathways.

5.4.1 RPE inflammasome activation is a feature of the model

NLRP3 inflammasome activation, one of the fundamental innate immune defense mechanisms, has recently been studied for its role in the development of AMD.[200] Our earlier study indicated that a single Aβ injection resulted in a peak in pro-inflammation at 4 days post-injection, but then dramatically subsided.[113] In the current study, we extended the duration of pro-inflammation from 4 to 14 days by making sequential injections of Aβ every 4 days to better mimic a chronic inflammatory microenvironment in the outer retina. Our results demonstrated that longer exposure to pro-inflammation triggered robust NF-κB p65 subunit translocalization in RPE nuclei, elevated levels of total caspase-1 immunoreactivity, and enhanced secretion of mature products IL-1β and IL-18. Collectively, these results support inflammasome activity in the RPE.

Sequential injections of Aβ also provide a good model to study Aβ's role in inflammasome activation in the eye. Considered as one of the pathological hallmarks in AD, the deposition of Aβ in the AD brain is associated with elevated NLRP3 inflammasome activity, particularly the elevation of IL-1β production.[201-203] Using microglia culture models, Halle et al. demonstrated the importance of NLRP3 inflammasome activation for the recruitment of microglia to Aβ deposits in the AD brain.[123] Heneka et al. further discovered that in the absence of NLRP3 or caspase-1, mice carrying mutations associated with familial AD were largely protected from spatial memory loss, and demonstrated reduced IL-1β secretion and enhanced Aβ clearance.[202] However, the involvement of these pathways has not been well established in the eye tissue. As a continuation from our previous studies,[113] our current Aβ multi-injection model recapitulates seminal features associated with each step of the NLRP3 inflammasome activation cascades.

5.4.2 Pyroptosis and apoptosis may contribute to RPE cell death in this model

The involvement of NLRP3 inflammasome activation in RPE has been studied in many different AMD models.[32, 34, 145, 204] However, once the inflammasome is activated, little is known of the exact biological events that occur and whether these events lead to cell death. Using rodent and non-human primate models, Doyle and colleagues demonstrated the efficacy of IL-18 treatment as a potential alternative, adjuvant therapy for CNV.[35, 43, 205] On the other hand, Ambati and collaborators showed evidence that IL-18 drives RPE degeneration after NLRP3 inflammasome activation in murine models.[36, 206] In the current study, we also assessed the changes after activation of the NLRP3 inflammasome by Aβ. Intriguingly, after prolonged pro-inflammation in outer retina, we found enlarged or swollen RPE cells and significant increases in the proteolytic

cleavage of full-length GSDMD in the RPE-choroid tissues. As reported in earlier studies, the cytolytic effects of pyroptosis are mediated by the oligomerization of the GSDMD's N-terminal fragments (N-GSDMD) in the cellular membrane, resulting in the cell-burst pore formation.[207] Hence, it confirms the activation of pyroptotic pathway in the Aβ injected animals.[197] Therefore, we have demonstrated the co-existence of two events that occur after inflammasome activation: the secretion of mature pro-inflammatory cytokines, including the inflammasome products (IL-18 and IL-1β) and morphological and western blot evidence that supports the GSDMD-mediated pyroptotic pathway activation in RPE cells. Such an orchestrated response has also been seen in non-ocular cell types.[208]

Unlike pyroptosis, which rapidly lyses the cell, apoptosis is considered a non-inflammatory and non-cytolytic form of programmed cell death. From a canonical point of view, pyroptosis is biochemically characterized as caspase-1 dependent and caspase-3 independent, whereas apoptosis is caspase-3 dependent and caspase-1 independent. Interestingly, in the current study, we observed parallel cleavage of both caspase-1 and caspase-3 in the RPE tissue, challenging the dogma of their mutual exclusivity. Although it is biologically impossible for one single cell to undergo both distinctive cell death pathways, it is still likely for one type of tissue, such as the RPE monolayer in the retina, to accommodate these pathways in a spatially discrete and stimulus dose-dependent manner. One study using murine bone marrow derived macrophages exploited the potential of crosstalk between pyroptosis and apoptosis. The authors exhibited a DNA-dose dependent integral model for cell death, with apoptosis seen at a lower-dose of DNA stimulation and pyroptosis at higher doses. They further concluded that such an explicit response is regulated through caspase-8 activation.[209]

5.5 Conclusion

In conclusion, we have demonstrated the activation of two distinct cell death pathways in RPE following prolonged pro-inflammation induced by drusen component, Aβ. For the first time, we show that GSDMD cleavage is associated with inflammasome activation in RPE, providing the molecular basis for pyroptosis participation in this model. The biochemical events revealed here will benefit future endeavors in the search of therapeutic agents to slow down, or even prevent, RPE cell death in AMD.

Chapter 6: The reduction of XIAP is associated with NLRP3 inflammasome activation in RPE: implications for AMD pathogenesis

6.1 Introduction

AMD is a complex disease with various risk factors contributing to its pathogenesis. Despite the fact that the exact molecular basis underlying AMD is not yet fully understood, several candidate cellular and biochemical pathways associated with its development have been hypothesized. Our work (Chapter 5) and those of others, point towards the activation of the NLRP3 inflammasome as a pathway associated with RPE cell demise[36]. A salient factor in the development and homeostasis of all organs and tissues is the balance between cell death and cell survival. There are many routes to cell death and it remains challenging to determine which pathway a particular cell population takes under developmental or pathological conditions[210]. In keeping with this idea, it appears that the NLRP3 inflammasome is a powerful double-edged sword that needs precise, well-balanced regulation. Clinically, inflammasome antagonists are being explored as novel therapeutics for treating human immune diseases.[38, 211] The inhibition of inflammasome activity can potentially be achieved at four different levels along its activation pathway[38]. These include blocking cell membrane receptors (e.g., P2X7 receptor for ATP), controlling cytoplasmic second messengers (e.g., K^+, cathepsin B, ROS), preventing inflammasome components from assembling, and antagonizing released cytokine products and/or their cognate receptors. Given the fact that NLRP3 inflammasome senses a variety of activation signals, it is arguably more beneficial to slow down or stop the inflammasome assembly and subsequently, the release of pro-inflammatory cytokines. Undoubtedly, further investigation is warranted to uncover the

uncharted cell survival mechanisms that inhibit inflammasome activity, and thus suppress RPE atrophy in GA.

As mentioned in Chapter 1.1.9, XIAP is a classic potent anti-apoptosis factor, which has been recently shown to be involved in NLRP3 inflammasome activation in non-ocular cells.[81, 82, 212] However, it has not yet been characterized in RPE, the relevant cell type afflicted in AMD. The purpose of the research conducted in this chapter is to provide a closer look at XIAP's immune regulatory role.

6.2 Methods

6.2.1 XIAP plasmid construct

The design of the XIAP plasmid was modified with advice of Dr. Catherine Tsilfidis (University of Ottawa): the generic mammalian cytomegalovirus (CMV) promoter was engineered to drive the transcription of hemagglutinin-XIAP fragment (HA-XIAP) in an eukaryotic expression vector pcDNA3.1(+) (Invitrogen, Carlsbad, CA). Restriction enzyme sites were introduced to flank the HA-XIAP fragment (BamHI on the 5' end, XhoI on the 3' end) using the following PCR primer pair: BamHI-HA-XIAP 5'-TTTCGGATCCATGTACCCATAC-3'; HA-XIAP-XhoI 5'-TCTCCTCGAGGGGCTTAAGATCTATTTAAGAC-3'. To ligate the HA-XIAP fragment with the pcDNA3.1(+) backbone, both DNA sequences were digested by BamHI/XhoI enzyme mixture at 37°C for overnight. Next, the ligators were separated by 2-D DNA gel electrophoresis. Only the band with correct molecular weight (sum of HA-XIAP and pcDNA3.1(+)) was incised for gel digestion and DNA purification (QIAquick PCR Purification

Kit, Qiagen, Toronto ON, Canada). The pcDNA3.1(+)-HA-XIAP plasmid was then transformed into *E. coli* DH5α competent cells and spread onto LB-agar-ampicillin culture plate for overnight growth of ampicillin-resistant bacterial colonies. Single, large *E. coli* colonies were then inoculated into LB-ampicillin liquid medium for plasmid amplification and extraction (QIAamp DNA Mini Kit, Qiagen, Toronto ON, Canada). The extracted plasmids were digested with BamHI/XhoI enzymes and run on DNA gels again to verify the proper molecular weight and plasmid integrity (Figure 6-1). The plasmid concentrations and A260/A280 ratios were determined by a spectrometer (Bio-Tek Synergy H1). To assure the accuracy of XIAP sequence, the extracted plasmid was further analyzed by sequencing (primer sequences: 5'-GGCTAACTAGAGAACCC-3' and 5'-CCTGGTCAGAACACAG-3').

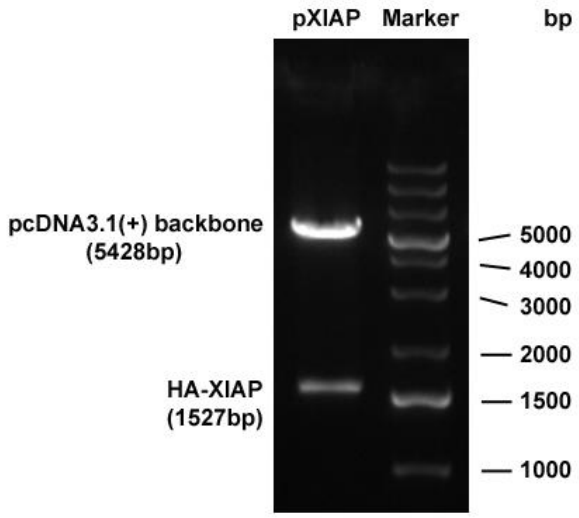

Figure 6-1 Restriction enzyme digestion of XIAP plasmid to verify correct insertion

The XIAP plasmid construct extracted from *E. coli* overnight cultures was digested by BamHI/XhoI restriction enzymes. The digested DNA fragments were separated in 1% agarose gel showing a large band of pcDNA3.1(+) backbone at ~5400bp and a small band of HA-XIAP at ~1500bp, compared to their theoretical molecular weight in parentheses.

6.2.2 *In vitro* model of inflammasome activation

To fully assess the molecular mechanisms underlying the inflammasome activation in RPE, low-passage ARPE-19 cells were used. Cells were maintained in complete culture medium, including DMEM/F12, high glucose, 1% penicillin/streptomycin and 10% fetal bovine serum (FBS), and incubated at 37ºC in a humidified atmosphere of 95% air and 5% CO_2. To activate the inflammasome, ARPE-19 cells were seeded in complete culture medium in 6-well plates at a density of 6 x 10^5 cells per well and cultured for overnight. Then the cells were washed twice in DMEM/F12 medium before subject to various stimulation conditions. L-leucyl-L-leucine methyl ester (Leu-Leu-OMe; Chem-Impex International, Wood Dale, IL), a lysosomotropic agent endocytosed by cells and converted into $(LeuLeu)_n$-OMe (n>3) in lysosomes causing lysosomal destabilization,[213] was applied with or without the recombinant human IL-1α pre-incubation at 10 ng/mL for 48 h ('priming'). Leu-Leu-OMe concentration of 1 mM was proven effective to destabilize RPE lysosomes according to previously established protocol.[32] After 3 h of Leu-Leu-OMe stimulation (1 mL/well at 1 mM), cell culture supernatants were collected and cells were lysed in 200 µL/well ice-cold RIPA buffer supplemented with protease inhibitors. After centrifugation at 14,800 rpm, 4°C for 20 min, 900 µL of cell-free culture supernatant and 200 µL of cell lysates for each stimulation conditions were stored at -20°C.

6.2.3 XIAP siRNA knockdown and plasmid overexpression

The validated *Silencer*® Select human XIAP 21-mer siRNA, which have been functionally tested to reduce human XIAP gene expression, the recommended *Silencer*® Select negative control siRNA that is experimentally tested not to target any gene product, and the *Silencer*® Select GAPDH positive control siRNA were purchased from Life Technologies. Preliminary tests were

run in house to assure the minimal off-target effects and the efficiency of siRNA delivery. ARPE-19 cells transfected with or without the negative control siRNA did not exhibit significant difference in XIAP mRNA levels (data not shown). The XIAP siRNA knockdown procedures were conducted as per the manufacturer's protocols. Briefly, ARPE-19 cells in complete culture medium were seeded into 6-well plates at a density of 6×10^5 cells per well one day before the siRNA transfection. At the time of transfection, ARPE-19 cells were at ~80% confluence. The cells were first washed twice in DMEM/F12 only medium and then 3 mL of serum-/antibiotics-free DMEM/F12 medium was added onto each well. A lipid-based transfection reagent, RNAiMAX (Invitrogen), was used to prepare the siRNA-lipid complex in serum-/antibiotics-free DMEM/F12 medium. A series of three different XIAP siRNA final concentrations were tested during a 48 h-incubation period: 2.5 nM, 5.0 nM and 10 nM, of which the lowest effective dose (2.5 nM) was determined by reverse transcription PCR (RT-PCR) of XIAP mRNA (Figure 6-4A). For the rest of the *in vitro* XIAP siRNA experiments, a final concentration of 2.5 nM and incubation duration of 48 h were used throughout. The effectiveness of siRNA knockdown was further assured by XIAP western blot.

To overexpress XIAP in ARPE-19 cells, the XIAP plasmid (pcDNA3.1(+)-HA-XIAP) and its vector control (pcDNA3.1(+) plasmid without the insertion of the HA-XIAP transgene) were transfected into the cells following our established protocol.[102] Briefly, transfection was performed in the 6-well plate format, using 2 ug total DNA for each well. A 30 h transfection incubation regime was applied, followed by 3 h inflammasome activation by Leu-Leu-OMe (1 mL per well at 1 mM).

6.2.4 Reverse transcription PCR (RT-PCR)

Total RNA of ARPE-19 cells from different stimulation condition groups (in triplicates) were extracted using ultRNA Column Purification kit (Applied Biological Materials). 1 μg total RNA from each well was reverse transcribed into cDNA using the High-Capacity cDNA Reverse Transcription kit (Applied Biosystems). RT-PCR was carried out on the 7500 Fast Real-time PCR System (Applied Biosystems) using the following cycling conditions: 95°C for 30 s, 50°C for 30 s, 72°C for 30 s, 40 cycles. RT-PCR primer sequences can be found in Table 6-1. Melting curve analysis was automatically performed right after the cycles' completion. The results were expressed as mRNA fold-change relative to the control group after normalization to the reference gene, using the $2^{-\Delta\Delta CT}$ method.

Human Gene	Forward Primer (5'-3')	Reverse Primer (5'-3')
X-linked inhibitor of apoptosis (XIAP)	CAGACTATGCTCACCTAACC	CCAAAAGTAAAGATCCGTGC
18S RNA (reference gene for siRNA assays)	GTAACCCGTTGAACCCCA	CCATCCAATCGGTAGTAG
Glyceraldehyde 3-phosphate dehydrogenase (GAPDH) (reference gene for plasmid overexpression)	TCCCTCCAAAATCAAGTGG	GGCTGTTGTCATACTTCTC

Table 6-1 List of RT-PCR primer sequences used in Chapter 6 for ARPE-19 cells.

6.2.5 Animal tissue samples

All animal procedures were approved by the Animal Care Committee of the University of British Columbia, and conformed to the guidelines of the Canadian Council on Animal Care and in accordance with the Resolution on the Use of Animals in Research of the Association of Research in Vision and Ophthalmology. Rat eye tissue protein lysates from previous chapters' experiments were used again in this chapter to evaluate the association between XIAP and NLRP3 inflammasome. These tissue protein sample groups include: $A\beta_{1-40}$ + vinpo vs $A\beta_{1-40}$ + vehicle (N = 5 per group, see Chapter 4 for details); ATAC vs NO ATAC (N = 6 per group, see Chapter 2 for details).

6.2.6 Western blot

To detect the secreted IL-18 and caspase-1 in ARPE-19 cell culture supernatant after Leu-Leu-OMe stimulation, 10 μL of the StrataClean resin solution (hydroxylated silica particles, Agilent Technologies, Santa Clara, CA) was added into each of the 900 μL culture supernatant samples. Next, the sample-resin slurry was vortexed to achieve a homogeneous distribution and incubated them at 4 °C for 2 h on a 360-degree rotator. Concentrated supernatant proteins were then collected by pelleting the StrataClean resin at 14,800 rpm, 4 °C for 20 min and the non-protein liquid phase removed. The resin-protein complexes were then resuspended in 1x reducing loading buffer (40 μL per sample) and denatured at 95 °C for 5 min to release the bound proteins. The resin-sample-loading buffer solution was pelleted, and the upper phase protein-containing solution was loaded onto gels.

To detect the intracellular proteins, cell protein lysates were quantified by BCA assay (Pierce, Thermo Fisher Scientific) for total protein concentrations and run on gels under reducing conditions. Established blotting procedures were followed to visualize the proteins of interest.[171] A list of primary antibodies used in western blot is included (Table 6-2). As an internal protein loading control, GAPDH was detected. The protein band intensity of XIAP (57 kD), cleaved caspase-1 p20 (20 kD) and GAPDH (36 kD) was individually measured using Image J (NIH, Bethesda MD) and converted into ratios relative to GAPDH. The final relative intensity of XIAP, cleaved caspase-1 p20 was normalized to the control group (naïve, non-stimulated ARPE-19 cells).

Antigen	Antibody	Dilution	Source
Interleukin-18 (IL-18)	Rabbit polyclonal	1:1000	Santa Cruz Biotechnology, Dallas TX
X-linked inhibitor of apoptosis (XIAP)	Mouse monoclonal	1:1000	BD Transduction Laboratories, San Jose CA
Caspase-1	Mouse monoclonal	1:1000	R&D Systems, Minneapolis, MN
GAPDH	Mouse monoclonal	1:10,000	EMD Millipore, Billerica, MA

Table 6-2 List of primary antibodies used in Chapter 6

6.2.7 Statistical analysis

Data are presented as Mean ± SD. All experiments were repeated three times. Statistical analysis was performed using GraphPad Prism version 7 (GraphPad Software). To compare two groups, Mann-Whitney *U* test was used for western blot analysis of animal tissue samples, whereas one-tailed Student's *t*-test was used for RT-PCR analysis of XIAP mRNA levels after plasmid

transfection. To compare more than two groups, a Kruskal-Wallis and a post hoc Dunn's multiple comparison test was used for western blot analysis of ARPE-19 cell lysates, whereas a one-way ANOVA and a post hoc Bonferroni multiple comparison test was used for RT-PCR analysis of XIAP mRNA levels after siRNA knockdown. Statistical significance level was set at $p<0.05$.

6.3 Results

6.3.1 XIAP is involved in the inflammasome activation step

The concept that XIAP may regulate the inflammasome pathway is novel. There is little knowledge as to what role XIAP might play in the immune regulation, especially in the inflammasome cascade. In our previous study, we established an *in vivo* model of inflammasome activation in RPE, demonstrating robust caspase-1 immunoreactivity and cytokine secretion (IL-18 and IL-1β) (Figures 5-1, 5-3). Intriguingly, in that model, we also found evidence of concomitant XIAP reduction at both the mRNA and protein levels when the inflammasome was activated (Figure 5-7). This prompted us to further investigate XIAP and its potential association with inflammasome activity. Using vinpocetine, a potent NF-κB blocker, we were able to show a strong inhibition of caspase-1 cleavage in a prior study (see Chapter 4).[102] However, when we tested the same set of protein samples for XIAP by western blotting, there was no significant difference in XIAP protein abundance, suggesting that XIAP is not affected by the NF-κB 'priming' signal (Figure 6-2A). We then looked at the involvement of XIAP in the pathway associated with the 'activation' signal. From our earlier study, MAC induced caspase-1 cleavage by the 'activation' pathway, and this was prevented by ATAC, a drug known to prevent MAC

formation (see Chapter 2).[171] By testing these samples, we found that XIAP protein level was increased by more than 50% when animals were given ATAC, compared to controls (Figure 6-2B), indicating that XIAP is regulated by the inflammasome activity.

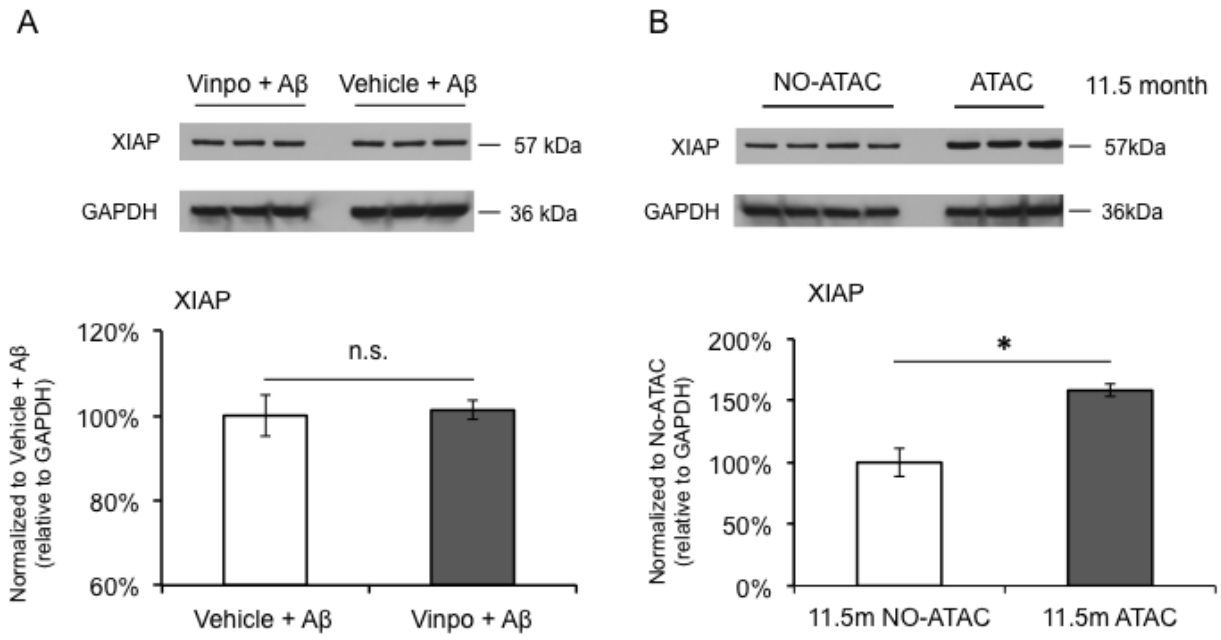

Figure 6-2 XIAP protein level is associated with inflammasome activation step.

XIAP western blot was performed using rat eye tissue protein lysates from previous studies.[102, 171] Significant difference in XIAP protein levels was observed between ATAC-fed animals and No-ATAC controls (N = 6, Mann-Whitney, *p<0.05). There was no difference in XIAP levels with vinpocetine administration compared to control.

6.3.2 Reduction of XIAP protein under inflammasome activation *in vitro*

To verify this inverse correlation between XIAP and the inflammasome activity, we tested ARPE-19 cells under four conditions: non-stimulated ARPE-19 cells (Ctrl); ARPE-19 cells primed with IL-1α for 48 h; ARPE-19 cells stimulated with Leu-Leu-OMe for 3 h; ARPE-19 cells first primed with IL-1α for 48 h and subsequently stimulated with Leu-Leu-OMe for 3 h.

Comparisons among the four groups revealed strong cleaved caspase-1 p20 bands in the cell lysates from Leu-Leu-OMe alone and IL-1α + Leu-Leu-OMe combined stimulation groups, confirming inflammasome activity. Comparing XIAP protein levels in these four groups revealed that there was a greater than 50% decrease in XIAP band intensity in the presence of Leu-Leu-OMe stimulation, compared to Ctrl and IL-1α priming alone groups (*p<0.05). However, IL-1α + Leu-Leu-OMe combined stimulation did not further reduce the XIAP level (Figure 6-3).

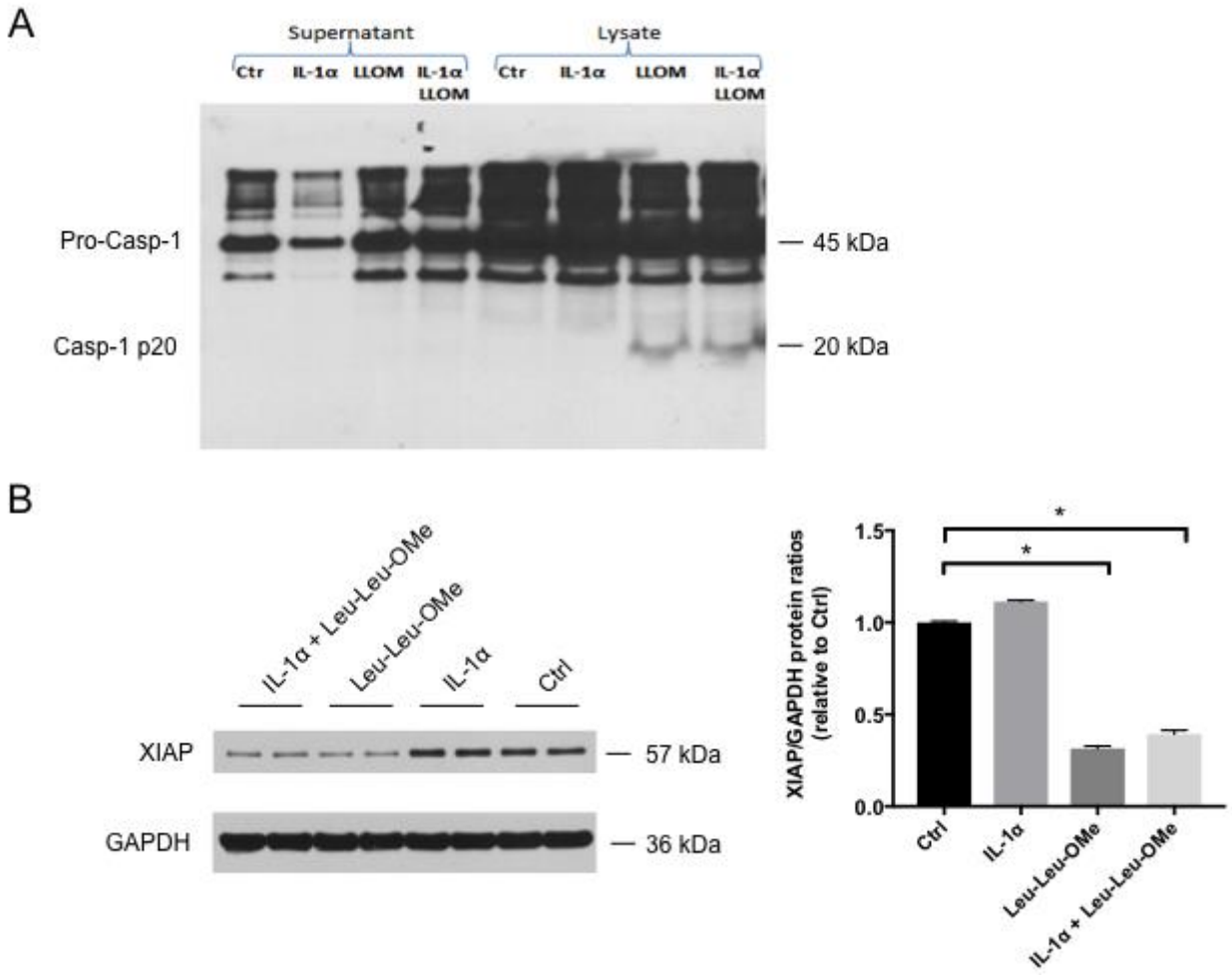

Figure 6-3 Leu-Leu-OMe stimulation alone is sufficient to activate inflammasome and reduce the XIAP protein level.

(A) Caspase-1 western blot was performed using ARPE-19 cell culture supernatants and cell lysates from four stimulation groups: non-stimulated RPE; IL-1α primed RPE; Leu-Leu-OMe (LLOM) stimulated RPE; IL-1α primed and LLOM stimulated RPE. The cleaved caspase-1 (Casp-1) p20 bands were observed under LLOM stimulation regardless of IL-1α priming. (B) XIAP protein levels were studied using cell lysates from the same groups, where LLOM stimulation was able to decrease XIAP in RPE cells with or without IL-1α priming, compared to non-stimulated RPE cells or cells only primed with IL-1α (N = 3, Kruskal-Wallis, $*p<0.05$).

6.3.3 XIAP siRNA knockdown promotes IL-18 release but not caspase-1 cleavage

Next, we studied the kinetics between the decline of XIAP protein and the caspase-1 cleavage, with the assumption that transient knockdown of XIAP will change the level of caspase-1 cleavage if XIAP reduction is a prerequisite for inflammasome activation. RT-PCR assays were used to select the lowest effective dose of XIAP siRNA after a 48 h transfection period. It appeared that XIAP siRNA was effective at 2.5 nM, the lowest of all three concentrations tested, causing a reduction in XIAP mRNA level of more than 75% (Figure 6-4A) and a dramatic decrease in XIAP protein level (Figure 6-4B). When combined with Leu-Leu-OMe (LLOMe) stimulation, the 2.5 nM XIAP siRNA induced an even greater depletion of XIAP protein in ARPE-19 cells (Figure 6-4B), compared to non-stimulated cells. However, such changes in XIAP did not correlate with the level of caspase-1 cleavage, with XIAP siRNA having no observable effects on the intensity of the cleaved caspase-1 p20 bands (Figure 6-4B). Nonetheless, we saw a steady increase of released IL-18 in the culture supernatants of siRNA-Leu-Leu-OMe combined stimulation, compared to those with only Leu-Leu-OMe stimulation (Figure 6-4B). Neither the XIAP siRNA alone nor the non-stimulated RPE cells secreted IL-18, confirming that IL-18 secretion is a downstream event of inflammasome activation and insufficient XIAP levels leads to enhanced IL-18 secretion during inflammasome activation.

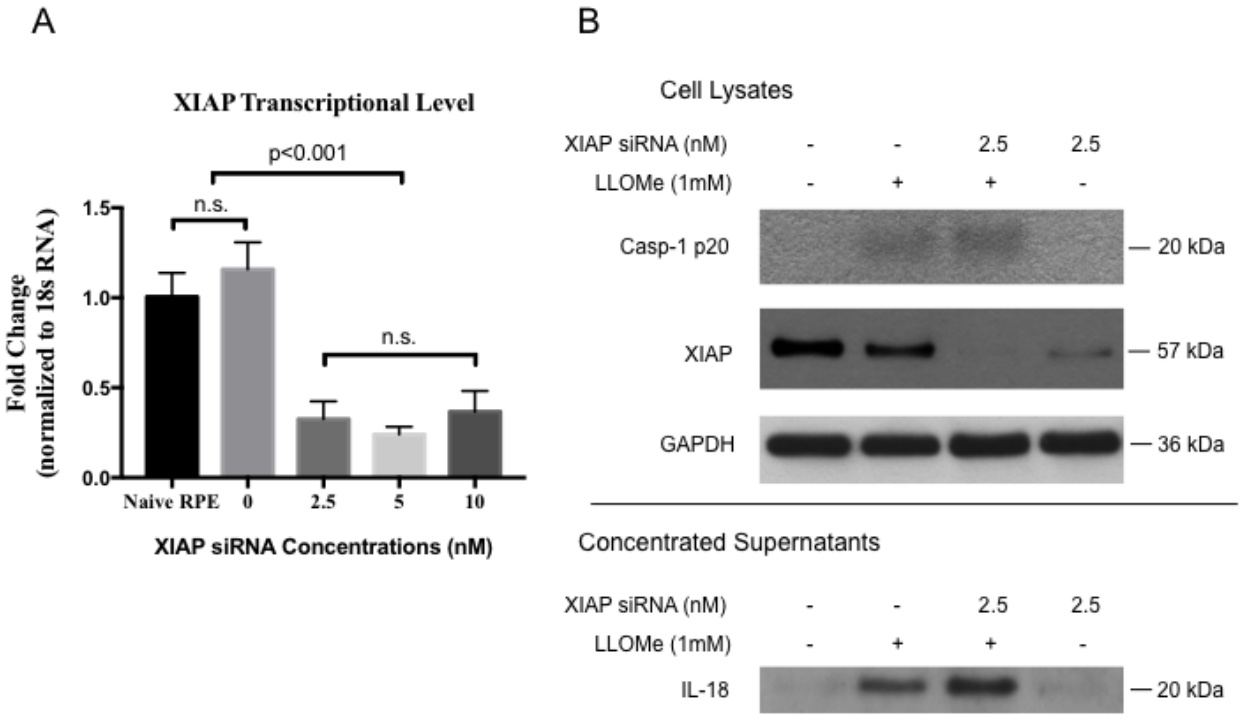

Figure 6-4 XIAP siRNA knockdown in ARPE-19 cells enhances IL-18 release, but not caspase-1 cleavage. (A) The selection of effective XIAP siRNA concentration was determined by RT-PCR assays, where a lower dose of XIAP siRNA (2.5 nM) achieved more than 75% inhibition on XIAP mRNA. Increasing the XIAP siRNA concentrations (5 nM or 10 nM) did not provide additional inhibition. N = 3, one-way ANOVA, $p<0.001$. (B) ARPE-19 cell lysates and culture supernatants from different stimulation groups were collected for protein analysis. LLOMe stimulation alone triggered caspase-1 cleavage, IL-18 secretion and XIAP reduction. Cells pre-treated with XIAP siRNA exhibited more IL-18 secretion and further decrease of XIAP, but not caspase-1 cleavage, compared to LLOMe alone group. LLOMe: Leu-Leu-OMe.

6.3.4 Inflammasome activation reduces the XIAP level post-translationally

A decline of protein abundance is generally the result of either: (1) insufficient gene expression (transcriptional and/or translational) or (2) undesirable post-translational regulation. To better understand the mechanism responsible for downregulation of XIAP under inflammasome

activation, we constructed an XIAP overexpression plasmid and transfected ARPE-19 cells before inflammasome activation. If aberrantly low XIAP gene expression occurred in response to Leu-Leu-OMe induced inflammasome activation, then we predicted that overexpressing XIAP by plasmid transfection should counter balance the effects. However, it is less likely for Leu-Leu-OMe to influence the NF-κB priming pathway since the literature suggests it as an activation signal.[32] We showed that transfection of the XIAP plasmid led to an upregulation of XIAP mRNA level by 15,000 fold compared to vector control (Figure 6-5A, *p<0.05). XIAP protein level was also increased dramatically (Figure 6-5B). Surprisingly, there were also more lower molecular weight bands (17 kDa, 25 kDa, 34 kDa, 43 kDa) present in the XIAP plasmid transfected group after inflammasome activation was induced, compared to the vector transfected and the non-transfected control cells, suggesting inflammasome-related post-translational regulation of XIAP.

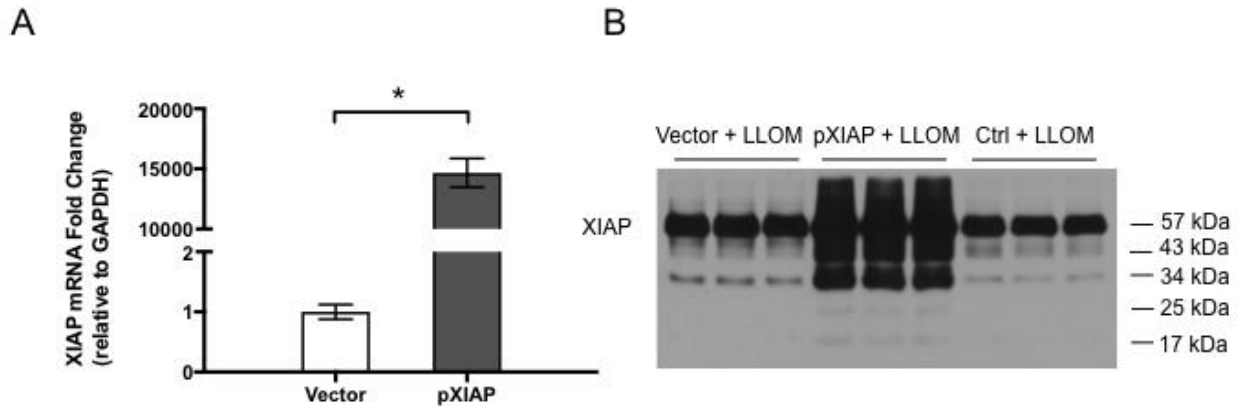

Figure 6-5 Inflammasome activation lowered XIAP protein level post-translationally.

(A) Transfection of the XIAP plasmid increased its mRNA transcription by ~15000 fold, compared to the vector control (N = 3, Student's *t*-test, *p<0.05). (B) Under Leu-Leu-OMe (LLOM) induced inflammasome activation,

ARPE-19 cells transfected with the XIAP plasmid exhibited more lower molecular weight XIAP bands (less than 57 kD), compared to the non-transfected cells or cells transfected with the control vector.

6.4 Discussion

6.4.1 XIAP: more than just an anti-apoptotic factor

XIAP is well known for its role in regulating apoptosis. In fact, it is even considered as the most potent caspase inhibitor *in vitro*.[214] However, compared to its anti-apoptotic function, little is known about XIAP's involvement in immune regulation. Mutations in the XIAP gene were found to result in a primary immunodeficiency condition in humans, named X-linked lymphoproliferative syndrome 2 (XLP2, OMIM entry number: 300635),[215] while XIAP polymorphisms are responsible for idiopathic periodic fever,[216] suggesting that XIAP may play a key role in immune homeostasis. In a recent review, Beug et al. further examined the relationship between the members of inhibitors of apoptosis proteins family (IAPs) and inflammasome activity.[217] The authors conclude that IAPs are involved in many aspects of the innate and adaptive immunity, either through the regulation of NF-κB and MAPK pathways or through the control of inflammasome activity. So far, examples of IAPs, in particular XIAP, regulating inflammasome activity have been reported mainly in immune cells.[81, 212, 218] However, research shows that inflammasome activation is a fundamental defense mechanism used by not only immune cells but also epithelial cells.[219-221] Indeed, several research groups have independently demonstrated the existence of inflammasome activity in RPE, a type of ocular epithelial cells.[32, 34, 36, 145] But none of those studies have looked into the question of whether XIAP regulates the assembly or activity of the inflammasome. In this study, we sought to investigate an inverse

relationship between XIAP and inflammasome activation from one of our established animal models of AMD (see Chapter 5). By comparing our data with two other models (Chapter 2 and 4), we were able to map the XIAP into the inflammasome's activating signal pathway (Figure 6-2), and to exclude the involvement of the NF-κB pathway in XIAP-inflammasome interactions.

6.4.2 Inflammasome mediated XIAP reduction is required for IL-18 secretion

To address the question of whether XIAP functions as a positive or negative regulator, we performed XIAP siRNA knockdown experiments on ARPE-19 cells with, or without, the Leu-Leu-OMe induced inflammasome activation. We showed that knocking down XIAP strengthens the cells' capacity to secrete IL-18 when inflammasome activation is induced, without changing the caspase-1 cleavage level (Figure 6-4B). Considered counter-intuitive at first, this finding makes sense when we take into account the recent report on human patients diagnosed with XLP2 disease (XIAP deficiency), where strikingly elevated IL-18 concentrations were discovered in these patients' sera samples which remained high after treatment despite the fact that other pro-inflammatory cytokines returned to the normal range.[222] Moreover, longitudinal examination of these patients revealed marked increase of IL-18 serum concentration, suggesting a clinical association between XIAP deficiency and high IL-18 levels. Of note, the loss of XIAP protein alone in ARPE-19 cells did not trigger inflammasome activation (i.e. no caspase-1 p20 bands, Figure 6-4B) or IL-18 secretion, compared to naïve ARPE-19 cells. Therefore, it indicates XIAP is a negative regulator of inflammasome-mediated IL-18 secretion. Nevertheless, the molecular structural basis that enables the XIAP-mediated regulation of IL-18 secretion remains unknown and warrants future investigation.

In addition to the augmented IL-18 secretion, we also reported no change of caspase-1 cleavage in response to XIAP siRNA, which suggests XIAP is downstream of caspase-1 activation. Considering we have also showed an inverse correlation between caspase-1 cleavage and XIAP reduction, it is probable that inflammasome activation causes the reduction in XIAP. To support this interpretation, we overexpressed XIAP in ARPE-19 cells and then induced inflammasome activation. Interestingly, a clear trend of more full length XIAP (57 kDa) turning into small fragments (Figure 6-5B) was observed in XIAP plasmid transfected cells, which is consistent with another study where caspase-1 cleavage and XIAP degradation are both present in injured rat neurons and suppressing caspase-1 cleavage helped to retain XIAP in its full length form.[212] Moreover, our data showed a further reduction of XIAP protein abundance when ARPE-19 cells were subject to stimulation with both Leu-Leu-OMe (inflammasome activation) and XIAP siRNA, compared to the cells treated with XIAP siRNA alone (Figure 6-4B), supporting the idea that XIAP can be downregulated by the active inflammasome. The observed XIAP-caspase-1 relation here is likely cell type specific, as caspase-1's cleavage levels were increased by XIAP siRNA knockdown in murine macrophage cell line, RAW264.7 (Supplementary Figure 3). Collectively, these findings favor the notion that XIAP is positioned downstream of caspase-1 in ARPE-19 cells. Whether XIAP is a natural substrate of, or indirectly influenced by, caspase-1 in RPE cells needs further investigation.

6.5 Conclusion

In this study, we identified a novel role of XIAP in regulating IL-18, an inflammasome-related cytokine secretion. Using a combined approach of siRNA and protein overexpression, we were able, for the first time, to pinpoint XIAP's position along the inflammasome activation pathway.

The results reported here help provide insights into the biological consequences of inflammasome activation in RPE and reveal the caspase-1/XIAP/IL-18 axis as a target for broader applications in AMD biology and treatment design.

Chapter 7: Conclusion

7.1 Significance and strengths

AMD is a degenerative eye disease with individual, societal, governmental and global impact. The global costs of visual impairment due to AMD are estimated to be $255 billion in direct health care.[9] More sobering is the fact that lack of effective treatment exists for the prevalent, but yet incurable late stage dry AMD that leads to RPE and photoreceptor death. Therefore, it is paramount to further research into the molecular basis of RPE cell death in order to achieve better clinical treatments for dry AMD. The results from this dissertation provide several original contributions to the field of AMD research.

7.1.1 Inflammasome activation contributes to low-grade chronic inflammation in RPE during aging

As the leading risk factor, aging brings significant, irreversible changes to RPE tissues, affecting cellular processes including metabolic pathways, impaired mechanism of autophagy, disrupted proteolytic and lysosomal function, decline in ability to combat oxidative stress and enhanced mitochondrial dysfunction.[223] However, the fact that not everyone gets AMD draws a clear line between normal aging and the age-related pathological changes in AMD.[84] Therefore, it is vital to elucidate the biological events facilitating the transition from normal aging to AMD in RPE tissues. Given its multifactorial nature, human AMD-like pathology can be initiated and replicated in different ways using animal models.[70, 157, 224-227] The search for a common pathway that connects all risk factors to the ultimate AMD pathogenesis is a daunting task for today's AMD researchers. Various single nucleotide polymorphisms (SNPs) have been shown to

predispose individuals to higher risk of AMD, but so far there has been no single "master gene" of AMD.[140, 228-230] Low-grade inflammation is a feature of normal aging and maintains tissue homeostasis.[231] Inflammation becomes chronic when tissue stressors persist for a significant length of time, which in turn contributes to the initiation of age-related diseases.[92] Our data (Chapter 2) support this idea by demonstrating the age-dependent accumulation of two pro-inflammatory tissue stressors, MAC and Aβ (both drusen components), in RPE-choroid tissues. We further showed an endogenous, constitutive level of caspase-1 activation, which can be blocked by the application of the MAC inhibitor ATAC. The causal relationship established between age-dependent MAC deposition and the endogenously induced caspase-1 activity suggests a crucial role of inflammasome activation in aged rodents. Thus, our results indicate that monitoring, or even suppressing, the inflammasome-mediated inflammation in RPE may be a way to control, or delay, the transition from normal aging to pathological aging in AMD.

7.1.2 Aβ: a novel inflammasome inducer in RPE

Aβ is one of the major pathological peptides that is responsible for the onset and progression of AD. It is involved in many aspects of AD pathology and more recently has been implicated in the activation of the inflammasome pathway. Both the immune cells and the brain tissues from AD animal models exhibit robust inflammasome activity associated with Aβ accumulation.[123, 202] More interestingly, Aβ deposition is not limited to the brain but also present in the retina of an amyloid precursor protein/presenilin (APP/PS1, Tg2576) bitransgenic mouse strain, causing pro-inflammatory responses and neurodegeneration.[100] Much stronger evidence for the role of Aβ in retinal degeneration, in particular AMD, is found in studies of drusen composition in which the accumulation of Aβ in drusen deposits is associated with the inflammatory status in AMD donor

eyes.[50, 62, 66] Furthermore, using a primary human RPE cell culture model, we previously suggested that Aβ triggers a pro-inflammatory response, based on microarray data.[65] However, no study has been conducted to reveal the mechanisms underlying the Aβ induced inflammatory responses in AMD. Whether the inflammasome pathway is activated by Aβ in RPE similarly to the immune and neuronal cells in AD is not known. In this dissertation, I contributed to this knowledge gap by studying the relationship between upregulated inflammasome activity and cell death mechanisms in RPE after intravitreal Aβ injections (Chapter 3, 5). As proof-of-principle, I also demonstrate the merits of using vinpocetine, a specific NF-κB inhibitor, to ameliorate Aβ-induced inflammasome activity (Chapter 4). All together, these findings emphasize a crucial role that Aβ plays in the inflammasome pathway in RPE and provide first-of-its-kind knowledge to promote the awareness of inflammasome involvement in AMD pathogenesis.

7.1.3 XIAP's role in inflammasome activity: a part-time job?

XIAP is considered as one of the most efficient regulators of the apoptotic form of programmed cell death in mammalian cells.[232] Besides its 'full-time job' in keeping apoptosis in check, recent studies identify XIAP's potential in other biological contexts, for instance, immune regulation.[217] It is reported that XIAP is specifically required to combat against certain types of bacterial infections via the regulation of nucleotide-binding and oligomerization domain (NOD)-dependent immune responses.[233-236] However, there are few studies that report XIAP's role in "sterile" (non-infectious) inflammation. My work in Chapter 6 adds to this line of investigation by identifying XIAP's involvement in inflammasome activation in RPE. The data reported here demonstrated correlations between the levels of XIAP and inflammasome activities. Mechanistically, the results suggest that hyperactivity of the inflammasome causes harm to the

RPE—by degrading XIAP, which in turn would likely make the cells more vulnerable to other deleterious AMD-related stimuli in the environment.

7.2 Limitation

While this work has made several contributions to our understanding of AMD, there are a number of limitations of the study, as detailed below.

7.2.1 Route of ocular Aβ administration: intravitreal vs subretinal

There are many ways to deliver drugs to the retina. In AMD treatment, such administration can be achieved by intravitreal and periocular injection (subconjunctival, subtenon, and posterior juxtascleral).[237] The intravitreal injection offers a direct route for the molecules to enter the vitreous, and is the current strategy used for anti-VEGFs treatments for wet AMD. However, there are three major drawbacks limiting the therapeutic efficacy of intravitreally delivered drugs. First, the distribution of injected molecules is size-dependent, with small molecules more easily penetrating through and reaching the retina. This is a significant challenge for retinal gene delivery due to the high binding affinity between vitreous and the cationic lipids/DNA complexes.[238] Second, the inner limiting membrane of the retina constitutes a physical barrier for intravitreally delivered drugs to enter retina. Lastly, the half-life of intravitreally delivered drugs varies significantly depending on their hydrophilicity and molecular weight to avoid elimination from the vitreous.[239] To circumvent the size barrier, in my study, a relatively small molecule, the oligomeric form of Aβ (< 20 KDa in size) was injected intravitreally into the rodent eye (Chapter 3-5). For comparison, intravitreal injection of Avastin (one of the commonly used humanized anti-VEGF antibody with a molecular weight of 148 KDa) reaches the choroid of the outer retina

and is effective at suppressing CNV. The benefits of choosing the intravitreal injection route are to achieve a direct and fast delivery to the vitreous and to maintain a relatively sustainable Aβ level. The retinal penetration of the injected Aβ molecules was demonstrated using immunohistochemistry, showing a strong retinal layer presence (reaching the RPE layer) at Day 1 post-injection. However, such Aβ retinal presence became much weaker at Day 4 post-injection, resulting in the peaks of most inflammatory gene responses at Day 4 (Chapter 3). In comparison, using the surgically more challenging subretinal injection benefits from: (1) closer range RPE-Aβ contact (less interference from other retinal cell types) and (2) longer-lasting effects on RPE up to Day 7 post-injection.[120] This approach is also suitable for retinal gene therapy. However, subretinal injections have their own set of limitations. For instance, retinal detachment and the disruption of retinal layers often occur as the major side effects of this more invasive delivery approach. After weighing these factors, I chose the intravitreal delivery for the animal studies throughout this dissertation.

7.2.2 ARPE-19 cell line vs human primary RPE cells

In this dissertation, *in vitro* cell culture models were used to explore the mechanistic aspect of RPE's responses to Aβ and inflammasome activation, providing us with additional information to the *in vivo* animal studies. A vital question to ask, when selecting an RPE cell culture model, is if the chosen type of cells resembles the native RPE's functional and physiological phenotypes *in situ*. The immortalized ARPE-19 cell line has been widely used as a dependable alternative to native RPE under a great number of experimental conditions. These cells express several RPE specific genes, such as retinoid isomerohydrolase (RPE65) and cellular retinaldehyde-binding protein (CRALBP), and retain the capacity to phagocytose photoreceptor outer segments, a key

function of native RPE.[204] However, the use of ARPE-19 cells does come with a limitation in that these cells tend to lose their phenotypes after multiple passages, likely due to a process called epithelial-mesenchymal transition.[240] In Chapter 4 and Chapter 6, low-passage ARPE-19 cells (passage 10 or lower), as suggested previously,[241] were used to establish the ARPE-19/NF-κB-luciferase reporter cell line and to conduct inflammasome activation assays because they are more likely to resemble native RPE in functionality than high-passage cells. Human primary RPE cells, on the other hand, may possess the best model of native RPE *in vitro* as they preserve many key characteristics of the functional human RPE. Adult human primary RPE cells are thought to be the most physiologically and functionally mature model of *in vitro* RPE.[242] But human primary RPE cultures have inherent weakness such as limited number of expansions,[243] the heterogeneity of the donor eyes' genetic background, and the considerable length of time to achieve a statistically significant sample size for donor eyes. Therefore, we chose the more practical approach of using the ARPE-19 cell line. Future studies with human primary RPE cultures will allow us to validate and extend the findings observed from ARPE-19 cells.

7.2.3 RPE-specific vs choroidal macrophage-mediated responses *in vivo*

The ability to dissect RPE-choroid from neuroretina was demonstrated in our earlier work[113, 171] and those of others.[244] However, it is possible that in the RPE-choroid sample, the choroidal component with macrophages, may also contribute to the inflammasome activity in our *in vivo* work. Testing for activated macrophages by immunohistochemistry in paraffin sections or by microdissection of choroidal tissue alone[75] may help us better understand the migration of immune cells from choroid in our Aβ-injected animal groups. It is possible that the choroidal macrophages, important immune cells associated with AMD,[84, 245] in combination with RPE

(studied here) may both work to exacerbate the chronic inflammatory milieu in the AMD eye. Therefore, *in vitro* work on cultured RPE cells and choroidal macrophages will allow us to define the role of each cell type without the confounding effects from the other.

7.2.4 Other limitations

In Chapter 3, I demonstrated Aβ's ability in triggering NLRP3 inflammasome activation when compared to the reverse peptide or PBS vehicle control groups. Based on those findings, I continued to explore ways to suppress the inflammasome activity and chose to investigate the therapeutic merits of vinpocetine in Chapter 4. The comparisons were then made between the two animal groups, Aβ + Vehicle (i.e. DMSO) and Aβ + vinpocetine (containing the same amount of DMSO), by which I successfully demonstrated the inhibitory role of vinpocetine in the inflammasome pathway in RPE. However, it would have been better to include a treatment naïve group (i.e. Aβ only group) in the study, which would allow us to appreciate the role of DMSO in those experimental conditions, especially when DMSO has been previously reported to carry anti-inflammatory properties.[188]

In Chapter 6, siRNA experiments were used to probe the relationship between the XIAP protein level and the NLRP3 inflammasome activation. All the control siRNAs including a positive control GAPDH siRNA and a negative control non-targeting siRNA were purchased at the same time from the same commercial vendor as the XIAP siRNA. They were tested in the preliminary assays to ensure the sequence-specific knockdown of XIAP in ARPE-19 cells. Subsequently, only the XIAP siRNA transfected and the non-transfected ARPE-19 cells were used in the comparisons throughout Chapter 6, given that the preliminary results suggested similar levels of

XIAP gene expression in both the non-transfected and the negative control siRNA transfected ARPE-19 cells. It would have been better to include all siRNA controls in every siRNA experiment. Alternatively, scramble siRNAs can also be used as negative controls in siRNA experiments. However, these scramble siRNAs are synthesized by randomizing or reversing the same nucleotide sequence as the target (or test) siRNA and must be confirmed not to recognize any known genes or miRNA regions. Compared to the non-targeting siRNA negative controls, this scramble siRNA control strategy is less practical and often impossible.

7.3 Future directions

7.3.1 Biological roles of inflammasome-mediated IL-18 secretion: friend or foe?

Being one of the mature cytokines processed by the active caspase-1, the biological consequence of IL-18 secretion remains a controversial topic in AMD research. Opposing findings from different research groups have presented contradictory data regarding this issue. On one hand, IL-18 is hypothesized to be a detrimental pro-apoptotic factor to RPE in dry AMD.[206, 246] In line with this model, Tarallo et al. and Kim et al. together mechanistically uncovered a caspase-8-mediated apoptotic RPE cell death pathway in MyD88- and Fas ligand-dependent manner in response to IL-18 secretion,[36, 74] suggesting IL-18's involvement in dry AMD but not in CNV. On the other hand, using recombinant IL-18, Doyle et al. shows effective reduction in lesion size in experimental animal models of CNV,[35, 43, 205] promoting the protective role of IL-18 in CNV. In Chapter 3, the acute Aβ intravitreal stimulation triggers the elevation of several NLRP3 inflammasome related genes, including IL-18. The data demonstrate marked increase of IL-18 mRNA and protein in RPE-choroid at post-injection Day 4 and Day 14, respectively. However,

no significant change of VEGF levels (both mRNA and protein) was observed at those time points. When RPE cells were exposed to chronic Aβ intravitreal stimulation (Chapter 5), augmented IL-18 protein levels were evident in RPE-choroid tissues along with an increase of active caspase-3 and cleaved GSDMD fragments, with no sign of aberrant choroidal vessel growth. Furthermore, knocking down XIAP, a potent anti-apoptotic factor, led to enhanced IL-18 secretion in cultured ARPE-19 cells under inflammasome activation (Chapter 6). Collectively, my data suggest that IL-18 serves as a "threat" rather than a "helper" to RPE cells in the context of dry AMD. Nonetheless, in order to fully address this issue, an RPE-choroidal endothelial cell co-culture model should be useful for testing the exact role of RPE-derived IL-18 on choroid vasculature.

7.3.2 Mechanisms of IL-18 secretion in RPE and the influence by XIAP

In Chapter 6, I demonstrated the secretion of IL-18 after inflammasome activation in ARPE-19 cells. I also showed that lowering XIAP protein levels by RNA interference could further enhance IL-18 secretion. However, the detailed mechanisms underlying these findings are still unknown. Given that the IL-18 precursor protein lacks the signal peptide sequence for transmembrane exocytosis, its mature product cannot exit the cell via the canonical secretory pathway.[247] Instead, the unconventional protein secretion, or endoplasmic reticulum/Golgi-independent protein secretion mechanism, is likely involved. More specifically, reports suggest that IL-18 is translocated from the cytosol into secretory lysosomes for exocytosis.[248] Whether this process exists in RPE cells and is regulated by inflammasome activity remains unclear. However, IL-1β, the other cytokine product released after inflammasome activation was shown by Martin-Sanchez et al. to be released by membrane permeabilization in parallel with the death

of the secreting cell.[249] The authors further clarified that this type of IL-1β release is independent of the non-specific leakage of proteins during common cell death events, indicating it is a tightly controlled process. Considering IL-18 is another secreted cytokine downstream of inflammasome activation, it is likely to share a similar mechanism with IL-1β and to invoke cell death along with its secretion. Therefore, it brings up the opportunity for us to further evaluate XIAP's role in the potential cell death phenotype associated with IL-18 secretion.

7.3.3 Ubiquitylation and deubiquitylation: new for inflammasome regulation

Ubiquitylation is a common post-translational modification of proteins through a cascade of enzymatic activity of ubiquitin ligases. It has multiple effects on proteasome- or lysosome-mediated protein degradation, cell signal transduction and protein activity regulation. According to the type and length of ubiquitin linkage, there are three major forms of protein ubiquitylation currently studied, including lysine 48 (K48) linked ubiquitylation, lysine 63 (K63) linked ubiquitylation and methionine 1 (Met 1) linked linear ubiquitylation.[250] Mounting evidence has implicated the involvement of ubiquitylation in AMD pathophysiology. By looking at the retinal distribution of several class III ubiquitin-conjugating enzymes in mice, Mirza et al. reported robust protein expression of one such enzyme, UbcM2, in murine photoreceptors and RPE cells. The authors further experimented with UbcM2's protective effects on photoreceptors using an acute bright-light-damage model. It was shown that mice with only one copy of functional UbcM2 allele were protected from acute excessive light damage to photoreceptors, suggesting a strong relationship between UbcM2-mediated ubiquitylation and photoreceptor survival.[251] In human RPE cells, it is evident that there is an active ubiquitin-proteasome mediated protein degradation pathway, with low endogenous levels of ubiquitin to fight against cellular

stressors.[252] In the context of AMD, Ramos de Carvalho et al. tested the proteasome activity of primary human RPE cells in response to complement factor C3a, another known drusen component. C3a stimulation significantly reduced proteasome activity without changing its component at either protein or mRNA levels, indicating a potential functional suppression of the proteasome in primary human RPE.[253] On the other hand, the family of deubiquitinating enzymes (DUBs) is another force balancing protein activity. Glenn and colleagues reported altered proteomic profiling of ARPE-19 cells cultured on advanced glycation end products (AGEs, known drusen component) modified Matrigel BM extract compared to non-AGE modified control BM. Of note, by immunocytochemistry, the authors were able to localize upregulated protein expression of a DUB protein, ubiquitin carboxyterminal hydrolase-1 (UCH-L1), in AGE-stimulated ARPE-19 cells, suggesting a potential role for DUBs in AMD pathogenesis.[254]

However, few reports exist on the roles of both ubiquitinating and deubiquitinating enzymes in NLRP3 inflammasome regulation. Recently, Py and colleagues demonstrated that BRCC3, a JAMM domain-containing zinc metalloprotease DUB, promotes NLRP3 inflammasome activation by deubiquitinating the mixed K64 and K48 ubiquitin chains on both the NACHT and LRR domains of NLRP3.[255] The authors further suggested that the deubiquitylation of NLRP3 was critical for inflammasome activation based on the facts that inhibiting BRCC3 could abolish NLRP3 inflammasome activation under a diverse range of classic "activation signals", including K^+ efflux, ROS overproduction and lysosomal destabilization. Perhaps more intriguing is the report by Rodgers et al. of the discovery that the linear ubiquitylation of the ASC adaptor protein by the linear ubiquitin assembly complex (LUBAC) is also essential for NLRP3 inflammasome

activation, independent of NF-κB activity[256] (Figure 7-1). Clinically, these studies provide potential alternative approaches for the treatment of inflammasome related diseases, such as AMD, by better controlling the ubiquitylation levels of separate NLRP3 inflammasome components, instead of targeting secreted levels of the mature pro-inflammatory cytokines.

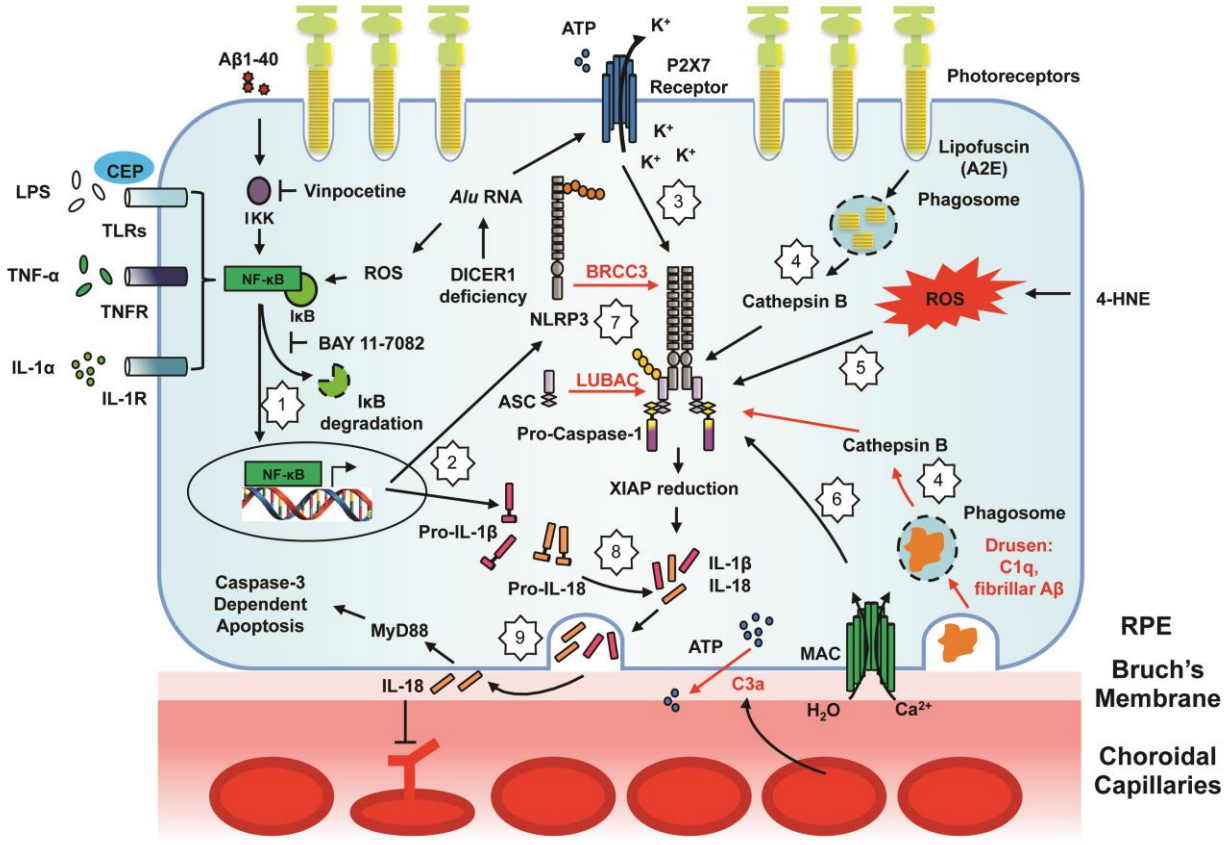

Figure 7-1 Summary of NLRP3 inflammasome activation and regulation in RPE

(1) Priming of the RPE by one of the following factors (LPS, TNF-α, IL-1α, CEP, and $A\beta_{1-40}$) is needed in order to activate the NF-κB pathway, which can be specifically blocked by vinpocetine or BAY11-7082. Intriguingly, DICER1 deficiency induced *Alu* RNA accumulation has also been shown to prime NF-κB signaling, independent of toll-like receptors (TLRs). (2) Once the NF-κB pathway is active, it promotes the transcription of NLRP3 and pro-IL-1β. (3-7) For the production of mature IL-1β and IL-18; separate inflammasome components are assembled as a

multiprotein complex triggered by one of the following mechanisms: K^+ efflux via P2X7 receptor activation in response to extracellular ATP accumulation or intracellular *Alu* RNA (3); cytoplasmic cathepsin B released from destabilized phagolysosomes of lipofuscin/A2E (4); ROS overproduction caused by 4-HNE (5); MAC formation (6). Other NLRP3 inflammasome activation mechanisms that have been reported in immune cells but not validated in RPE cells are shown in red text and arrows. These include drusen components (C1q and fibrillar Aβ) induced lysosomal damage (4), C3a triggered ATP efflux, BRCC3-mediated deubiquitylation and LUBAC-mediated ubiquitylation (7). (8) Successful assembly of NLRP3 inflammasome triggers autoproteolysis of pro-caspase-1 into active caspase-1, which further reduces XIAP and converts pro-IL-1β and pro-IL-18 into bioactive peptides. (9) The biological significance of NLRP3 inflammasome activation is to release active IL-1β and IL-18 into extracellular space through exocytosis. The secreted IL-1β will facilitate inflammation process in the tissue whereas IL-18 will either promote caspase-3 dependent RPE apoptosis via MyD88 signaling or suppress neovascular vessels growth in the choroid capillaries.

7.4 Summary

Much of our knowledge of the mechanisms associated with activation and regulation of the inflammasome comes from studies in immune cells. Validation of these mechanisms in ocular cells, such as RPE and photoreceptors, will be useful for designing inflammasome-related treatment strategies for chronic inflammatory diseases of the retina, such as AMD. The results from my dissertation work may guide the development of new strategies for the implementation of earlier treatments towards prevention of AMD. Hopefully my work will lead to new treatment strategies and lead to a brighter future for individuals who suffer from this devastating eye disease, improving the quality of life for those individuals and their families.

Bibliography

1. Ambati J, Atkinson JP, Gelfand BD. Immunology of age-related macular degeneration. *Nature reviews Immunology* 2013;13:438-451.

2. Strasburger H, Rentschler I, Juttner M. Peripheral vision and pattern recognition: a review. *J Vis* 2011;11:13.

3. Reh TA. The development of the retina. In: Hinton DR (ed), *Retina*: Elsevier; 2013:330-341.

4. Kim HT, Kim JW. Compartmentalization of vertebrate optic neuroephithelium: external cues and transcription factors. *Mol Cells* 2012;33:317-324.

5. Panda-Jonas S, Jonas JB, Jakobczyk-Zmija M. Retinal pigment epithelial cell count, distribution, and correlations in normal human eyes. *American journal of ophthalmology* 1996;121:181-189.

6. Strauss O. The retinal pigment epithelium in visual function. *Physiol Rev* 2005;85:845-881.

7. Boulton M, Dayhaw-Barker P. The role of the retinal pigment epithelium: topographical variation and ageing changes. *Eye* 2001;15:384-389.

8. World-Health-Organization. Age-related macular degeneration. *Prevention of blindness and visual impairment--priority eye diseases*: World Health Organization; 2014.

9. Access-Economics. The global economic cost of visual impairment. Vienna, Austria: AMD Alliance International; 2010.

10. Friedman DS, Katz J, Bressler NM, Rahmani B, Tielsch JM. Racial differences in the prevalence of age-related macular degeneration: the Baltimore Eye Survey. *Ophthalmology* 1999;106:1049-1055.

11. Cruickshanks KJ, Klein R, Klein BE. Sunlight and age-related macular degeneration. The Beaver Dam Eye Study. *Archives of ophthalmology* 1993;111:514-518.

12. Vingerling JR, Dielemans I, Hofman A, et al. The prevalence of age-related maculopathy in the Rotterdam Study. *Ophthalmology* 1995;102:205-210.

13. Friedman DS, O'Colmain BJ, Munoz B, et al. Prevalence of age-related macular degeneration in the United States. *Archives of ophthalmology* 2004;122:564-572.

14. Age-Related Eye Disease Study Research G. A randomized, placebo-controlled, clinical trial of high-dose supplementation with vitamins C and E, beta carotene, and zinc for age-related macular degeneration and vision loss: AREDS report no. 8. *Archives of ophthalmology* 2001;119:1417-1436.

15. Age-Related Eye Disease Study 2 Research G. Lutein + zeaxanthin and omega-3 fatty acids for age-related macular degeneration: the Age-Related Eye Disease Study 2 (AREDS2) randomized clinical trial. *JAMA : the journal of the American Medical Association* 2013;309:2005-2015.

16. Chew EY, Clemons TE, Agron E, et al. Long-term effects of vitamins C and E, beta-carotene, and zinc on age-related macular degeneration: AREDS report no. 35. *Ophthalmology* 2013;120:1604-1611 e1604.

17. Woodell A, Rohrer B. A mechanistic review of cigarette smoke and age-related macular degeneration. *Advances in experimental medicine and biology* 2014;801:301-307.

18. Davis MD, Gangnon RE, Lee LY, et al. The Age-Related Eye Disease Study severity scale for age-related macular degeneration: AREDS Report No. 17. *Archives of ophthalmology* 2005;123:1484-1498.

19. Fine SL, Berger JW, Maguire MG, Ho AC. Age-related macular degeneration. *The New England journal of medicine* 2000;342:483-492.

20. Anderson DH, Mullins RF, Hageman GS, Johnson LV. A role for local inflammation in the formation of drusen in the aging eye. *American journal of ophthalmology* 2002;134:411-431.

21. Klein ML, Ferris FL, 3rd, Armstrong J, et al. Retinal precursors and the development of geographic atrophy in age-related macular degeneration. *Ophthalmology* 2008;115:1026-1031.

22. Camelo S. Potential Sources and Roles of Adaptive Immunity in Age-Related Macular Degeneration: Shall We Rename AMD into Autoimmune Macular Disease? *Autoimmune diseases* 2014;2014:532487.

23. Iannaccone A, Neeli I, Krishnamurthy P, et al. Autoimmune biomarkers in age-related macular degeneration: a possible role player in disease development and progression. *Advances in experimental medicine and biology* 2012;723:11-16.

24. Menu P, Vince JE. The NLRP3 inflammasome in health and disease: the good, the bad and the ugly. *Clinical and experimental immunology* 2011;166:1-15.

25. Lamkanfi M, Vande Walle L, Kanneganti TD. Deregulated inflammasome signaling in disease. *Immunological reviews* 2011;243:163-173.

26. Davis BK, Wen H, Ting JP. The inflammasome NLRs in immunity, inflammation, and associated diseases. *Annual review of immunology* 2011;29:707-735.

27. Franchi L, Eigenbrod T, Munoz-Planillo R, Nunez G. The inflammasome: a caspase-1-activation platform that regulates immune responses and disease pathogenesis. *Nature immunology* 2009;10:241-247.

28. Lamkanfi M, Dixit VM. Mechanisms and functions of inflammasomes. *Cell* 2014;157:1013-1022.

29. Kayagaki N, Warming S, Lamkanfi M, et al. Non-canonical inflammasome activation targets caspase-11. *Nature* 2011;479:117-121.

30. Lawlor KE, Vince JE. Ambiguities in NLRP3 inflammasome regulation: is there a role for mitochondria? *Biochimica et biophysica acta* 2014;1840:1433-1440.

31. Sutterwala FS, Haasken S, Cassel SL. Mechanism of NLRP3 inflammasome activation. *Annals of the New York Academy of Sciences* 2014;1319:82-95.

32. Tseng WA, Thein T, Kinnunen K, et al. NLRP3 inflammasome activation in retinal pigment epithelial cells by lysosomal destabilization: implications for age-related macular degeneration. *Invest Ophthalmol Vis Sci* 2013;54:110-120.

33. Bauernfeind FG, Horvath G, Stutz A, et al. Cutting edge: NF-kappaB activating pattern recognition and cytokine receptors license NLRP3 inflammasome activation by regulating NLRP3 expression. *Journal of immunology* 2009;183:787-791.

34. Kerur N, Hirano Y, Tarallo V, et al. TLR-independent and P2X7-dependent signaling mediate Alu RNA-induced NLRP3 inflammasome activation in geographic atrophy. *Invest Ophthalmol Vis Sci* 2013;54:7395-7401.

35. Doyle SL, Ozaki E, Brennan K, et al. IL-18 attenuates experimental choroidal neovascularization as a potential therapy for wet age-related macular degeneration. *Sci Transl Med* 2014;6:230ra244.

36. Tarallo V, Hirano Y, Gelfand BD, et al. DICER1 loss and Alu RNA induce age-related macular degeneration via the NLRP3 inflammasome and MyD88. *Cell* 2012;149:847-859.

37. Juliana C, Fernandes-Alnemri T, Kang S, Farias A, Qin F, Alnemri ES. Non-transcriptional priming and deubiquitination regulate NLRP3 inflammasome activation. *The Journal of biological chemistry* 2012;287:36617-36622.

38. Di Virgilio F. The therapeutic potential of modifying inflammasomes and NOD-like receptors. *Pharmacological reviews* 2013;65:872-905.

39. Munoz-Planillo R, Kuffa P, Martinez-Colon G, Smith BL, Rajendiran TM, Nunez G. K(+) efflux is the common trigger of NLRP3 inflammasome activation by bacterial toxins and particulate matter. *Immunity* 2013;38:1142-1153.

40. Hornung V, Bauernfeind F, Halle A, et al. Silica crystals and aluminum salts activate the NALP3 inflammasome through phagosomal destabilization. *Nature immunology* 2008;9:847-856.

41. Zhou R, Yazdi AS, Menu P, Tschopp J. A role for mitochondria in NLRP3 inflammasome activation. *Nature* 2011;469:221-225.

42. Misawa T, Takahama M, Kozaki T, et al. Microtubule-driven spatial arrangement of mitochondria promotes activation of the NLRP3 inflammasome. *Nature immunology* 2013;14:454-460.

43. Doyle SL, Campbell M, Ozaki E, et al. NLRP3 has a protective role in age-related macular degeneration through the induction of IL-18 by drusen components. *Nature medicine* 2012;18:791-798.

44. Mevorach D. Clearance of dying cells and systemic lupus erythematosus: the role of C1q and the complement system. *Apoptosis : an international journal on programmed cell death* 2010;15:1114-1123.

45. Anderson DH, Radeke MJ, Gallo NB, et al. The pivotal role of the complement system in aging and age-related macular degeneration: hypothesis re-visited. *Progress in retinal and eye research* 2010;29:95-112.

46. Khandhadia S, Cipriani V, Yates JR, Lotery AJ. Age-related macular degeneration and the complement system. *Immunobiology* 2012;217:127-146.

47. Asgari E, Le Friec G, Yamamoto H, et al. C3a modulates IL-1beta secretion in human monocytes by regulating ATP efflux and subsequent NLRP3 inflammasome activation. *Blood* 2013;122:3473-3481.

48. Laudisi F, Spreafico R, Evrard M, et al. Cutting edge: the NLRP3 inflammasome links complement-mediated inflammation and IL-1beta release. *Journal of immunology* 2013;191:1006-1010.

49. Triantafilou K, Hughes TR, Triantafilou M, Morgan BP. The complement membrane attack complex triggers intracellular Ca2+ fluxes leading to NLRP3 inflammasome activation. *Journal of cell science* 2013;126:2903-2913.

50. Johnson LV, Leitner WP, Rivest AJ, Staples MK, Radeke MJ, Anderson DH. The Alzheimer's A beta -peptide is deposited at sites of complement activation in pathologic deposits associated with aging and age-related macular degeneration. *Proceedings of the National Academy of Sciences of the United States of America* 2002;99:11830-11835.

51. Anderson DH, Talaga KC, Rivest AJ, Barron E, Hageman GS, Johnson LV. Characterization of beta amyloid assemblies in drusen: the deposits associated with aging and age-related macular degeneration. *Experimental eye research* 2004;78:243-256.

52. Isas JM, Luibl V, Johnson LV, et al. Soluble and mature amyloid fibrils in drusen deposits. *Investigative ophthalmology & visual science* 2010;51:1304-1310.

53. Haass C, Selkoe DJ. Soluble protein oligomers in neurodegeneration: lessons from the Alzheimer's amyloid beta-peptide. *Nature reviews Molecular cell biology* 2007;8:101-112.

54. Iwata N, Tsubuki S, Takaki Y, et al. Identification of the major Abeta1-42-degrading catabolic pathway in brain parenchyma: suppression leads to biochemical and pathological deposition. *Nature medicine* 2000;6:143-150.

55. Madani R, Poirier R, Wolfer DP, et al. Lack of neprilysin suffices to generate murine amyloid-like deposits in the brain and behavioral deficit in vivo. *Journal of neuroscience research* 2006;84:1871-1878.

56. Kayed R, Head E, Thompson JL, et al. Common structure of soluble amyloid oligomers implies common mechanism of pathogenesis. *Science* 2003;300:486-489.

57. Walsh DM, Klyubin I, Fadeeva JV, et al. Naturally secreted oligomers of amyloid beta protein potently inhibit hippocampal long-term potentiation in vivo. *Nature* 2002;416:535-539.

58. Klein WL, Krafft GA, Finch CE. Targeting small Abeta oligomers: the solution to an Alzheimer's disease conundrum? *Trends in neurosciences* 2001;24:219-224.

59. Kirkitadze MD, Bitan G, Teplow DB. Paradigm shifts in Alzheimer's disease and other neurodegenerative disorders: the emerging role of oligomeric assemblies. *Journal of neuroscience research* 2002;69:567-577.

60. Caughey B, Lansbury PT. Protofibrils, pores, fibrils, and neurodegeneration: separating the responsible protein aggregates from the innocent bystanders. *Annual review of neuroscience* 2003;26:267-298.

61. Luibl V, Isas JM, Kayed R, Glabe CG, Langen R, Chen J. Drusen deposits associated with aging and age-related macular degeneration contain nonfibrillar amyloid oligomers. *The Journal of clinical investigation* 2006;116:378-385.

62. Dentchev T, Milam AH, Lee VM, Trojanowski JQ, Dunaief JL. Amyloid-beta is found in drusen from some age-related macular degeneration retinas, but not in drusen from normal retinas. *Molecular vision* 2003;9:184-190.

63. Hoh Kam J, Lenassi E, Jeffery G. Viewing ageing eyes: diverse sites of amyloid Beta accumulation in the ageing mouse retina and the up-regulation of macrophages. *PLoS One* 2010;5.

64. Yoshida T, Ohno-Matsui K, Ichinose S, et al. The potential role of amyloid beta in the pathogenesis of age-related macular degeneration. *The Journal of clinical investigation* 2005;115:2793-2800.

65. Kurji KH, Cui JZ, Lin T, et al. Microarray analysis identifies changes in inflammatory gene expression in response to amyloid-beta stimulation of cultured human retinal pigment epithelial cells. *Invest Ophthalmol Vis Sci* 2010;51:1151-1163.

66. Crabb JW, Miyagi M, Gu X, et al. Drusen proteome analysis: an approach to the etiology of age-related macular degeneration. *Proceedings of the National Academy of Sciences of the United States of America* 2002;99:14682-14687.

67. Riera CE, Dillin A. Can aging be 'drugged'? *Nature medicine* 2015;21:1400-1405.

68. Terman A, Kurz T, Navratil M, Arriaga EA, Brunk UT. Mitochondrial turnover and aging of long-lived postmitotic cells: the mitochondrial-lysosomal axis theory of aging. *Antioxid Redox Signal* 2010;12:503-535.

69. Sarks JP, Sarks SH, Killingsworth MC. Evolution of geographic atrophy of the retinal pigment epithelium. *Eye (Lond)* 1988;2 (Pt 5):552-577.

70. Kaneko H, Dridi S, Tarallo V, et al. DICER1 deficit induces Alu RNA toxicity in age-related macular degeneration. *Nature* 2011;471:325-330.

71. Bressler SB, Bressler, N.M. Age-related Macular Degeneration: Non-neovascular Early AMD, Intermediate AMD, and Geographic Atrophy In: Ryan SJ (ed), *Retina*: Elsevier; 2014:1150-1182.

72. Gao H, Hollyfield JG. Aging of the human retina. Differential loss of neurons and retinal pigment epithelial cells. *Investigative ophthalmology & visual science* 1992;33:1-17.

73. Iyer SS, Pulskens WP, Sadler JJ, et al. Necrotic cells trigger a sterile inflammatory response through the Nlrp3 inflammasome. *Proceedings of the National Academy of Sciences of the United States of America* 2009;106:20388-20393.

74. Kim Y, Tarallo V, Kerur N, et al. DICER1/Alu RNA dysmetabolism induces Caspase-8-mediated cell death in age-related macular degeneration. *Proceedings of the National Academy of Sciences of the United States of America* 2014;111:16082-16087.

75. Newman AM, Gallo NB, Hancox LS, et al. Systems-level analysis of age-related macular degeneration reveals global biomarkers and phenotype-specific functional networks. *Genome medicine* 2012;4:16.

76. Leonard KC, Petrin D, Coupland SG, et al. XIAP protection of photoreceptors in animal models of retinitis pigmentosa. *PloS one* 2007;2:e314.

77. Liston P, Fong WG, Korneluk RG. The inhibitors of apoptosis: there is more to life than Bcl2. *Oncogene* 2003;22:8568-8580.

78. Kaufmann T, Strasser A, Jost PJ. Fas death receptor signalling: roles of Bid and XIAP. *Cell Death Differ* 2012;19:42-50.

79. Gao J, Wang A, Cui JZ, Tsilfidis C, Matsubara JA. XIAP protects RPE cells from oligomeric Aβ1-40 induced cell death. *ARVO E-abstract Orlando USA* 2014.

80. Shan H, Ji D, Barnard AR, et al. AAV-mediated gene transfer of human X-linked inhibitor of apoptosis protects against oxidative cell death in human RPE cells. *Invest Ophthalmol Vis Sci* 2011;52:9591-9597.

81. Vince JE, Wong WW, Gentle I, et al. Inhibitor of apoptosis proteins limit RIP3 kinase-dependent interleukin-1 activation. *Immunity* 2012;36:215-227.

82. Licandro G, Ling Khor H, Beretta O, et al. The NLRP3 inflammasome affects DNA damage responses after oxidative and genotoxic stress in dendritic cells. *Eur J Immunol* 2013;43:2126-2137.

83. de Rivero Vaccari JP, Lotocki G, Marcillo AE, Dietrich WD, Keane RW. A molecular platform in neurons regulates inflammation after spinal cord injury. *J Neurosci* 2008;28:3404-3414.

84. Ardeljan D, Chan CC. Aging is not a disease: distinguishing age-related macular degeneration from aging. *Progress in retinal and eye research* 2013;37:68-89.

85. Rodriguez-Muela N, Koga H, Garcia-Ledo L, et al. Balance between autophagic pathways preserves retinal homeostasis. *Aging Cell* 2013;12:478-488.

86. Chen M, Muckersie E, Forrester JV, Xu H. Immune activation in retinal aging: a gene expression study. *Investigative ophthalmology & visual science* 2010;51:5888-5896.

87. Ricklin D, Hajishengallis G, Yang K, Lambris JD. Complement: a key system for immune surveillance and homeostasis. *Nature immunology* 2010;11:785-797.

88. Mullins RF, Schoo DP, Sohn EH, et al. The membrane attack complex in aging human choriocapillaris: relationship to macular degeneration and choroidal thinning. *Am J Pathol* 2014;184:3142-3153.

89. Mullins RF, Dewald AD, Streb LM, Wang K, Kuehn MH, Stone EM. Elevated membrane attack complex in human choroid with high risk complement factor H genotypes. *Experimental eye research* 2011;93:565-567.

90. Cao S, Ko A, Partanen M, et al. Relationship between systemic cytokines and complement factor H Y402H polymorphism in patients with dry age-related macular degeneration. *American journal of ophthalmology* 2013;156:1176-1183.

91. Seth A, Cui J, To E, Kwee M, Matsubara J. Complement-associated deposits in the human retina. *Investigative ophthalmology & visual science* 2008;49:743-750.

92. Xu H, Chen M, Forrester JV. Para-inflammation in the aging retina. *Progress in retinal and eye research* 2009;28:348-368.

93. Chen H, Liu B, Lukas TJ, Neufeld AH. The aged retinal pigment epithelium/choroid: a potential substratum for the pathogenesis of age-related macular degeneration. *PloS one* 2008;3:e2339.

94. Whitmore SS, Sohn EH, Chirco KR, et al. Complement activation and choriocapillaris loss in early AMD: implications for pathophysiology and therapy. *Progress in retinal and eye research* 2015;45:1-29.

95. Lakkaraju A, Toops KA, Xu J. Should I stay or should I go? Trafficking of sub-lytic MAC in the retinal pigment epithelium. *Advances in experimental medicine and biology* 2014;801:267-274.

96. Xu H, Chen M. Targeting the complement system for the management of retinal inflammatory and degenerative diseases. *Eur J Pharmacol* 2016;787:94-104.

97. Lueck K, Wasmuth S, Williams J, et al. Sub-lytic C5b-9 induces functional changes in retinal pigment epithelial cells consistent with age-related macular degeneration. *Eye* 2011;25:1074-1082.

98. Lee M, Guo JP, Schwab C, McGeer EG, McGeer PL. Selective inhibition of the membrane attack complex of complement by low molecular weight components of the aurin tricarboxylic acid synthetic complex. *Neurobiology of aging* 2012;33:2237-2246.

99. Lee M, Guo JP, McGeer EG, McGeer PL. Aurin tricarboxylic acid self-protects by inhibiting aberrant complement activation at the C3 convertase and C9 binding stages. *Neurobiology of aging* 2013;34:1451-1461.

100. Ning A, Cui J, To E, Ashe KH, Matsubara J. Amyloid-beta deposits lead to retinal degeneration in a mouse model of Alzheimer disease. *Investigative ophthalmology & visual science* 2008;49:5136-5143.

101. Jiang K, To E, Cui JZ, Cao S, Gao J, Matsubara JA. Drusen and Pro-inflammatory Mediators in the Post-Mortem Human Eye. *Journal of clinical & experimental ophthalmology* 2012;3:208.

102. Liu RT, Wang A, To E, et al. Vinpocetine inhibits amyloid-beta induced activation of NF-kappaB, NLRP3 inflammasome and cytokine production in retinal pigment epithelial cells. *Experimental eye research* 2014;127C:49-58.

103. Shen Y, Yang L, Li R. What does complement do in Alzheimer's disease? Old molecules with new insights. *Translational neurodegeneration* 2013;2:21.

104. Prakasam A, Muthuswamy A, Ablonczy Z, et al. Differential accumulation of secreted AbetaPP metabolites in ocular fluids. *J Alzheimers Dis* 2010;20:1243-1253.

105. Ferriani VP, Barbosa JE, de Carvalho IF. Complement haemolytic activity (classical and alternative pathways), C3, C4 and factor B titres in healthy children. *Acta paediatrica (Oslo, Norway : 1992)* 1999;88:1062-1066.

106. Cao S, Walker GB, Wang X, Cui JZ, Matsubara JA. Altered cytokine profiles of human retinal pigment epithelium: oxidant injury and replicative senescence. *Molecular vision* 2013;19:718-728.

107. Rogers J, Cooper NR, Webster S, et al. Complement activation by beta-amyloid in Alzheimer disease. *Proceedings of the National Academy of Sciences of the United States of America* 1992;89:10016-10020.

108. Velazquez P, Cribbs DH, Poulos TL, Tenner AJ. Aspartate residue 7 in amyloid beta-protein is critical for classical complement pathway activation: implications for Alzheimer's disease pathogenesis. *Nature medicine* 1997;3:77-79.

109. Perkins ND. The diverse and complex roles of NF-kappaB subunits in cancer. *Nat Rev Cancer* 2012;12:121-132.

110. Huang Y, Krein PM, Muruve DA, Winston BW. Complement factor B gene regulation: synergistic effects of TNF-alpha and IFN-gamma in macrophages. *Journal of immunology* 2002;169:2627-2635.

111. Moon MR, Parikh AA, Pritts TA, et al. Complement component C3 production in IL-1beta-stimulated human intestinal epithelial cells is blocked by NF-kappaB inhibitors and by transfection with ser 32/36 mutant IkappaBalpha. *J Surg Res* 1999;82:48-55.

112. Yu DY, Huang ZM, Murakami S, Takahashi M, Nonaka M. Specific binding of a hepatoma nuclear factor to the NF.kappa B/H2TF1 recognition motif found in the C4 promoter, but not in the Slp promoter. *Journal of immunology* 1989;143:2395-2400.

113. Liu RT, Gao J, Cao S, et al. Inflammatory mediators induced by amyloid-beta in the retina and RPE in vivo: implications for inflammasome activation in age-related macular degeneration. *Invest Ophthalmol Vis Sci* 2013;54:2225-2237.

114. Leibowitz HM, Krueger DE, Maunder LR, et al. The Framingham Eye Study monograph: An ophthalmological and epidemiological study of cataract, glaucoma, diabetic retinopathy, macular degeneration, and visual acuity in a general population of 2631 adults, 1973-1975. *Survey of ophthalmology* 1980;24:335-610.

115. Bird AC, Bressler NM, Bressler SB, et al. An international classification and grading system for age-related maculopathy and age-related macular degeneration. The International ARM Epidemiological Study Group. *Survey of ophthalmology* 1995;39:367-374.

116. Hogg RE, Stevenson MR, Chakravarthy U, Beirne RO, Anderson RS. Early features of AMD. *Ophthalmology* 2007;114:1028.

117. Hageman GS, Luthert PJ, Victor Chong NH, Johnson LV, Anderson DH, Mullins RF. An integrated hypothesis that considers drusen as biomarkers of immune-mediated processes at the

RPE-Bruch's membrane interface in aging and age-related macular degeneration. *Progress in retinal and eye research* 2001;20:705-732.

118. Klein R, Klein BE, Tomany SC, Meuer SM, Huang GH. Ten-year incidence and progression of age-related maculopathy: The Beaver Dam eye study. *Ophthalmology* 2002;109:1767-1779.

119. Yehoshua Z, Rosenfeld PJ, Albini TA. Current Clinical Trials in Dry AMD and the Definition of Appropriate Clinical Outcome Measures. *Semin Ophthalmol* 2011;26:167-180.

120. Bruban J, Glotin AL, Dinet V, et al. Amyloid-beta(1-42) alters structure and function of retinal pigmented epithelial cells. *Aging Cell* 2009;8:162-177.

121. Walsh DT, Bresciani L, Saunders D, et al. Amyloid beta peptide causes chronic glial cell activation and neuro-degeneration after intravitreal injection. *Neuropathol Appl Neurobiol* 2005;31:491-502.

122. Dahlgren KN, Manelli AM, Stine WB, Jr., Baker LK, Krafft GA, LaDu MJ. Oligomeric and fibrillar species of amyloid-beta peptides differentially affect neuronal viability. *The Journal of biological chemistry* 2002;277:32046-32053.

123. Halle A, Hornung V, Petzold GC, et al. The NALP3 inflammasome is involved in the innate immune response to amyloid-beta. *Nature immunology* 2008;9:857-865.

124. Nakazawa T, Kayama M, Ryu M, et al. Tumor necrosis factor-alpha mediates photoreceptor death in a rodent model of retinal detachment. *Investigative ophthalmology & visual science* 2011;52:1384-1391.

125. Howlett DR, Bate ST, Collier S, et al. Characterisation of amyloid-induced inflammatory responses in the rat retina. *Exp Brain Res* 2011;214:185-197.

126. Landa G, Butovsky O, Shoshani J, Schwartz M, Pollack A. Weekly vaccination with Copaxone (glatiramer acetate) as a potential therapy for dry age-related macular degeneration. *Curr Eye Res* 2008;33:1011-1013.

127. Anderson PJ, Watts H, Hille C, et al. Glial and endothelial blood-retinal barrier responses to amyloid-beta in the neural retina of the rat. *Clin Ophthalmol* 2008;2:801-816.

128. Walsh DT, Montero RM, Bresciani LG, et al. Amyloid-beta peptide is toxic to neurons in vivo via indirect mechanisms. *Neurobiol Dis* 2002;10:20-27.

129. Guo L, Normando EM, Nizari S, Lara D, Cordeiro MF. Tracking longitudinal retinal changes in experimental ocular hypertension using the cSLO and spectral domain-OCT. *Investigative ophthalmology & visual science* 2010;51:6504-6513.

130. Davis D, Zhang, A., Etienne, C., Huang, I., Malit, M. Tech Note 2861: Principles of Curve Fitting for Multiplex Sandwich Immunoassays. Hercules, CA: Bio-Rad; 2012.

131. Seddon JM, George S, Rosner B, Rifai N. Progression of age-related macular degeneration: prospective assessment of C-reactive protein, interleukin 6, and other cardiovascular biomarkers. *Archives of ophthalmology* 2005;123:774-782.

132. Bian ZM, Elner SG, Yoshida A, Elner VM. Human RPE-monocyte co-culture induces chemokine gene expression through activation of MAPK and NIK cascade. *Experimental eye research* 2003;76:573-583.

133. Martinon F, Burns K, Tschopp J. The inflammasome: a molecular platform triggering activation of inflammatory caspases and processing of proIL-beta. *Molecular cell* 2002;10:417-426.

134. Elner SG, Elner VM, Jaffe GJ, Stuart A, Kunkel SL, Strieter RM. Cytokines in proliferative diabetic retinopathy and proliferative vitreoretinopathy. *Curr Eye Res* 1995;14:1045-1053.

135. Noma H, Funatsu H, Mimura T, Harino S, Hori S. Vitreous levels of interleukin-6 and vascular endothelial growth factor in macular edema with central retinal vein occlusion. *Ophthalmology* 2009;116:87-93.

136. Wang J, Ohno-Matsui K, Yoshida T, et al. Amyloid-beta up-regulates complement factor B in retinal pigment epithelial cells through cytokines released from recruited macrophages/microglia: Another mechanism of complement activation in age-related macular degeneration. *J Cell Physiol* 2009;220:119-128.

137. Ma W, Zhao L, Fontainhas AM, Fariss RN, Wong WT. Microglia in the mouse retina alter the structure and function of retinal pigmented epithelial cells: a potential cellular interaction relevant to AMD. *PloS one* 2009;4:e7945.

138. Rosenbaum DM, Degterev A, David J, et al. Necroptosis, a novel form of caspase-independent cell death, contributes to neuronal damage in a retinal ischemia-reperfusion injury model. *Journal of neuroscience research* 2010;88:1569-1576.

139. Mullins RF, Russell SR, Anderson DH, Hageman GS. Drusen associated with aging and age-related macular degeneration contain proteins common to extracellular deposits associated with atherosclerosis, elastosis, amyloidosis, and dense deposit disease. *FASEB journal : official publication of the Federation of American Societies for Experimental Biology* 2000;14:835-846.

140. Klein RJ, Zeiss C, Chew EY, et al. Complement factor H polymorphism in age-related macular degeneration. *Science* 2005;308:385-389.

141. Mo FM, Proia AD, Johnson WH, Cyr D, Lashkari K. Interferon gamma-inducible protein-10 (IP-10) and eotaxin as biomarkers in age-related macular degeneration. *Investigative ophthalmology & visual science* 2010;51:4226-4236.

142. Holtkamp GM, Kijlstra A, Peek R, de Vos AF. Retinal pigment epithelium-immune system interactions: cytokine production and cytokine-induced changes. *Progress in retinal and eye research* 2001;20:29-48.

143. Planck SR, Huang XN, Robertson JE, Rosenbaum JT. Retinal pigment epithelial cells produce interleukin-1 beta and granulocyte-macrophage colony-stimulating factor in response to interleukin-1 alpha. *Curr Eye Res* 1993;12:205-212.

144. Nakazawa T, Matsubara A, Noda K, et al. Characterization of cytokine responses to retinal detachment in rats. *Molecular vision* 2006;12:867-878.

145. Kauppinen A, Niskanen H, Suuronen T, Kinnunen K, Salminen A, Kaarniranta K. Oxidative stress activates NLRP3 inflammasomes in ARPE-19 cells--implications for age-related macular degeneration (AMD). *Immunology letters* 2012;147:29-33.

146. Jaffe GJ, Van Le L, Valea F, et al. Expression of interleukin-1 alpha, interleukin-1 beta, and an interleukin-1 receptor antagonist in human retinal pigment epithelial cells. *Experimental eye research* 1992;55:325-335.

147. Elner VM, Scales W, Elner SG, Danforth J, Kunkel SL, Strieter RM. Interleukin-6 (IL-6) gene expression and secretion by cytokine-stimulated human retinal pigment epithelial cells. *Experimental eye research* 1992;54:361-368.

148. Hangai M, Yoshimura N, Honda Y. Increased cytokine gene expression in rat retina following transient ischemia. *Ophthalmic Res* 1996;28:248-254.

149. Schutyser E, Struyf S, Van Damme J. The CC chemokine CCL20 and its receptor CCR6. *Cytokine Growth Factor Rev* 2003;14:409-426.

150. Chen Y, Yang P, Li F, Kijlstra A. The effects of Th17 cytokines on the inflammatory mediator production and barrier function of ARPE-19 cells. *PloS one* 2011;6:e18139.

151. Bian ZM, Elner SG, Khanna H, Murga-Zamalloa CA, Patil S, Elner VM. Expression and functional roles of caspase-5 in inflammatory responses of human retinal pigment epithelial cells. *Investigative ophthalmology & visual science* 2011;52:8646-8656.

152. Yang P, McKay BS, Allen JB, Jaffe GJ. Effect of NF-kappa B inhibition on TNF-alpha-induced apoptosis in human RPE cells. *Investigative ophthalmology & visual science* 2004;45:2438-2446.

153. Yang P, Peairs JJ, Tano R, Zhang N, Tyrell J, Jaffe GJ. Caspase-8-mediated apoptosis in human RPE cells. *Investigative ophthalmology & visual science* 2007;48:3341-3349.

154. Dunaief JL, Dentchev T, Ying GS, Milam AH. The role of apoptosis in age-related macular degeneration. *Archives of ophthalmology* 2002;120:1435-1442.

155. Xia Y, Novak R, Lewis J, Duckett CS, Phillips AC. Xaf1 can cooperate with TNFalpha in the induction of apoptosis, independently of interaction with XIAP. *Mol Cell Biochem* 2006;286:67-76.

156. Kempkensteffen C, Fritzsche FR, Johannsen M, et al. Down-regulation of the pro-apoptotic XIAP associated factor-1 (XAF1) during progression of clear-cell renal cancer. *BMC Cancer* 2009;9:276.

157. Malek G, Johnson LV, Mace BE, et al. Apolipoprotein E allele-dependent pathogenesis: a model for age-related retinal degeneration. *Proceedings of the National Academy of Sciences of the United States of America* 2005;102:11900-11905.

158. Chan CC, Ross RJ, Shen D, et al. Ccl2/Cx3cr1-deficient mice: an animal model for age-related macular degeneration. *Ophthalmic Res* 2008;40:124-128.

159. Ambati J, Anand A, Fernandez S, et al. An animal model of age-related macular degeneration in senescent Ccl-2- or Ccr-2-deficient mice. *Nature medicine* 2003;9:1390-1397.

160. Chen M, Forrester JV, Xu H. Dysregulation in retinal para-inflammation and age-related retinal degeneration in CCL2 or CCR2 deficient mice. *PloS one* 2011;6:e22818.

161. Wang Y, Wang VM, Chan CC. The role of anti-inflammatory agents in age-related macular degeneration (AMD) treatment. *Eye* 2011;25:127-139.

162. Masters SL, O'Neill LA. Disease-associated amyloid and misfolded protein aggregates activate the inflammasome. *Trends Mol Med* 2011;17:276-282.

163. Tschopp J, Schroder K. NLRP3 inflammasome activation: The convergence of multiple signalling pathways on ROS production? *Nature reviews Immunology* 2010;10:210-215.

164. Ding JD, Johnson LV, Herrmann R, et al. Anti-amyloid therapy protects against retinal pigmented epithelium damage and vision loss in a model of age-related macular degeneration. *Proceedings of the National Academy of Sciences of the United States of America* 2011;108:E279-287.

165. Szatmari SZ, Whitehouse PJ. Vinpocetine for cognitive impairment and dementia. *Cochrane Database Syst Rev* 2003;CD003119.

166. Tamaki N, Matsumoto S. [Agents to improve cerebrovascular circulation and cerebral metabolism--vinpocetine]. *Nihon Rinsho* 1985;43:376-378.

167. Jeon KI, Xu X, Aizawa T, et al. Vinpocetine inhibits NF-kappaB-dependent inflammation via an IKK-dependent but PDE-independent mechanism. *Proceedings of the National Academy of Sciences of the United States of America* 2010;107:9795-9800.

168. Segovia J, Sabbah A, Mgbemena V, et al. TLR2/MyD88/NF-kappaB pathway, reactive oxygen species, potassium efflux activates NLRP3/ASC inflammasome during respiratory syncytial virus infection. *PloS one* 2012;7:e29695.

169. Bouwmeester T, Bauch A, Ruffner H, et al. A physical and functional map of the human TNF-alpha/NF-kappa B signal transduction pathway. *Nat Cell Biol* 2004;6:97-105.

170. Blackwell TS, Christman JW. The role of nuclear factor-kappa B in cytokine gene regulation. *Am J Respir Cell Mol Biol* 1997;17:3-9.

171. Zhao T, Gao J, Van J, et al. Age-related increases in amyloid beta and membrane attack complex: evidence of inflammasome activation in the rodent eye. *J Neuroinflammation* 2015;12:121.

172. Pereira C, Agostinho P, Oliveira CR. Vinpocetine attenuates the metabolic dysfunction induced by amyloid beta-peptides in PC12 cells. *Free Radic Res* 2000;33:497-506.

173. Lee J, Rhee MH, Kim E, Cho JY. BAY 11-7082 is a broad-spectrum inhibitor with anti-inflammatory activity against multiple targets. *Mediators Inflamm* 2012;2012:416036.

174. Lemon B, Tjian R. Orchestrated response: a symphony of transcription factors for gene control. *Genes Dev* 2000;14:2551-2569.

175. Napetschnig J, Wu H. Molecular basis of NF-kappaB signaling. *Annu Rev Biophys* 2013;42:443-468.

176. Polgar M, Vereczkey L, Nyary I. Pharmacokinetics of vinpocetine and its metabolite, apovincaminic acid, in plasma and cerebrospinal fluid after intravenous infusion. *J Pharm Biomed Anal* 1985;3:131-139.

177. Zhao YY, Yu JZ, Li QY, Ma CG, Lu CZ, Xiao BG. TSPO-specific ligand vinpocetine exerts a neuroprotective effect by suppressing microglial inflammation. *Neuron Glia Biol* 2011;7:187-197.

178. Chang SH, Dong C. Signaling of interleukin-17 family cytokines in immunity and inflammation. *Cell Signal* 2011;23:1069-1075.

179. Dinarello CA. Immunological and inflammatory functions of the interleukin-1 family. *Annual review of immunology* 2009;27:519-550.

180. Lin T, Walker GB, Kurji K, et al. Parainflammation associated with advanced glycation endproduct stimulation of RPE in vitro: implications for age-related degenerative diseases of the eye. *Cytokine* 2013;62:369-381.

181. Chen Y, Kijlstra A, Chen Y, Yang P. IL-17A stimulates the production of inflammatory mediators via Erk1/2, p38 MAPK, PI3K/Akt, and NF-kappaB pathways in ARPE-19 cells. *Molecular vision* 2011;17:3072-3077.

182. Medina AE. Vinpocetine as a potent antiinflammatory agent. *Proceedings of the National Academy of Sciences of the United States of America* 2010;107:9921-9922.

183. Strowig T, Henao-Mejia J, Elinav E, Flavell R. Inflammasomes in health and disease. *Nature* 2012;481:278-286.

184. Kavita U, Mizel SB. Differential sensitivity of interleukin-1 alpha and -beta precursor proteins to cleavage by calpain, a calcium-dependent protease. *The Journal of biological chemistry* 1995;270:27758-27765.

185. Yazdi AS, Guarda G, Riteau N, et al. Nanoparticles activate the NLR pyrin domain containing 3 (Nlrp3) inflammasome and cause pulmonary inflammation through release of IL-1alpha and IL-1beta. *Proceedings of the National Academy of Sciences of the United States of America* 2010;107:19449-19454.

186. Kim SJ, Ahn JW, Kim H, et al. Two beta-strands of RAGE participate in the recognition and transport of amyloid-beta peptide across the blood brain barrier. *Biochem Biophys Res Commun* 2013;439:252-257.

187. Meneghini V, Bortolotto V, Francese MT, et al. High-mobility group box-1 protein and beta-amyloid oligomers promote neuronal differentiation of adult hippocampal neural progenitors via receptor for advanced glycation end products/nuclear factor-kappaB axis: relevance for Alzheimer's disease. *J Neurosci* 2013;33:6047-6059.

188. Chang CK, Llanes S, Schumer W. Inhibitory effect of dimethyl sulfoxide on nuclear factor-kappa B activation and intercellular adhesion molecule 1 gene expression in septic rats. *J Surg Res* 1999;82:294-299.

189. Wong WL, Su X, Li X, et al. Global prevalence of age-related macular degeneration and disease burden projection for 2020 and 2040: a systematic review and meta-analysis. *Lancet Glob Health* 2014;2:e106-116.

190. Age-Related Eye Disease Study Research G. A Simplified Severity Scale for Age-Related Macular Degeneration: AREDS Report No. 18. *Archives of ophthalmology* 2005;123:1570-1574.

191. Amoaku WM, Chakravarthy U, Gale R, et al. Defining response to anti-VEGF therapies in neovascular AMD. *Eye* 2015;29:721-731.

192. Bergsbaken T, Fink SL, Cookson BT. Pyroptosis: host cell death and inflammation. *Nat Rev Microbiol* 2009;7:99-109.

193. Gao J, Liu RT, Cao S, et al. NLRP3 inflammasome: activation and regulation in age-related macular degeneration. *Mediators Inflamm* 2015;2015:690243.

194. Liu RT, Wang A, To E, et al. Vinpocetine inhibits amyloid-beta induced activation of NF-kappaB, NLRP3 inflammasome and cytokine production in retinal pigment epithelial cells. *Exp Eye Res* 2014;127:49-58.

195. Sarroukh R, Cerf E, Derclaye S, et al. Transformation of amyloid beta(1-40) oligomers into fibrils is characterized by a major change in secondary structure. *Cell Mol Life Sci* 2011;68:1429-1438.

196. Stine WB, Jungbauer L, Yu C, LaDu MJ. Preparing synthetic Abeta in different aggregation states. *Methods Mol Biol* 2011;670:13-32.

197. Shi J, Zhao Y, Wang K, et al. Cleavage of GSDMD by inflammatory caspases determines pyroptotic cell death. *Nature* 2015;526:660-665.

198. He WT, Wan H, Hu L, et al. Gasdermin D is an executor of pyroptosis and required for interleukin-1beta secretion. *Cell Res* 2015;25:1285-1298.

199. Kayagaki N, Stowe IB, Lee BL, et al. Caspase-11 cleaves gasdermin D for non-canonical inflammasome signalling. *Nature* 2015;526:666-671.

200. Celkova L, Doyle SL, Campbell M. NLRP3 Inflammasome and Pathobiology in AMD. *J Clin Med* 2015;4:172-192.

201. Olsen I, Singhrao SK. Inflammasome Involvement in Alzheimer's Disease. *J Alzheimers Dis* 2016;54:45-53.

202. Heneka MT, Kummer MP, Stutz A, et al. NLRP3 is activated in Alzheimer's disease and contributes to pathology in APP/PS1 mice. *Nature* 2013;493:674-678.

203. Salminen A, Ojala J, Suuronen T, Kaarniranta K, Kauppinen A. Amyloid-beta oligomers set fire to inflammasomes and induce Alzheimer's pathology. *J Cell Mol Med* 2008;12:2255-2262.

204. Anderson OA, Finkelstein A, Shima DT. A2E induces IL-1ss production in retinal pigment epithelial cells via the NLRP3 inflammasome. *PloS one* 2013;8:e67263.

205. Doyle SL, Lopez FJ, Celkova L, et al. IL-18 Immunotherapy for Neovascular AMD: Tolerability and Efficacy in Nonhuman Primates. *Investigative ophthalmology & visual science* 2015;56:5424-5430.

206. Hirano Y, Yasuma T, Mizutani T, et al. IL-18 is not therapeutic for neovascular age-related macular degeneration. *Nature medicine* 2014;20:1372-1375.

207. Liu X, Zhang Z, Ruan J, et al. Inflammasome-activated gasdermin D causes pyroptosis by forming membrane pores. *Nature* 2016;535:153-158.

208. Sborgi L, Ruhl S, Mulvihill E, et al. GSDMD membrane pore formation constitutes the mechanism of pyroptotic cell death. *The EMBO journal* 2016;35:1766-1778.

209. Sagulenko V, Thygesen SJ, Sester DP, et al. AIM2 and NLRP3 inflammasomes activate both apoptotic and pyroptotic death pathways via ASC. *Cell Death Differ* 2013;20:1149-1160.

210. Hurtley SM. Apoptosis, necrosis, and pyroptosis. *Science* 2016;352:48-50.

211. Lopez-Castejon G, Pelegrin P. Current status of inflammasome blockers as anti-inflammatory drugs. *Expert opinion on investigational drugs* 2012;21:995-1007.

212. de Rivero Vaccari JP, Lotocki G, Marcillo AE, Dietrich WD, Keane RW. A molecular platform in neurons regulates inflammation after spinal cord injury. *J Neurosci* 2008;28:3404-3414.

213. Uchimoto T, Nohara H, Kamehara R, Iwamura M, Watanabe N, Kobayashi Y. Mechanism of apoptosis induced by a lysosomotropic agent, L-Leucyl-L-Leucine methyl ester. *Apoptosis : an international journal on programmed cell death* 1999;4:357-362.

214. Eckelman BP, Salvesen GS. The human anti-apoptotic proteins cIAP1 and cIAP2 bind but do not inhibit caspases. *The Journal of biological chemistry* 2006;281:3254-3260.

215. Rigaud S, Fondaneche MC, Lambert N, et al. XIAP deficiency in humans causes an X-linked lymphoproliferative syndrome. *Nature* 2006;444:110-114.

216. Ferretti M, Gattorno M, Chiocchetti A, et al. The 423Q polymorphism of the X-linked inhibitor of apoptosis gene influences monocyte function and is associated with periodic fever. *Arthritis Rheum* 2009;60:3476-3484.

217. Beug ST, Cheung HH, LaCasse EC, Korneluk RG. Modulation of immune signalling by inhibitors of apoptosis. *Trends Immunol* 2012;33:535-545.

218. Yabal M, Muller N, Adler H, et al. XIAP restricts TNF- and RIP3-dependent cell death and inflammasome activation. *Cell Rep* 2014;7:1796-1808.

219. Hirota JA, Hirota SA, Warner SM, et al. The airway epithelium nucleotide-binding domain and leucine-rich repeat protein 3 inflammasome is activated by urban particulate matter. *J Allergy Clin Immunol* 2012;129:1116-1125 e1116.

220. Santana PT, Martel J, Lai HC, et al. Is the inflammasome relevant for epithelial cell function? *Microbes Infect* 2016;18:93-101.

221. Peeters PM, Wouters EF, Reynaert NL. Immune Homeostasis in Epithelial Cells: Evidence and Role of Inflammasome Signaling Reviewed. *Journal of immunology research* 2015;2015:828264.

222. Wada T, Kanegane H, Ohta K, et al. Sustained elevation of serum interleukin-18 and its association with hemophagocytic lymphohistiocytosis in XIAP deficiency. *Cytokine* 2014;65:74-78.

223. Sharma K, Sharma NK, Anand A. Why AMD is a disease of ageing and not of development: mechanisms and insights. *Front Aging Neurosci* 2014;6:151.

224. Choudhary M, Ding JD, Qi X, et al. PPARbeta/delta selectively regulates phenotypic features of age-related macular degeneration. *Aging (Albany NY)* 2016.

225. Fletcher EL, Jobling AI, Greferath U, et al. Studying Age-Related Macular Degeneration Using Animal Models. *Optometry and vision science : official publication of the American Academy of Optometry* 2014;91:878-886.

226. Hollyfield JG, Bonilha VL, Rayborn ME, et al. Oxidative damage-induced inflammation initiates age-related macular degeneration. *Nature medicine* 2008;14:194-198.

227. Pennesi ME, Neuringer M, Courtney RJ. Animal models of age related macular degeneration. *Molecular aspects of medicine* 2012;33:487-509.

228. Haines JL, Hauser MA, Schmidt S, et al. Complement factor H variant increases the risk of age-related macular degeneration. *Science* 2005;308:419-421.

229. Edwards AO, Ritter R, 3rd, Abel KJ, Manning A, Panhuysen C, Farrer LA. Complement factor H polymorphism and age-related macular degeneration. *Science* 2005;308:421-424.

230. Fritsche LG, Igl W, Bailey JN, et al. A large genome-wide association study of age-related macular degeneration highlights contributions of rare and common variants. *Nat Genet* 2016;48:134-143.

231. Riera CE, Merkwirth C, De Magalhaes Filho CD, Dillin A. Signaling Networks Determining Life Span. *Annu Rev Biochem* 2016;85:35-64.

232. Fuchs Y, Steller H. Live to die another way: modes of programmed cell death and the signals emanating from dying cells. *Nature reviews Molecular cell biology* 2015;16:329-344.

233. Krieg A, Correa RG, Garrison JB, et al. XIAP mediates NOD signaling via interaction with RIP2. *Proceedings of the National Academy of Sciences of the United States of America* 2009;106:14524-14529.

234. Bauler LD, Duckett CS, O'Riordan MX. XIAP regulates cytosol-specific innate immunity to Listeria infection. *PLoS Pathog* 2008;4:e1000142.

235. Prakash H, Albrecht M, Becker D, Kuhlmann T, Rudel T. Deficiency of XIAP leads to sensitization for Chlamydophila pneumoniae pulmonary infection and dysregulation of innate immune response in mice. *The Journal of biological chemistry* 2010;285:20291-20302.

236. Damgaard RB, Nachbur U, Yabal M, et al. The ubiquitin ligase XIAP recruits LUBAC for NOD2 signaling in inflammation and innate immunity. *Molecular cell* 2012;46:746-758.

237. Gaudana R, Ananthula HK, Parenky A, Mitra AK. Ocular drug delivery. *AAPS J* 2010;12:348-360.

238. Pitkanen L, Ruponen M, Nieminen J, Urtti A. Vitreous is a barrier in nonviral gene transfer by cationic lipids and polymers. *Pharm Res* 2003;20:576-583.

239. Urtti A. Challenges and obstacles of ocular pharmacokinetics and drug delivery. *Adv Drug Deliv Rev* 2006;58:1131-1135.

240. Kalluri R, Weinberg RA. The basics of epithelial-mesenchymal transition. *The Journal of clinical investigation* 2009;119:1420-1428.

241. Samuel W, Jaworski C, Postnikova OA, et al. Appropriately differentiated ARPE-19 cells regain phenotype and gene expression profiles similar to those of native RPE cells. *Molecular vision* 2017;23:60-89.

242. Stern JH, Temple S. Stem cells for retinal replacement therapy. *Neurotherapeutics* 2011;8:736-743.

243. Adijanto J, Philp NJ. Cultured primary human fetal retinal pigment epithelium (hfRPE) as a model for evaluating RPE metabolism. *Experimental eye research* 2014;126:77-84.

244. Woodell A, Coughlin B, Kunchithapautham K, et al. Alternative complement pathway deficiency ameliorates chronic smoke-induced functional and morphological ocular injury. *PloS one* 2013;8:e67894.

245. McLeod DS, Bhutto I, Edwards MM, Silver RE, Seddon JM, Lutty GA. Distribution and Quantification of Choroidal Macrophages in Human Eyes With Age-Related Macular Degeneration. *Investigative ophthalmology & visual science* 2016;57:5843-5855.

246. Ijima R, Kaneko H, Ye F, et al. Interleukin-18 induces retinal pigment epithelium degeneration in mice. *Investigative ophthalmology & visual science* 2014;55:6673-6678.

247. Stanley AC, Lacy P. Pathways for cytokine secretion. *Physiology (Bethesda)* 2010;25:218-229.

248. Blott EJ, Griffiths GM. Secretory lysosomes. *Nature reviews Molecular cell biology* 2002;3:122-131.

249. Martin-Sanchez F, Diamond C, Zeitler M, et al. Inflammasome-dependent IL-1beta release depends upon membrane permeabilisation. *Cell Death Differ* 2016;23:1219-1231.

250. Minton K. Inflammasome: Ubiquitin lines up for inflammasome activity. *Nature reviews Immunology* 2014.

251. Mirza S, Plafker KS, Aston C, Plafker SM. Expression and distribution of the class III ubiquitin-conjugating enzymes in the retina. *Molecular vision* 2010;16:2425-2437.

252. Zhang X, Zhou J, Fernandes AF, et al. The proteasome: a target of oxidative damage in cultured human retina pigment epithelial cells. *Investigative ophthalmology & visual science* 2008;49:3622-3630.

253. Ramos de Carvalho JE, Klaassen I, Vogels IM, et al. Complement factor C3a alters proteasome function in human RPE cells and in an animal model of age-related RPE degeneration. *Investigative ophthalmology & visual science* 2013;54:6489-6501.

254. Glenn JV, Mahaffy H, Dasari S, et al. Proteomic profiling of human retinal pigment epithelium exposed to an advanced glycation-modified substrate. *Graefe's archive for clinical and experimental ophthalmology = Albrecht von Graefes Archiv fur klinische und experimentelle Ophthalmologie* 2012;250:349-359.

255. Py BF, Kim MS, Vakifahmetoglu-Norberg H, Yuan J. Deubiquitination of NLRP3 by BRCC3 critically regulates inflammasome activity. *Molecular cell* 2013;49:331-338.

256. Rodgers MA, Bowman JW, Fujita H, et al. The linear ubiquitin assembly complex (LUBAC) is essential for NLRP3 inflammasome activation. *The Journal of experimental medicine* 2014;211:1333-1347.

Appendices

Appendix A Supplementary Figures

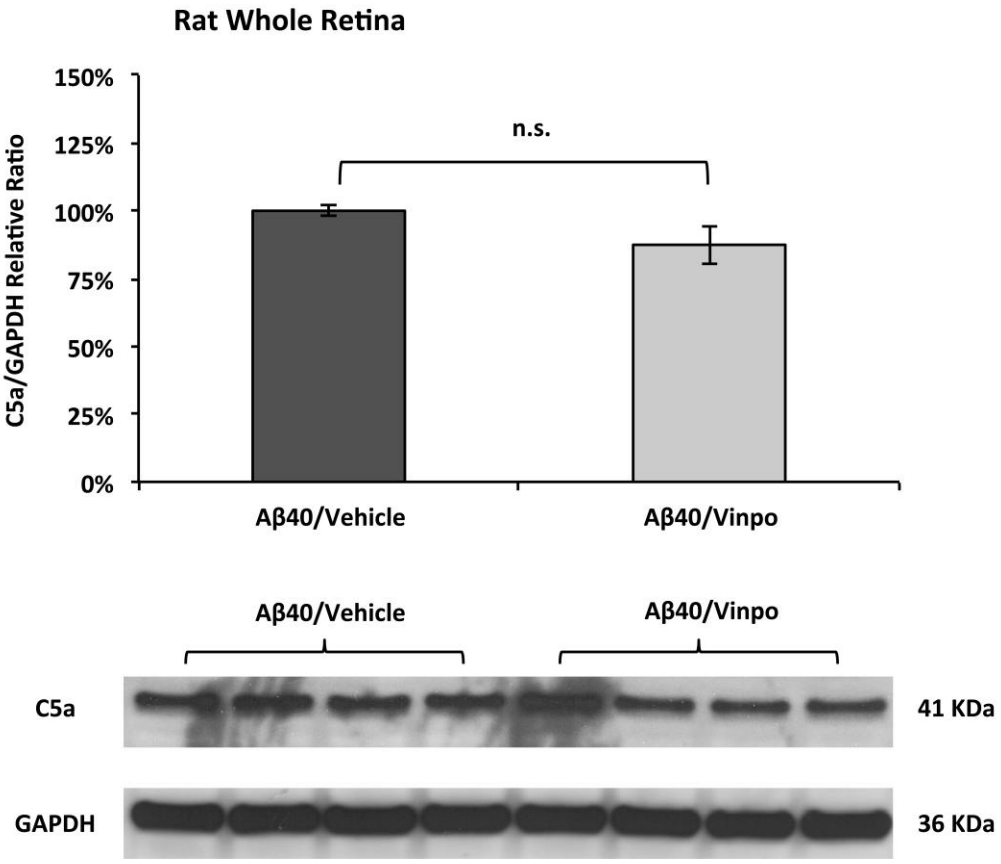

Supplementary Figure 1 C5a is not affected by vinpocetine-mediated NF-κB inhibition.

Since the intraocular $A\beta_{1\text{-}40}$ injection has been previously implicated in promoting NF-κB activation and NLRP3 inflammasome activation,[113] we assessed the level of activated C5 (C5a) as a surrogate marker for complement activation and MAC formation when NF-κB activity was specifically inhibited by vinpocetine. Western blot of retina protein lysates shows equal amounts of C5a (MW = 41 kDa; rabbit polyclonal C5a complement antibody, cat# 250565) in the vinpocetine-treated group, when compared to vehicle controls (Mann-Whitney, $p > 0.05$; $N = 5$). For a full description of the experimental procedures, refer to Chapter 4.

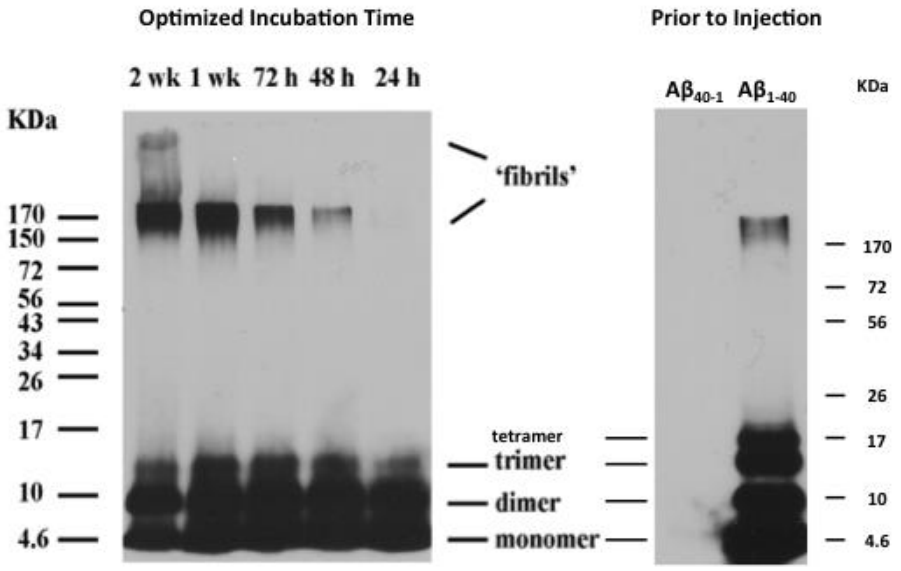

Amyloid-beta Peptide Amino Acid Sequences

Aβ1-40: Asp-Ala-Glu-Phe-Arg-His-Asp-Ser-Gly-Tyr-Glu-Val-His-His-Gln-Lys-Leu-Val-Phe-Phe-Ala-Glu-Asp-Val-Gly-Ser-Asn-Lys-Gly-Ala-Ile-Ile-Gly-Leu-Met-Val-Gly-Gly-Val-Val

Aβ40-1: Val-Val-Gly-Gly-Val-Met-Leu-Gly-Ile-Ile-Ala-Gly-Lys-Asn-Ser-Gly-Val-Asp-Glu-Ala-Phe-Phe-Val-Leu-Lys-Gln-His-His-Val-Glu-Tyr-Gly-Ser-Asp-His-Arg-Phe-Glu-Ala-Asp

Supplementary Figure 2 Preparation of oligomeric Aβ: optimization and injection.

Synthetic Aβ peptides were purchased and prepared following our published protocol.[171] A series of different incubation time points were tested for the optimal formation of Aβ oligomers (left). For *in vivo* rat eye injections, oligomeric Aβ peptide solutions (both $A\beta_{1\text{-}40}$ and the reverse control, $A\beta_{40\text{-}1}$) were incubated for 48 h, tested by the 6E10 anti-Aβ antibody in western blot (right), and then delivered to the animals.

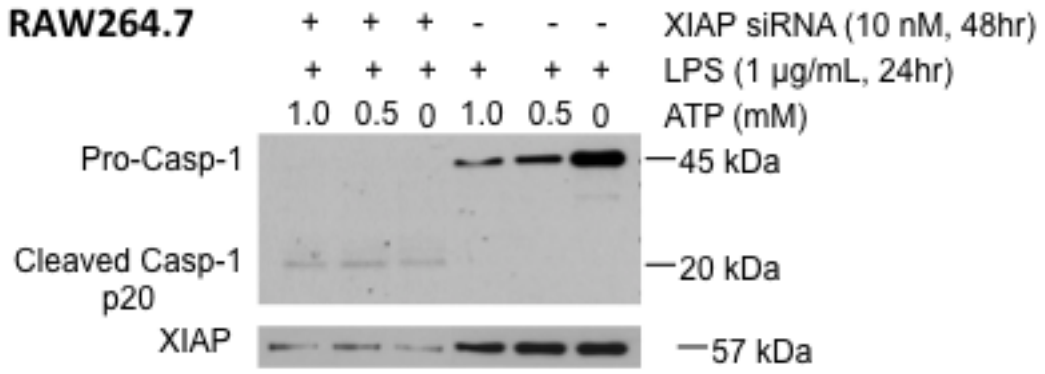

Supplementary Figure 3 XIAP siRNA knockdown enhances caspase-1 cleavage in murine macrophage cell line RAW264.7.

The murine macrophage RAW264.7 cell line was used as a positive control cell type to study the relationship between caspase-1 cleavage and XIAP protein level. Under the same LPS/ATP combined stimulation, RAW264.7 cells pretreated with 10 nM XIAP siRNA showed enhanced cleavage of full-length pro-caspase-1 (45 kD) into cleaved caspase-1 bands (20 kD).